NUMERICAL SIMULATIONS FOR THE OPTIMIZATION OF ONLINE WASH SYSTEMS FOR GAS TURBINES

A THESIS IN MECHANICAL ENGINEERING

Master of Science in Mechanical Engineering (MSME)

Presented to the faculty of the American University of Sharjah
College of Engineering in partial fulfillment of
the requirements for the degree

MASTER OF SCIENCE

By
Hamzeh Ahmed Nawar
B.S. 2009

Sharjah, UAE
May 2011

We approve the thesis of Hamzeh Ahmed Nawar | Date of signature

_____ _____

Dr. Essam Wahba
Assistant Professor
Department of Mechanical Engineering
Thesis Advisor

_____ _____

Dr. Mohamed Gadalla
Associate Professor
Department of Mechanical Engineering
Graduate Committee

_____ _____

Dr. Saad Ahmed
Professor
Department of Mechanical Engineering
Graduate Committee

_____ _____

Dr. Rami Haweeleh
Assistant Professor
Department of Civil Engineering
Graduate Committee

_____ _____

Dr. Mohammad Ameen Al-Jarrah
Department Head
Department of Mechanical Engineering

_____ _____

Dr. Hany El Kadi
Associate Dean
College of Engineering

_____ _____

Dr. Yousef Al-Assaf
Dean
College of Engineering

_____ _____

Dr. Gautam Sen
Vice-Provost
Research & Graduate study

NUMERICAL SIMULATIONS FOR THE OPTIMIZATION OF ONLINE WASH SYSTEMS FOR GAS TURBINES

Hamzeh Ahmed Nawar, Candidate for the Master of Science in Mechanical Engineering

American University of Sharjah, 2011

ABSTRACT

During gas turbine operation, large amounts of small particles are ingested along with the air inflow. As a result, the blade shape changes over time, hence affecting the air flow pattern and reducing efficiency. Field tests and operator experience have shown that online water washing systems help to regain power lost due to contaminant build up on the compressor blades. This technology involves injecting fine atomized sprays of water through nozzles into the air stream. Poorly designed online washing systems may result in inefficient operation that does not lead to the expected improvement in gas turbine efficiency. For this reason, the efficient design of compressor online washing systems is crucial if the desired output of performance recovery is to be realized. An optimum design requires controlling the water spray characteristics at the inlet to the compressor first stage.

The current work is based on a numerical approach to propose a generalized and structured methodology for optimizing gas turbine online washing systems. The approach is applied to optimize the design of the online washing system for the General Electric gas turbine model MS5002. Comparisons between the optimized design and the current design are also presented. Numerical optimization results show that an optimum design of the online washing system for MS5002 gas turbine is feasible for the following nozzles system: 11 axial nozzles and 12 radial nozzles, equally spaced. the optimized nozzle diameter is 1.5 mm, mass flow rate is 0.1672 kg/s, and half-cone angle is 15° for axial nozzles. For the radial nozzles, the optimized nozzle diameter is 1.1 mm, mass flow rate is 0.1533 kg/s, and half-cone angle is 54°. With this system droplet size in the range of $55 - 150\mu m$, impact velocity of 110-113 m/s, and water covers the entire outlet boundary of bell mouth uniformly.

KEYWORDS

Online wash for compressor, Numerical-based Optimization, Jet Breakup, Secondary Breakup Models

CONTENTS

LIST OF FIGURES

LIST OF TABLES

ACKNOWLEDGEMENT

In the name of Allah.

First of all, all praise and glory be to Allah, the Almighty, for enlightening my way and directing me to achieve this work successfully ensha'allah, and our beloved prophet Mohammad –may peace be upon him- the perfect example to be followed, all my wishes and prays go towards meeting you in paradise enshalla.

I would like to express my deep appreciation to my advisor Dr. Essam Wahba for guiding me through this work and for his valuable advice, patience and encouragement and also for providing me with the valuable material to develop this work.

Also I would like to express my appreciation to the examiner committee members and to all the faculty members of the mechanical engineering department for their guidance and advice.

To my favorite professors Dr. Ahmad Obaide and Dr. Sarim Al-Zubaidy, I cannot thank you enough for helping me to see my future and putting my plans, I will never forget you.

My deepest appreciation goes to my family. My parents who brought me to this life and supported me and guided me to reach this point. Also My brothers and sister who loved me. I wish I can return some of their favor upon me.

NOMENCLATURE

CAB: Cascade Atomization and breakup model

CFD: Computational fluid dynamic

d: Diameter

d_{32}: Sauter Mean Diameter, $\frac{\sum_k \dot{n}_k d_{p,k}^3}{\sum_k \dot{n}_k d_{p,k}^2}$

ETAB: Enhanced Taylor Analogy Breakup model

IGV: Inlet Guide Vanes

m: water to air mass flux ratio, $\frac{\rho_i V_i A_i}{\rho_g V_g A_g}$

$\dot{m}$: Mass flow rate

n: Number of droplets

Oh: Ohnesorge number, $\frac{\mu}{\sqrt{\rho_p \sigma d_p}}$

PDA: Phase Doppler Anemometry

PIV: Particle Imaging Velocimery

r: radius

q: momentum flux ratio, $\frac{\rho_l V_l^2}{\rho_g V_g^2}$

Re: Reynolds number, $\frac{\rho V_i d_i}{\mu}$

SMD: Sauter Mean Diameter, $\frac{\sum_k \dot{n}_k d_{p,k}^3}{\sum_k \dot{n}_k d_{p,k}^2}$

t: Breakup time

TAB: Taylor Analogy Breakup model.

V: Velocity

V_{slip}: Slip velocity, $V_l - V_a$

We: Weber number, $\frac{\rho_F V_{Slip}^2 d_p}{\sigma}$

x: Deviation of the droplet equator from its undeformed position

y: Dimensionless deformation of drops, $2(x/r)$

Greek letters

v: Dynamic viscosity

σ: Surface tension

ρ: Density

μ: Kinematic Viscosity

ε: *Error*

Subscripts

a: Air

cr: Critical

F: Fluid (Continuous medium)

g: Gas

i: Injection (of water)

l: Liquid

m: maximum

p: Particles

r: Relative

$req.$: required

Chapter 1

Introduction

Gas turbine efficiency depends significantly on the state of its compressor. During its operation, compressors suffer from the accumulation of fouling on the blades causing changes in the blades' airfoil shape. This, in turn, affects the aerodynamic characteristics and the surge limit of the blade by increasing the incident angle and the surface roughness which results in reduction of the compressor throat area . With time, this problem leads to reduction of the power output of the gas turbine, where 70-80% of gas turbine overall performance loss is caused by fouling [1]. Burning higher amount of fuel becomes necessity to compensate for the reduction of efficiency, in a time where the world is suffering from the lack of oil resources and the increase of energy demand. Energy demand is expected to increase by 50% in 2050 than it was in 2005 [2].

It has been shown by a study published by the World Energy Council that there is a gap between the current average performance and the top optimized power plant, eliminating this gab saves approximately US$80 billion per year [3]. Nevertheless burning higher amount of fuel leads to increase of emissions to the atmosphere which is a growing problem worldwide.

Making the compressor operates near its design point requires keeping the blades clean and in shape. Although the installation of air filtration in the air intake reduces the contaminants carried with air entering the compressor, fouling is not avoidable [4]. Accordingly, the need of washing compressor blades regularly becomes necessity . Many approaches where adopted over time for this purpose, starting with the most obvious way, manual cleaning. despite the great benefits of this approach in delivering the desired performance recovery, clearly, it is not an efficient approach as it requires the shut down and dis-assembly of the engine to clean it [5]. As a more efficient approach, grid-blasting method was considered, where deposits removed by injecting charcoal, rice, nutshells, or synthetic resin particles in the direction of air while the engine is running. This approach does not require shutting

down the engine and less labor is needed [6]. However the potential of erosion is high due to the impact of solid particles into blades. Eventually a more reliable and efficient approach floats to surface, which is injecting water, with or without additions, where this approach can be done by two processes: online or offline washing [5].

Offline washing takes place while the power plant operates at very low rotational speed which requires to put the gas turbine off duty very frequently causing problem especially for heavy duty industrial gas turbine, Alternatively, the use of online washing system becomes the solution. As the use of online washing system does not replace the need of offline washing but it spans the interval between one offline wash to another, in other words online and offline are complementary.

Online washing operates while the power plant is running at full speed and full load [5] by injecting water from high pressure spray nozzles at the intake of gas turbine. Water injected at high speed causes the water to break up to micro level droplets impacting the compressor blades at high speed leading to the removal of the fouling accumulated on the blades. However, poorly designed online washing system results in useless design that does not deliver its essential purpose if the injected water particles impact the compressor casing instead of compressor blades or worse, compressor blades can suffer from erosion if the water droplet sizes impinging the blades exceed the acceptable limits. Moreover, it can affect the centrifugal forces on the blades if the water was not distributed uniformly across the whole cross-sectional area of the compressor [5].

According to what is mentioned above, the efficient design of compressor online washing system is crucial if the desired output of performance recovery to be realized. An optimized design must include: selecting the appropriate location to install the spray nozzles, controlling the water droplet size and speed at entrance to compressor first stage, selecting the proper nozzle cone angle to ensure the water covers the entire compressor cross-sectional area uniformly, deciding the required water-to-air ratio for the given engine based on its power output and operation conditions [7], and tracking the droplet path to reduce the amount of water drops impacting the compressor casing.

Due to the complicated nature of the multiphase problem associated with injecting water sprays in the continuous airstream, there is no direct method found in literature to quantitatively determining the spray characteristics (especially droplet size). Although there are many empirical equations found in literature to calculate the droplet Sauter Mean Diameter (SMD), these relations are valid for limited ranges and limited conditions. Alternatively, computational fluid dynamics (CFD) has provided many models describing the dynamics of liquid jets in gaseous flow that can be used to characterize the breakup process. Many numerical approaches were introduced in the literature to describe this phenomenon such as Taylor Analogy Breakup (TAB) [8], Reitz & Diwakar [9]. CFD comes as a very effective alternative for the costly experiments which require advanced optical techniques and special conditions to perform.

The current work is based on a numerical approach to propose a generalized and structured methodology for optimizing gas turbine online washing systems using ANSYS CFX 12.0 workbench which is supported with powerful tools that can be used to accomplish the desired objective of the current work

1.1. Literature Review

1.1.1. Historical background of compressor online washing development.

The Association of Power and Heat Generation Utilities [10] defined online washing as "At rated (nominal) shaft speed, generally demineralized water is injected into the engine upstream of the first compressor stage." As online and offline washing are complimentary the design of both systems is related, The idea of injecting water using spray nozzles started with the offline washing approach and gradually started to develop to online washing by the early 1970s, as washing started to take place at higher rotational speeds [5].

At the early time of putting online washing into practice, unsatisfactory results were obtained in terms of power recovery as Elser [11] showed in 1973 on an aero-derivative engines, where a slow recovery of output power of 3.9% was observed during over than 1375 hours.

In 1980s, better designs were introduced for online washing that took into account the properties of the injected sprays and an acceptable performance of washing was observed at high rotational speeds but reduced load [5]. By 1989,

Thames et al. [12] realized that online washing cannot replace offline washing but it can keep compressor blades clean between one offline washing to another. It was noticed that spray characteristics play a major role in the efficiency of cleaning, and in 1980s the problem of erosion was highlighted due to large droplets impacting the blade [5]. After that designers started to pay more attention to the location and distribution of spray nozzles.

In 1991, MacDermon suggested to inject the water across the airstream rather than parallel to it to allow the water to penetrate deep in the airstream and prevent droplets from impacting the compressor casing [13]. Backer and Bohn claimed that to avoid erosion, injected water should cover the entire cross-sectional area of the compressor [14]. The relation between droplet size and efficiency of cleaning came to picture as an important factor for efficient cleaning, the impact of large droplets increases the potential of erosion, however large droplets can penetrate easier in the airstream and propagate farther to later stages of compressor. On the other hand small droplet sizes follow the air stream line and reduce the efficiency of cleaning [5].

In 1990s, a trend of quantitatively addressing the acceptable limits of droplet size based on Sauter Mean Diameter (SMD) started, many different ranges were published, as those ranges depend on many different factors. Eventually there was a fair agreement that keeping the SMD in the range of 50-250μm results in erosion free efficient cleaning [15,16].

In the beginning of the current century the importance of water-to-air ratio was further investigated. It was found in literature that water-to-air ratio in the range of 0.2%-0.7% is recommended for engines up to 50MW [6,17,18,19]. . It was claimed that going for higher water-to-air rations plays a key role in enhancing the cleaning efficiency while droplet size plays a secondary role [17,18,20,21].

1.1.2. General background in spray characterization: Experimental Techniques & Numerical Approaches

Experimental Techniques

With regard to experimental studies, spray characteristics (especially droplet size of spray) have presented a challenge for decades to be quantitatively measured where the atomization degree is characterized by the spray droplet size [22]. The importance of understanding the liquid breakup processes in gaseous flow rised due

to the fact that jet breakup is a fundamental process for many industrial applications, mainly: cooling, fire systems, combustion, and washing. At the early times, a qualitative understanding of spray characteristics was dominant rather than quantitative, it was related to the operative parameters, mainly operative pressure. The need of quantitatively determining the spray characteristics came to picture initially for the purpose of the optimization of combustion systems as droplet size is an important parameter.

Over time, many techniques have been used for measuring droplet size and speed experimentally, these techniques are commonly based on optical methods, as they do not affect the flow, such as: high speed cameras, Particle Imaging Velocimetry (PIV), Phase Doppler Anemometry (PDA), Laser Diffraction, Pulsed Photography, Shadowgraph, Tomographic Visualization and others.

Recently, Santagelo [22] studied the solid cone water mist spray injected from CJX 1140 B1SG nozzle type with high operative pressure in the range 6-8 MPa, using optical techniques, quantitative description of droplet size and flux distribution, initial velocity and cone angle were reported. Droplet size was measured using Laser Diffraction technique, while initial velocity and cone angle was evaluated using PIV technique. The results reported showed that cone angle is independent of operative pressure and it decreases as the distance from nozzle increases, where it is around 30° near the orifice and decreases to 16-17° in few millimeters away from the nozzle. SMD tends to decrease with the operative pressure, where 68, 65, and 62μm where reported for operative pressure values of 6, 7, and 8 MPa respectively.

Sedarsky [23] studied the breakup of water jet in cross flow air using different optical techniques: high speed shadowgraph, PIV, and ballistic imaging under a wide range of Weber numbers (We) and momentum flux ratios (q). Quantitative results of droplet size, SMD, were reported and presented.

Liu and Wei-Feng [24] studied the effect of liquid nozzle diameter on the performance of co-axial air-blast atomizer. Water/air mass flux ratio investigated was in the range 0.137-16.6. Malvern laser particle size was used to measure SMD. The reported results showed that liquid nozzle diameter has an effect on SMD for large mass flux ratios while is has no effect at low mass flux ratios. A decrease of SMD

was noticed with liquid injection diameter followed by an increase for large mass flux ratios.

Table 1.1, presents a summary of similar experimental studies found in literature using different techniques for measuring: droplet size, velocity, cone angle, and penetration depth.

Table 1. 1, summary of experimental studies carried out to investigate the spray characteristics using different techniques.

Author	Study Type	Main parameters	Measuring technique	Reported results
Paolo E. Santagelo [22]	Water jet in still air	Injection pressure range 6-8 MPa	PIV	Droplet Size and dispersion
David Sedarsky [23]	Water jet in transverse air flow (cross-flow)	We, Re, q and d_i	PIV, HSS and BI	Droplet size, Penetration length
Sung Wook Park [25]	Mono-cross dispersed diesel droplets in a cross-flow air stream	frequency of droplet generator and We	Long distance microscope and CCD camera	Drop let size and droplet deformation rate
Yuegui Zhou [26]	Y-jet nozzle with high liquid flow rate in still air	$\dot{m}$, Injection pressure and nozzle structure size	A collection of lens with a focal length of $600mm$	Droplet size
C.-L. Ng [27]	Non turbulent liquid (water and athylachohol) jets in air cross-flow	Re_l, V_g, d_i, q and We	Pulsed photography, shadowgraph, and high-speed imaging	Droplet size, velocities and trajectory
J. C. LASHERAS [28]	Round water jet by a high-speed annular air jet	Re_l and V_g	high-speed visualizations and PDA	Droplet size and breakup type
Zh. Zhang [29]	Water jet in air cross-flow	Nozzle geometry	PDA	Droplet Size
R. Ragucci [30]	Water jet in air cross-flow	V_g, Re, We, and q	PIV	Droplet velocity vectors
A.Cavaliere [31]	Liquid jet in high-pressure air cross-flow	Nozzle diameter, V_g, and Re	Tomographic visualization technique	Jet trajectory
Pie-Kuan Wu [32]	Liquid jet in subsonic air cross flow	We, Re, Mach number and q		Droplet size and breakup type
K. A. Sallam [33]	Liquid jet in gaseous cross flow	We, Re, Mach number and q		Droplet deformation rate, and velocity
K. A. Sallam [34]	Liquid (water and athanol) jets in still air	We, Re, q and initial jet diameter		Relative cross stream drop velocities and Mean surface efficiency factors
Z.Liu and R. D. Reitz [35]	liquid drops injected into a transverse high	Droplet size, Re, V_a and We	Long distance microscope and 35mm camera	Droplet distortion rate

	velocity air			
Hai-Feng Liu, Wei-Feng [24]	coaxial two-fluid airblast atomizers	mass flux ratio (m), Injection velocity, nozzle diameter	PIV and Malvern Laser Particle Sizer	SMD

Numerical Approach

During 1980s researchers tried to model the secondary breakup process of liquid jet in gaseous flow, starting with the famous approach introduced by Reitz & Diwakar in 1987 [9]. The proposed model showed good performance compared to experimental data. Also Taylor Analogy Breakup (TAB) model was introduced by P.J.O'Rourke and A.A. Amsdem in 1987 [8], this model assumes that droplet distortion can be modeled as one-dimensional, forced, damped harmonic oscillation similar to the mass-spring system, also this model showed very good acceptance. After that two models were developed from the TAB model: Enhanced Taylor Analogy Breakup (ETAB) model [36] and Cascade Atomization and breakup (CAB) model (Miller A. and Gidaspow D, 1992). The mentioned models adopt the "blob" method which assumes that liquid blobs having the diameter of the injector are introduced to the continuous flow and undergoes breakup based on the balance of the inertial and surface tension forces [37]. Later in 2002, Schmehl introduced Schmehl Breakup model [38], where this model uses experimental data to approximate the droplet deformation and breakup times.

Recently, Bade [39] compared experimental results with a CFD approach using Fluent, using a low speed (15.4 m/s) wind tunnel. The droplet size, velocity distribution, and spray shape was investigated. The study aimed to investigate the effect of the incident angle of the injector on the mentioned spray characteristics. Hollow cone angle nozzle was used at low flow rate. The computational method showed very good agreement with experimental data measured using Phase Doppler Interferometer (PDI).

Tanner [40] used TAB model to investigate the breakup process of liquid fuel jet in constant-volume cell. Solid-cone diesel fuel was modeled and the secondary breakup of droplets has been investigated.

Table 1.2, presents a summary of similar studies found in literature used numerical approaches to investigate the spray characteristics and compared to experimental results.

Table 1. 2, summary of studies carried out to investigate the spray characteristics using CFD

Author	Study Type	Main parameters	Measuring technique	Reported results
Paolo E. Santagelo [41]	High pressure water-mist spray in still air	Injection pressure	Advanced laser-based diagnostics (Malvern Spraytec and PIV	Droplet Size and velocity
K. M. Bade [39]	Water jet in air (cross- and co-flow)	Incidence angle of injector	Doppler Interferometry System (DIS)	Droplet size, velocity distribution and spray shape
A. J. Yule [42]	Swirl atomizers operating at high water pressure	Injection pressure		experimental drop size, drop velocity and spray penetration data
F.X. Tanner [40]	Diesel Jet in air cross flow		Taylor analogy breakup model (TAB)	Droplet size and breakup type
S.C. Kuensberg [43]	Diesel Sprays	Injector Nozzle Geometry		In liquid penetration, spray angle and drop size

1.2. Research Approach and methodology

The main contribution of the current work is to propose a structured methodology based on numerical approach for optimizing on-line washing system of gas turbine that can be generally applied for any geometry. To fulfill this objective ANSYS 12.0 workbench was used. ANSYS CFX was used to model flow dynamic and Goal-Driven-Optimization tool was used to optimize the design.

The procedures adopted to achieve the study objective are listed below:

a. Selecting the most reliable numerical breakup model to use for modeling the flow dynamic of the problem

This step includes validating numerical jet breakup models against experimental studies. The tested CFD breakup models are: Reitz & Diwakar Breakup Model, Taylor Analogy Breakup (TAB) model, Enhanced Taylor Analogy Breakup

(ETAB model), Cascade Atomization and Breakup (CAB) model, and Schmehl Breakup model. Three cases were investigated:

- Water jet injected into still air.
- Water jet injected into cross-flow air.
- Water jet injected into co-flow air.

b. Numerical Optimization steps:

i. Introducing Geometry.

An approximate geometry of MS5002 gas turbine was used in this study. An existing design of the online washing system allows for comparisons with the present numerical-based design procedures

ii. Selecting the appropriate position of nozzles.

The location of nozzles was selected such that Weber number is highest to allow maximum droplet distortion which results in a minimum droplet spray size. At the same time position of nozzles must be selected such that momentum flux ratio is highest to allow injected water to penetrate farther in the airstream. Fortunately both conditions can be satisfied by injecting water inside the intake casing where airstream speed is minimum.

iii. Determining the optimum mass flow rate per nozzle for a practical range of nozzle diameters based on the acceptable limits of droplet size.

For each nozzle diameter, optimum range of mass flow rate per nozzle is obtained such that the spray droplet size is kept within the acceptable limits (SMD range 50-250μ) using goal-driven-optimization tool.

iv. Determining the required water mass flow rate for the system.

For the mentioned gas turbine power output, the optimum range of water-to-air ration can be determined, and the required water mass flow rate can be calculated.

v. Determining the required number of nozzles based on the water-to-air ratio and optimum mass flow rate per nozzle.

Based on the water-to-air ratio the total required mass flow rate of water can be determined, the number of required nozzles then can be calculated for different set of mass flow rate per nozzle.

vi. Determining the optimum cone angle of nozzles.

Optimum cone angle of nozzles is the angle at which the injected water would cover the entire cross-sectional area of compressor without water droplets impacting the compressor casing.

c. Comparing the optimized results with the exiting online wash system.

The results obtained for the optimized design are compared with real life existing gas turbine online wash system and recommendations are reported.

1.3. Research results and summary of key findings

As mentioned above the work was divided into three parts: 1) Selecting the most reliable numerical breakup model to use for the optimization procedures. 2) Performing the numerical optimization procedures 3) Comparing the optimized design with existing online wash system.

For part one, Reliability of several breakup models in estimating spray characteristics particularly droplet size was investigated, for three different cases. It was found that ETAB breakup model showed the best accuracy with Average absolute error of 14%, 13%, and 18% for Cases A, B, and C respectively. And with general tendency to slightly over estimating SMD values for cases A and B while it showed a non-monotonic tendency for case C.

For part 2, numerical-based optimization procedures were performed where ETAB breakup model was used for CFD simulations. An approximate geometry of MS5002 gas turbine was introduced for the optimization procedures. Constraints and criteria were collected from literature and set for the optimization procedures to ensure efficient washing without the potential of blades erosion. These constraints summarized as follow: SMD range of $50 - 250\ \mu m$, threshold velocity (Maximum impact velocity) of 1000 m/s, water-to-air ratio of 0.6%, minimum number of droplets impinging the compressor casing, and injected water covers the entire cross-sectional area of compressor. Two positions of nozzle were selected: axial and radial nozzles.

It was found that an optimum design of online washing system for MS5002 gas turbine is feasible for the following nozzles system: 23 nozzles, 11 axial nozzles and 12 radial nozzles, equally spaces and with operative and physical parameters of $d_n = 1.5\ mm$, mass flow rate of 0.1672 kg/s, and half-cone angle of 15° for axial nozzles. And for radial nozzles of $d_n = 1.1\ mm$, mass flow rate of 0.1533 kg/s, and

half-cone angle of 54°. With this system of nozzles all criteria and constraints were met. Droplet size in the range of $55 - 150\mu m$, impact velocity of 110-113 m/s, and water covers the entire outlet boundary of bell mouth uniformly.

For part 3, comparison between the optimized system and existing system of online washing for MS5002 gas turbine was presented. Both systems used the same axial and radial nozzle positions to allow comparison. Comparison of water-to-air ratio showed a very good agreement with 0.6% and 0.595% for optimized design and existing system respectively. For nozzles diameters existing design has lower values of nozzle diameters of 0.787 and 0.584 mm for axial and radial nozzles respectively, while optimized design has nozzle diameters values of 1.5 and 1.1 mm for axial and radial nozzles respectively. For mass flow rates existing design has higher values of operative mass flow rates.

Droplet mean diameter values for existing design were in the range of 25-90 $\boldsymbol{\mu}$m which is lower than the range of droplet diameters reported for the optimized design. According to the droplet size for existing design it was found that most of nozzles are operating in the inefficient washing region.

Chapter 2

Liquid Droplet Breakup Modeling

When liquid particles injected into a continuous gaseous medium with velocity lag between the dispersed particles and the continuous medium, reduction in size of liquid droplet occurs due to the aerodynamic forces exerted on the droplet surface. Understanding flow characteristics and properties, dynamic of water particles in airflow, and breakup regimes are important to enable the modeling of the breakup process adequately. In the current work the focus is limited to the injection of water sprays in airflow

2.1.Fluid flow characteristics

The investigated problem is a multiphase flow containing the liquid flow (water) injected in gaseous flow (air). The governing equations must include the effect of the continuous gaseous flow on the liquid droplets, and the effect of the water jet on the continuous flow [44].

To achieve the desired spray characteristics water jets should be issued at high-pressures to undergo the breakup process, hence water Reynolds number, Re_l, is relatively high ($Re_l > 4000$) and flow is classified as a turbulent flow [45]. Reynolds number is a dimensionless number relating the inertial forces, $\left(\frac{\rho V_i^2}{d_i}\right)$, to the viscous forces,$\left(\frac{\mu V_i}{d_i^2}\right)$. ρ is the density of the liquid, μ is the kinematic viscosity of the liquid, V_i is the injection velocity and d_i is the nozzle diameter.

$$Re_l = \frac{\rho V_i d_i}{\mu} \tag{2.1}$$

To understand the jet breakup process, many parameters are requires to be characterized and measured to describe the breakup process and spray characteristics adequately. The governing parameters must highlight breakup regimes, atomization degree, cone shape and velocity fields' distribution [22].

Breakup regimes are characterized by two dimensionless numbers: Weber number,We, and the Ohnesorge number, Oh. Weber number, We, defined as the ratio between forces that act to break apart a liquid structure and the surface tension acting to hold it together. For each type of flow (co-flow or cross-flow) We is defined in the appropriate way to emphasize the critical breakup process, for the proposed work We is defined in equation (1.2) below:

$$We = \frac{\rho_F V_{Slip}^2 d_p}{\sigma} \tag{2.2}$$

ρ_F is the density of the surrounding fluid (air), V_{slip} is the relative velocity between the gaseous flow and the liquid jet in the direction of the continuous flow, d_p is the diameter of the liquid droplet, and σ is the surface tension. Usually breakup process takes place in different regimes which are distinguished based on this number,

If the viscosity is relatively high it can affect the boundaries between different breakup regimes and the introduction of the Ohnesorge number,Oh, is required. Oh relates the viscous forces to the surface tension and it can be defined with respect to the flow regimes. A typical equation of this number is given by equation (1.3) below,

$$Oh = \frac{\mu}{\sqrt{\rho_p \sigma d_p}} \tag{2.3}$$

For the current work the effect of viscosity is not significant since the injected liquid is water which has relatively low viscosity, therefore the focus will be limited to the Weber number, We, since if $Oh < 1$ it has no effect on the breakup process [46].

Droplet size distribution and characteristic diameter of spray provide a clear representation of the atomization degree [22]. Usually droplet size distribution follows stochastic distribution approaches, however a simpler way of characterizing the atomization degree is to consider the characteristic Sauter Mean Diameter SMD, also known as D_{32}, and defined as follows [22]:

$$SMD = \frac{\sum_k \dot{n}_k d_{p,k}^3}{\sum_k \dot{n}_k d_{p,k}^2} \tag{2.4}$$

$d_{p,k}$ is the k[th] drop diameter and $\dot{n}_k$ is the rate of number of droplets having that diameter.

In cross-flows it is important to control the penetration of liquid jet into the gas for the purpose of achieving the required spray distribution. Jet penetration depth is defined as the distance to which the fluid dynamic disturbance associated with the injection extend [23]. This distance is controlled by the ratio,q, of jet momentum flux to gas momentum flux [23], this ratio is given by:

$$q = \frac{\rho_i V_i^2}{\rho_g V_g^2} \tag{2.5}$$

Subscript i indicates the initial liquid jet, and g denotes the gaseous flow.

Mass flow ratio is also commonly used to characterize the ratio between the mass flow rates of liquid to the mass flow rate of air in the control volume, Mass flow ratio is given by:

$$\mathrm{m} = \frac{\rho_\mathrm{i} \mathrm{V_i} \mathrm{A_i}}{\rho_\mathrm{g} \mathrm{V_g} \mathrm{A_g}} \tag{2.6}$$

2.2. Dynamics of water droplet breakup in gaseous flow

Injecting liquid spray into continuous gaseous flow with velocity lag between the dispersed liquid particles and the continuous gaseous medium results in size reduction in the liquid droplets. The distortion in droplet size can be characterized by the balance of aerodynamic forces acting on the droplet surface and surface tension. The velocity deviation between the liquid particles and the continuous medium play the key role in droplet breakup phenomenon [47]. The droplet formation in the continuous gaseous medium is very complicated and it takes place in two stages: primary breakup and secondary breakup, moreover both stages occur in many regimes, where these regimes can be distinguished based on the key governing parameter: Weber number, We.

2.2.1. Breakup processes regimes

As mentioned earlier breakup process for water jet takes place in two stages: primary breakup and secondary breakup. Primary breakup can be defined as the process at which continuous column of liquid initially breaks into drops, these drops undergo further breakup process to a finer drops these processes are defined as

secondary breakup [23]. Each of these two stages has different breakup regimes; the transition between these regimes is a function of Weber number,We.

- Primary breakup regimes.

Liquid jet into gaseous flow goes through a primary breakup process, Mazallon et al. (1999) found that breakup regime transitions of the liquid jet are determined by the Weber number, We, as follow: column breakup ($We < 4$), bag breakup ($4 \leq We < 30$) (modified by Sallam et al. (2004) [33]), multimode breakup ($30 \leq We < 110$), and shear breakup ($110 \leq We$) [27]. Those regimes are represented in figure 2.1 [33].

For the column breakup regime, (figure 2.1.b), liquid jet column starts to deform and take the shape of ellipsoidal cross section, and deflects in the direction of gas velocity V_g. This behavior caused by reduced gas pressure along the sides of the jet due to the acceleration of the gas across the liquid jet. For Bag breakup regime, (figure 2.1.c), the distance between liquid particles (nodes) starts to increase i.e. the liquid jet column width starts to increase in the direction of the low pressure in the sides of the jet taking the shape of Bag-like structure. Shear breakup regime, (figure 2.1.e), is similar to the previous two regimes but during this regime wavelike disturbance starts to appear in the upstream side of the deflected liquid jet, as a result of acceleration of a fluid of higher density toward a fluid of lower density. Multimode breakup, (figure 2.1.e), comes as a result of complex combination of the bag breakup and shear breakup properties, it can be considered as a transition between those regimes [33].

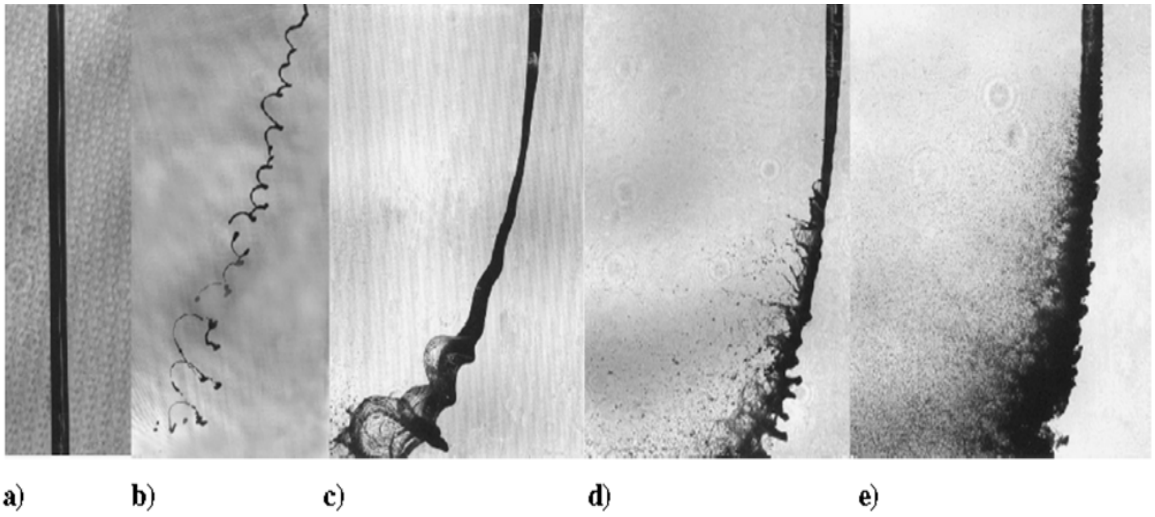

Figure 2. 1. [33], Visualization of primary breakup processes of round non-turbulent liquid jets in gaseous cross-flow: a) We = 0, no breakup; b) We = 3, column breakup; c) We = 8, bag breakup; d) We = 30, multimode breakup; and e) We = 220, shear breakup

- Secondary breakup regimes.

Secondary breakup regimes are similar to the primary breakup regimes (however droplets to be consider instead of continuous liquid column), it consists of three different regimes and again the transition between them is based on the Weber number,We: bag breakup regime$12 \geq We > 100$, stretching and thinning (stripping) regime$100 \geq We > 350$, and catastrophic regime $We \geq 350$ [25]. Figure 2.2 represents these regimes.

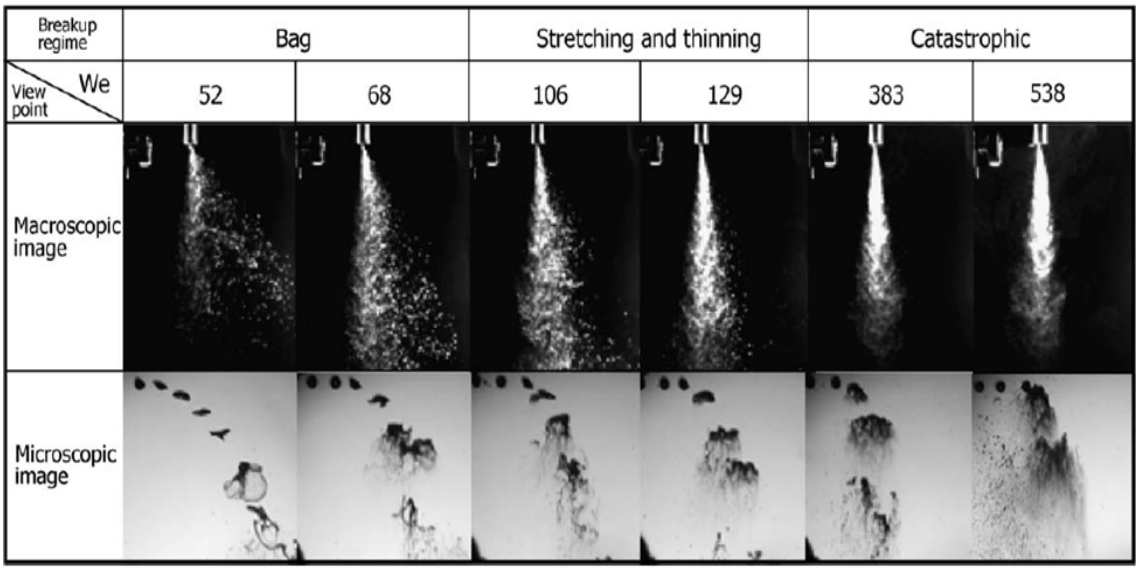

Figure 2. 2. [25], Secondary breakup regimes

2.2.2. Droplet breakup modeling: Numerical approach

As mentioned in chapter one, a trend to model secondary breakup started in 1980s, starting with Reitz & Diwakar Breakup model (R.D. Reitz and R. Diwakar 1987) [9] and Taylor Analogy Breakup (TAB) model (P.J.O'Rourke and A.A. Amsdem 1987) [8]. Two other models were developed from the TAB model: Enhanced Taylor Analogy Breakup (ETAB) model [36] and Cascade Atomization and Breakup Models (CAB) (Miller A. and Gidaspow D, (1992). After that R. Schmehl introduced the Schmehl Breakup model in 2002 [38].

Since the main concern is the final product in term of spray characteristics, modeling primary breakup has no practical use and tends to complicate the problem significantly, accordingly all the mentioned models are secondary breakup models and adopt the "blob" method which assumes that liquid blobs having the diameter of the injector are introduced to the continuous flow and undergoes breakup process based on the balance of the inertial forces and surface tension [37].

In some CFD packages, such as CFX, modeling using primary breakup option can be selected based on secondary breakup models, however this option is used to determine the initial conditions such as initial liquid velocity, yet spray characterization in the primary stage is not valid.

Assumptions and governing equations of each of the mentioned models are summarized below.

2.2.2.1. Reitz and Diwakar Breakup Model [9]

This model was introduced by R.D. Reitz and R. Diwakar [9] in 1987. The model classifies the breakup regimes into: bag breakup and striping breakup. The breakup of mother droplet to child droplets takes place if the Weber number,We, exceeds some critical value W_{cr}. The breakup process is governed by the following equation, which describes the change rate of the droplet radius:

$$\frac{dr_p}{dt} = \frac{-(r_p - r_{stable})}{t_{br}} \qquad (2.7)$$

r_p is the droplet radius prior to breakup, r_{stable} is the new radius of the stable droplet generated and t_{br} is the characteristics breakup time.

Values of r_{stable} and t_{br} are calculated based on the breakup regimes as follow:

Bag Breakup

$(We > W_{cr})$

$$t_{br} = C_1\sqrt{\frac{\rho_p r_p^3}{2\sigma}} \quad (2.8)$$

$$r_{stable} = \frac{\sigma}{\rho_F V_{slip}^2} \quad (2.9)$$

Stripping Breakup

$$\left(We/\sqrt{Re} > C_{S1}\right)$$

$$t_{br} = C_2 \frac{r}{V_{slip}}\sqrt{\frac{\rho_P}{\rho_F}} \quad (2.10)$$

$$r_{stable} = \frac{\sigma^2}{2\rho_F^2 V_{slip}^3 v} \quad (2.11)$$

The constantsC_1, C_2, W_{cr} and C_{S1} are listed in Table 2.1 below with their default values.

Table 2. 1, Reitz & Diwakar model constants

Constant	Default Value	Name
$\mathbf{C_1}$	π	Time Factor for Bag Breakup
$\mathbf{C_2}$	20	Time factor for Stripping
$\mathbf{W_{cr}}$	6.0	Critical Weber Number for bag
$\mathbf{C_{S1}}$	0.5	Weber Number Factor for Stripping

Reitz and Diwakar model is a multi-dimensional model it can characterize the interaction between injected liquid droplets and the contentious gaseous flow in dense

high-pressure sprays. This model accounts for the coupling effect between droplets and gas motion i.e. it accounts for the effect of gas on the droplets and also the effect of droplets on the gas turbulence. This model accounts for droplets breakup, droplets collision and coalescence as well. The approach of this model is based on the assumption that atomization and breakup are indistinguishable within the dense sprays near nozzle exit, therefore it assumes atomization takes place on the nozzle injector with droplet having diameter equal to the nozzle diameter. Once the droplet leaves the nozzle it goes through the breakup process due to the interaction with the gas [9].

2.2.2.2. Taylor Analogy Breakup (TAB) Model [8]

This model was proposed by P.J.O'Rourke and A.A. Amsdem in 1987, it assumes that droplet distortion can be modeled as one-dimensional, forced, dumped harmonic oscillation similar to the mass-spring system. Where the viscosity is assumed to be the dumping force and surface tension acts as a restoring force, this model uses a dimensionless value for the deformation of droplet size, $y = 2(x/r)$, where x described the deviation of the droplet equator from its non-deformed position [9] (figure 2.3), the modeling equation of y is expressed in equation (1.7) below:

$$\ddot{y} = \frac{5\mu_p}{\rho_p r^2}\dot{y} + \frac{8\sigma}{\rho_p r^3}y = \frac{2\rho_g V_{slip}^2}{3\rho_g r^2} \qquad (2.12)$$

Integrating this equation leads to a time dependents equation describing the particle distortion:

$$y(t) = We_{cr} + e^{-t/t_D}\left[(y_0 - We_{cr})\cos\omega t + \left(\frac{y_0}{\omega} + \frac{y_0 - We_{cr}}{\omega t_D}\right)\sin\omega t\right] \qquad (2.13)$$

Where,

$$t_D = \frac{2\rho_p r^2}{C_d}$$

$$\omega^2 = \frac{C_k\sigma}{\rho_p r^3} - \frac{1}{t_d^2}$$

For TAB model $\dot{y}(0) = y(0) = 0$

From equation (2.12) dimensionless particle distortiony, breakup occurs if $(y > 1)$ i.e. when the deviation of the droplet equator from its equilibrium position has become larger than half of the radius of the droplet [8].

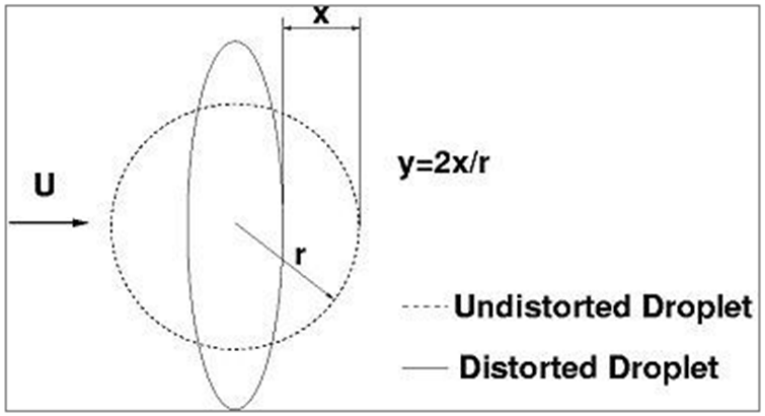

Figure 2. 3. [25], Particle Distortion

The Saunter mean radius (SMD) of the child droplets generated is calculated from the following equation:

$$\frac{r_{p,Parent}}{r_{p,Child}} = \left[1 + 0.4K + \frac{\rho_p r_{p,Parent}^3}{\sigma}\dot{y}_0^2\left(\frac{6K-5}{120}\right)\right] \quad (2.14)$$

This equation is based on the conservation of surface energy and energy bound in the distortion and oscillation of the parent droplet and surface energy and kinetic energy of the child droplets [8].

Table 2.2 below presents the model constants and their default values. [8]

Table 2. 2, TAB model Constants

Constant	Default Value	Name
$\mathbf{C_b}$	0.5	Critical Amplitude Coefficient
$\mathbf{C_d}$	5.0	Damping Coefficient
$\mathbf{C_f}$	1/3	External Force Coefficient
$\mathbf{C_k}$	8.0	Restoring Force Coefficient
$\mathbf{C_v}$	1.0	New Droplet Velocity Factor
K	10/3	Energy Ratio Factor

The weakness of this model is the large underestimation of the breakup time because the initial conditions are set to zero $\dot{y}(0) = y(0) = 0$, this leads to underestimation of penetration length.

2.2.2.3. Enhanced Taylor Analogy Breakup (ETAB) Model [18,32]

This model is based on the same assumptions of the TAB model except it models the breakup process based on the assumption that rate of child droplet generation $dn(t)/dt$, is proportional to the number of the child droplets according to the following equation:

$$\frac{d}{dt}n(t) = 2K_{br}n(t) \tag{2.15}$$

The constant K_{br}, depends on the break up regimes gives as:

$$K_{br} = \begin{cases} k_1\omega & We \leq We_t \\ k_2\omega\sqrt{we} & We > We_t \end{cases}$$

With We_t being the Weber number divides the bag breakup regimes from the stripping breakup regimes.

Droplet radius of the generated droplets is estimated by the following equation:

$$\frac{r_{p,Child}}{r_{p,Parent}} = e^{-K_{br}t} \tag{2.16}$$

Table 2.3 below shows the ETAB model constants and their default values. [8]

Table 2. 3, ETAB model constants

Constant	Default Value	Name
$\boldsymbol{K_1}$	2/9	Critical Amplitude Coefficient
$\boldsymbol{K_2}$	2/9	Damping Coefficient
$\boldsymbol{We_t}$	80	External Force Coefficient

2.2.2.4. Cascade Atomization and Breakup (CAB) Model [35]

This model is similar to the ETAB model except the constant K_{br} values defers as follow:

$$K_{br} = \begin{cases} k_1\omega & 5 < We < 80 \\ k_2\omega\sqrt{we} & 80 < We < 350 \\ k_3\omega We^{3/4} & 350 < We \end{cases}$$

The constants k_1 and k_2 are identical with TAB model and k_3=0.05

2.2.2.5. Schmehl Breakup Model [38]

This model was proposed by R. Schmehl [38] in 2002, it charachtarizes the breakup process in tow phases: phase one, is based on experimental results according experimental studies done by Hsinag et al [48] and plich eh al.[36]. it was showen experimentally irrespective of the breakup regimes, the time required to deform a partical from a sphere ito disk shape (see figure 2.3) is approximantely constant, and can be calculated as,

$$t_i = 1.6t^* \tag{2.17}$$

where t^* is the charactereristic time and calculated as follow:

$$t^* = \frac{d_p}{V_{slip}}\sqrt{\frac{\rho_p}{\rho_F}} \tag{2.18}$$

Phase two of the breakup, which charecterises the final destraction of droplets, is modeled by the following relations:

$$\frac{t_{br}}{t^*} = \begin{cases} 6(We-12)^{-0.25} & 12 \le We < 18 \\ 2.45(We-12)^{0.25} & 18 \le We < 45 \\ 141(We-12)^{-0.25} & 45 \le We < 351 \\ 0.766(We-12)^{0.25} & 351 \le We < 2670 \\ 5.5 & 2670 \le We \end{cases}$$

and for large Ohnesorge number ($Oh > 1$), the following relation is applied,

$$\frac{t_{br}}{t^*} = 4.5(1.2Oh^{0.74}) \tag{2.19}$$

similar Reitz and Diwakar model the breakup process takes place if the Weber number exceeds some critical value, We_{cr}, where the value of We_{cr} is calculated as follow:

$$We_{cr} = 12(1 + 1.077Oh^{1.6}) \tag{2.20}$$

Depending on the Weber number the following droplet breakup scenarios are possible:

A. Bag Breakup Regimes- Characterized by:

$$[12 \times (1 + 1.077Oh^{1.6})] < We < [20 \times (1 + 1.2Oh^{1.5})]$$

B. Multimode Regimes- Characterized by:

$$[20 \times (1 + 1.2Oh^{1.5})] < We < [32 \times (1 + 1.5Oh^{1.4})]$$

C. Shear Breakup Rrgimes- Characterized by:

$$[32 \times (1 + 1.5Oh^{1.4})] < We$$

For the three mentioned regimes child droplet sizes and normal velocity after breakup are computed, if the particle life time exceeds the breakup time, then breakup occurs.

Droplet size after breakup for Bag breakup and Multimode breakup is calculated by:

$$d_{32} = d_p \times (1.5Oh^{0.2}We_{corr}^{-0.25}) \quad (2.21)$$

Where,

$$We_{corr} = \frac{We}{(1+1.077Oh^{1.6})} \quad (2.22)$$

And for Shear breakup, the Child droplet size, $d_{32,red}$, is computed by:

$$d_{32,red} = \frac{We_{cr}\sigma}{\rho_F V_{Slip}^2} \quad (2.23)$$

Because this model divides the breackup process into two phases and the first phase is based on experimental data for breakup times it yields to better results in estimating the penetration depth.

Chapter 3

CFD Secondary Breakup Models Reliability

Droplet breakup is very complicated and multi-sided phenomenon. Operating conditions, liquid properties, continuous medium conditions and properties, and injection direction relative to gaseous flow play a significant role in modeling the breakup processes. For this reason modeling this problem requires to consider all the sides of the problem and the transition between breakup regimes should be carefully indicated. Although governing parameters, particularly Weber Number (We) and Ohnesorge number (Oh), are commonly used to indicate the transition point between different breakup regimes, the boundaries between these regimes are not obvious.

Different secondary breakup models are based on certain assumptions and different approaches, accordingly for different problems and conditions one model can reflects more accurate results than other models. The problem of the current work includes the breakup of water injected at co/cross airflow with velocity lag. Air is assumed to be at atmospheric pressure (100 kPa) and at room temperature (25°C).

Before carrying out the optimization procedures, the adequate secondary breakup model with best accuracy must be selected among the five models discussed in chapter two. Those five models are: Reitz & Diwakar Breakup model [9], Taylor Analogy Breakup (TAB) model [8], Taylor Analogy Breakup (ETAB) model [36] , Cascade Atomization and Breakup Models (CAB), and Schmehl Breakup model in 2002 [38].

To be able to select the appropriate model for the mentioned above conditions, the performance of those models must be compared to experimental data that were collected based on studies with similar conditions. Therefore the performance of these models was investigated against experimental data of studies were performed to

investigate the spray characteristics, mainly droplet size, of water sprays injected to air. Three cases were compared:

- Water jet injected into still air. Based on a study carried out by Paolo E. Santagelo [22].
- Water jet injected into cross-flow air. Based on a study carried out by David Sedarsky [23].
- Water jet injected into co-flow air. Based on two studies one carried out by Hai-Feng Liu [24], and the other study by Christopher M. Varga [49].

The mentioned above studies cover the conditions of the current work. After checking the reliability of the investigated models, the most accurate model can selected and range of errors analysis can be performed.

It is important to declare that reliability of breakup models model investigated in this work is based on the current problem conditions and not necessarily to reflect similar results for other problem with different conditions, such as combustion, where the injected liquid is fuel and the continuous medium is at high pressure.

3.1. Case A: Water jet injected into still air

The experimental data used for this task is the study carried out by Paolo E. Santagelo [22], in summary this paper study the effect of high pressure water jet in still air. The nozzle operative pressure values used in this study are 6, 7, and 8 MPa, the nozzle used in this study has diameter d_i of 0.5mm and it produces a solid cone spray. The reported results in this paper are the droplet size (SMD) and the dispersion.

3.1.1. Experimental setup

The experimental facility used in this paper is presented in Figure 3.1 The nozzle has been placed at 2 m height from the floor, PIV system with Malvern Spraytec Particle Sizer were used as data collection techniques. Nozzle type is (CJX 1140 B1SG manufactured by PNR Italia S.r.l.) with $d_i = 0.5mm$, as shown the data of droplet size were collected at a distance of 1 m from the nozzle orifice.

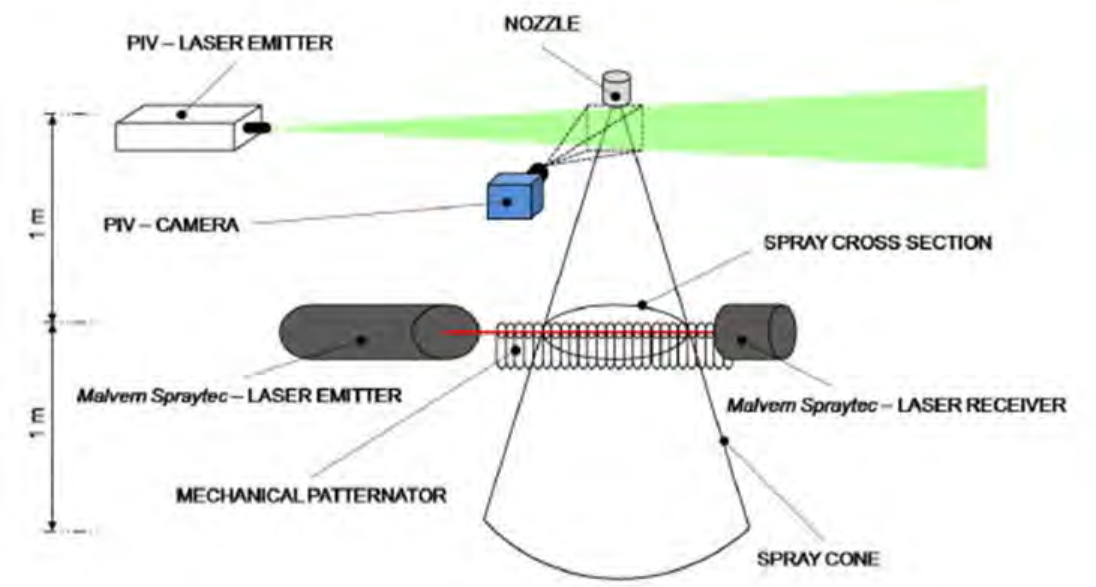

Figure 3. 1, Experimental facility of Paolo E. Santagelo study [22]

3.1.2. Computational Setup

CFD simulations were performed using ANSYS CFX, the geometry of the domain was set as a cylinder with a diameter of 1.5m and 1.2m length. The injection point was placed at the center of the cylinder a distance of 0.2m from the air inlet boundary. Mesh used in this simulation was 3D mesh with approximately 200000 total numbers of elements, with this number of elements results are mesh-independent.

Working fluids were assumed at 25℃ and the airflow at 100 kPa, the flow assumed to be turbulent and k-Epsilon method is used to characterize the turbulence effect. All boundaries were set to open boundary conditions. Droplet size, SMD, data were collected at the outlet boundary.

Three cases were analyzed in this study, the conditions of each case are summarized in Table 3.1.

Table 3. 1, Inputs to computational setup

Case number	Operative Pressure (MPa)	Half-Cone Angle (Degree)	Initial Velocity magnitude (m/s)
1	6	33.1	109.5
2	7	30.4	118.32
3	8	30.6	126.49

3.1.3. Results and discussions

The experimental result of SMD reported in Paolo E. Santagelo [22] study and the CFD simulation results of breakup models are presented in Figure 3.2. The tendency of experimental results and breakup models goes in the direction of decreasing droplet diameter, SMD, with the increase of operative pressure, this is because as the liquid injection pressure P_i increases the velocity lag between the dispersed water particles and the continuous medium increases, resulting in greater aerodynamic forces acting on the droplet surface and further distortion takes place.

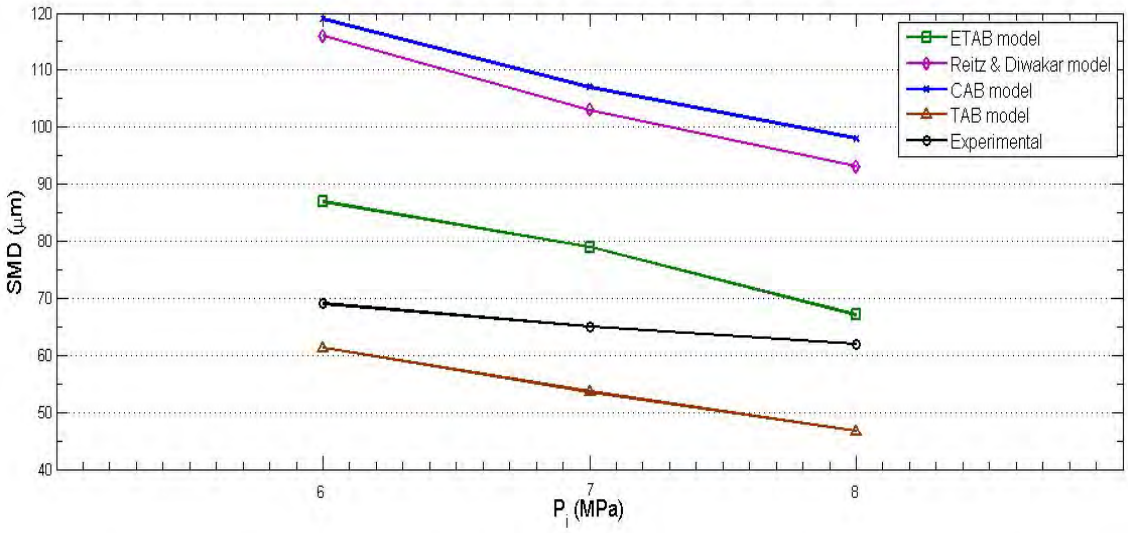

Figure 3. 2, Operative pressure vs. SMD for experimental results of Paolo E. Santagelo [22] study and breakup models

four of breakup models showed the same tendency in the direction of decreasing droplet size with increasing operative pressure, however as clearly shown

that TAB model and ETAB model show good agreement with the experimental results. TAB model tends to underestimate the droplet size and this proofs the statement mentioned in chapter 2 that TAB model tends to underestimate spray characteristics. ETAB model overestimated the droplet size slightly while Reitz & Diwakar and CAB models tend to greatly overestimate droplet size. Schmehl breakup model showed odd tendency for SMD, results of this model were not plotted.

Results shown in Figure 3.2 for breakup models are based on data collected at the outlet boundary of the computational domain, which is at an axial distance of 1 m from injection point to enable comparison with the experimental data which were collected at the same distance.

To enable a clear presentation of breakup models performance, Tables 3.2-6 show the variation of droplet mean particle diameter as it travels toward the outlet boundary. From the scope of the results obtained for case A, Reitz & Diwakar models tend to exaggerate other spray characteristics too, As shown in Table 3.2, time it takes droplet to reach it is final size for this model is highest among the investigated models, hence this model tends to overestimate penetration length, nevertheless it tends to overestimate cone angle also.

Contrary, TAB model tends to underestimate spray characteristics, particularly penetration length, as Table 3.3 presents droplet reach its final size at extremely short time, also it shows the lowest cone angle among the investigated models.

ETAB model tends to give moderate estimation of other spray characteristics, however there are not experimental data to judge its performance in term of penetration depth and cone angle. CAB model shows fair results for penetration depth and cone angle comparing to other breakup models. Schemhl model presented odd results for SMD, with 36.1, 84.3, and 32$\boldsymbol{\mu m}$ for $\boldsymbol{p_i}$ of 6, 7, and 8 MPa respectively.

Table 3. 2, Case A: Droplet Mean Particle Diameter variation as droplets travels towards outlet boundary vs. Operative Pressure, Results based on Reitz & Diwakar model

Reitz & Diwakar model		
Pressure (MPa)	SIDE VIEW	ISO. VIEW
6	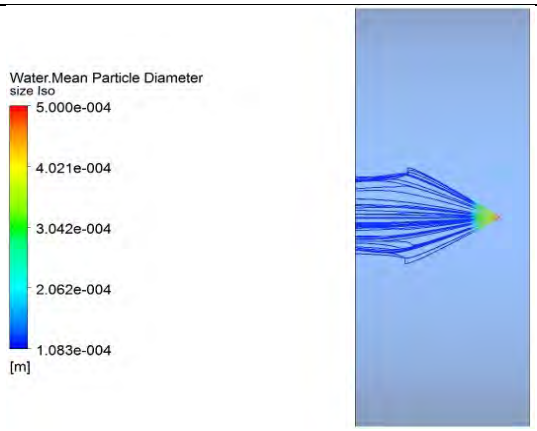	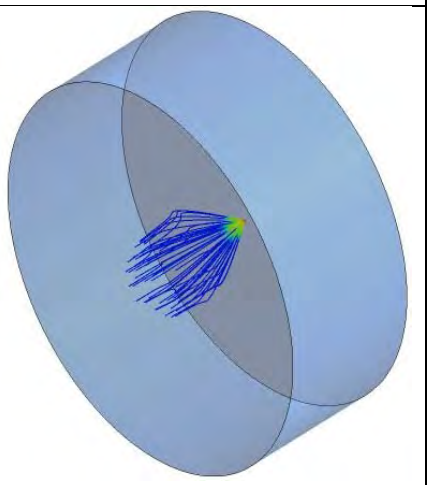
7	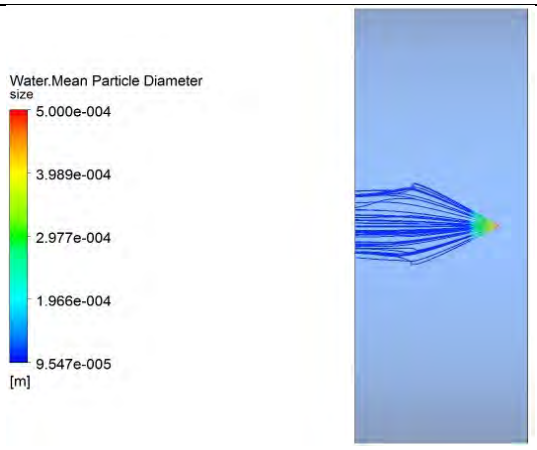	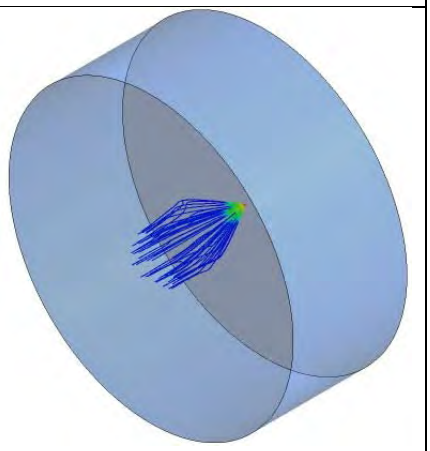
8	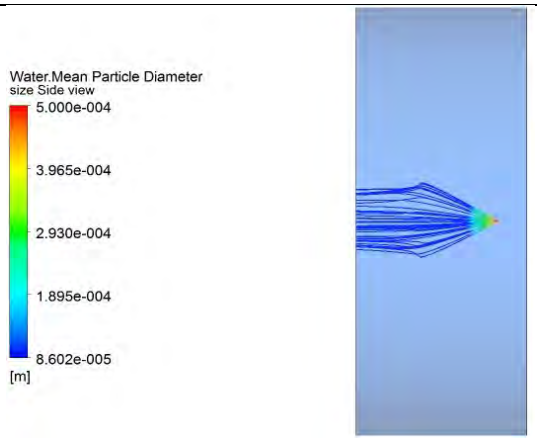	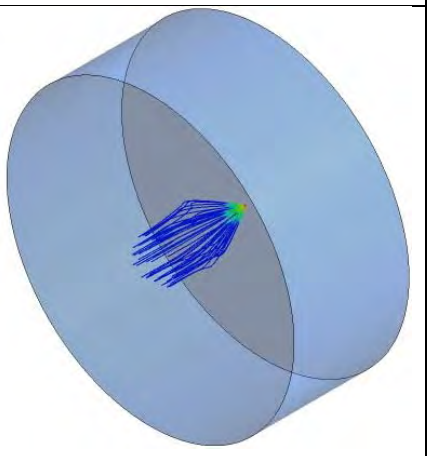

Table 3. 3, Case A: Droplet Mean Particle Diameter variation as droplets travels towards outlet boundary vs. Operative Pressure, Results based on TAB model

TAB model		
Pressure (MPa)	SIDE VIEW	ISO. VIEW
6	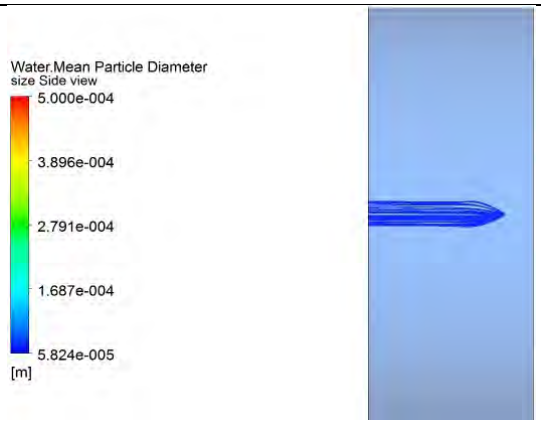	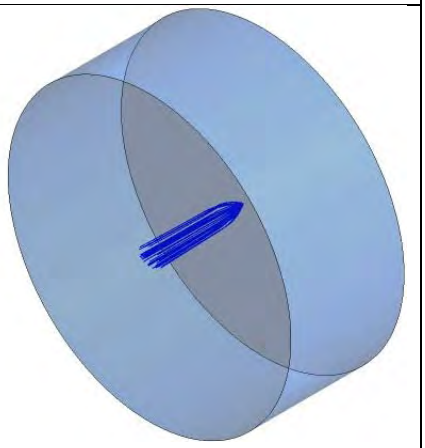
7	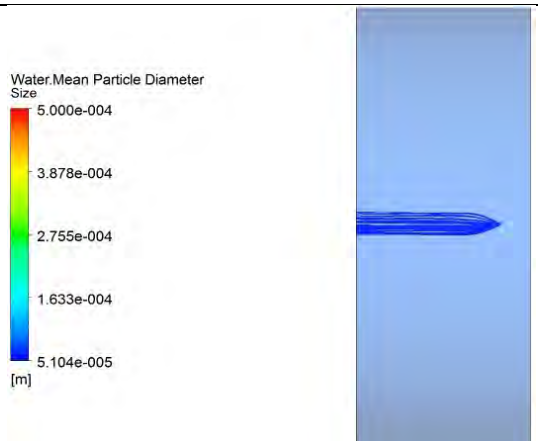	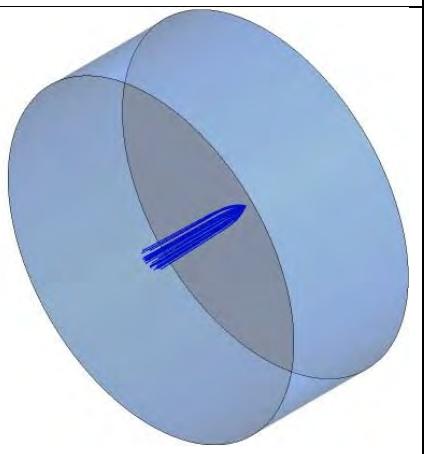
8	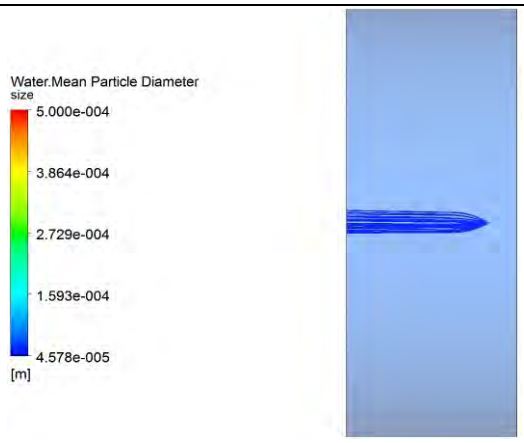	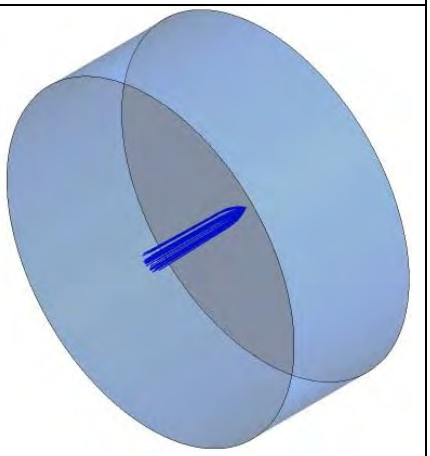

Table 3. 4, Case A: Droplet Mean Particle Diameter variation as droplets travels towards outlet boundary vs. Operative Pressure, Results based on ETAB model

ETAB model		
Pressure (MPa)	SIDE VIEW	ISO. VIEW
6	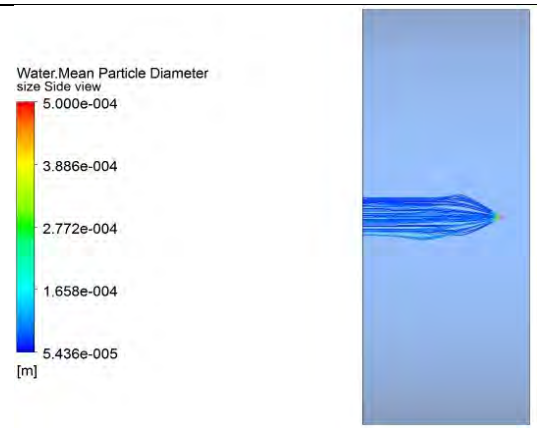	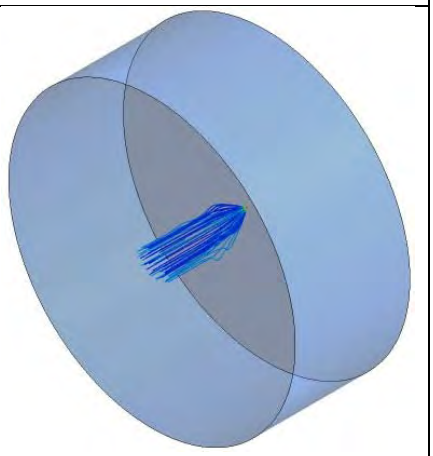
7	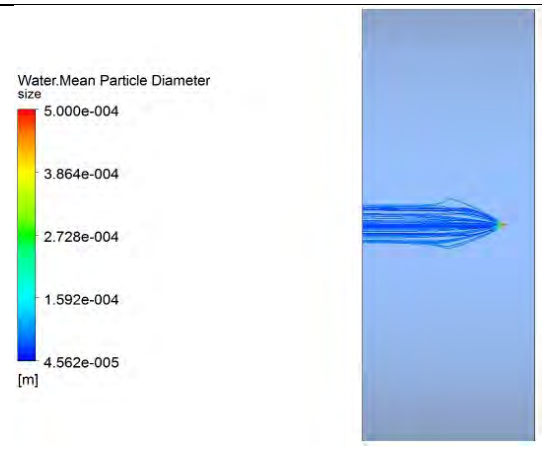	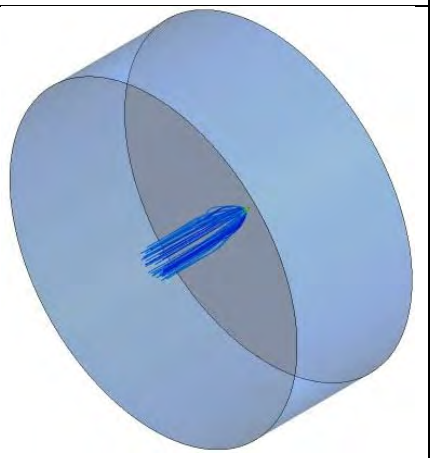
8	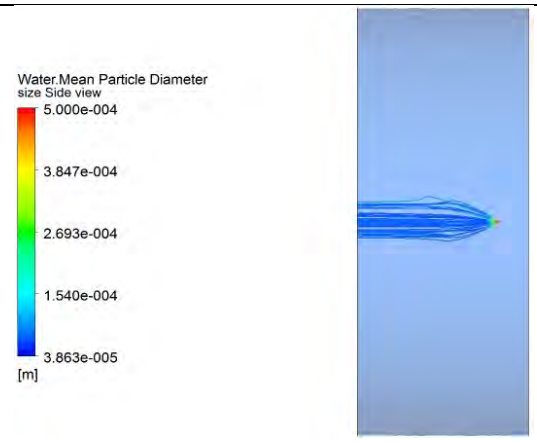	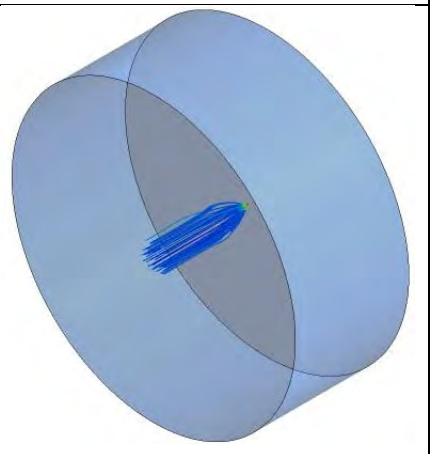

Table 3. 5, Case A: Droplet Mean Particle Diameter variation as droplets travels towards outlet boundary vs. Operative Pressure, Results based on CAB model

CAB model		
Pressure (MPa)	SIDE VIEW	ISO. VIEW
6	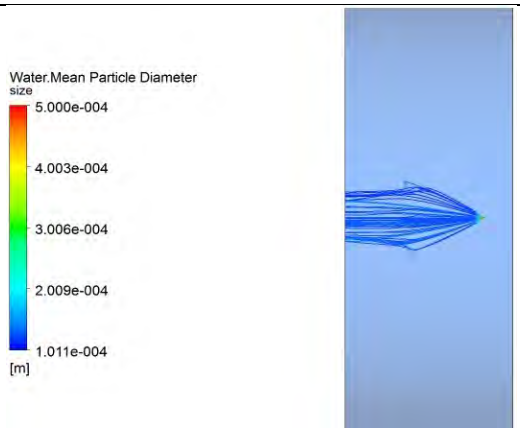	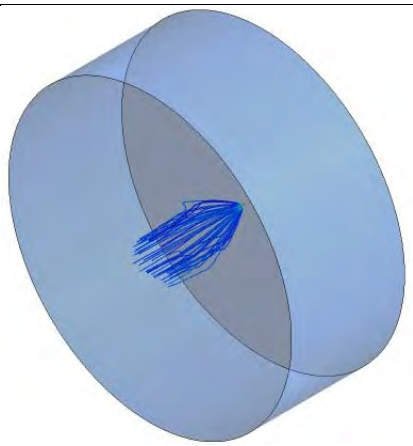
7	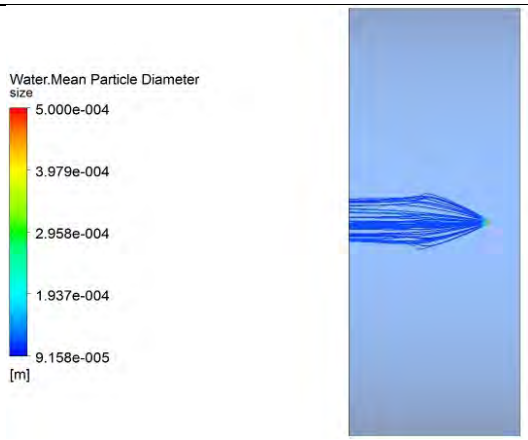	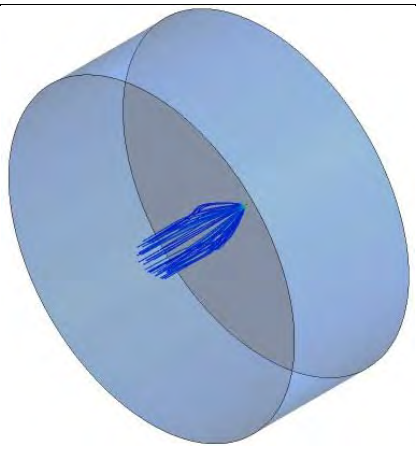
8	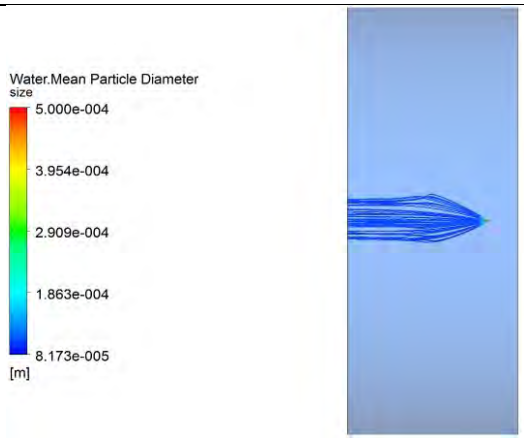	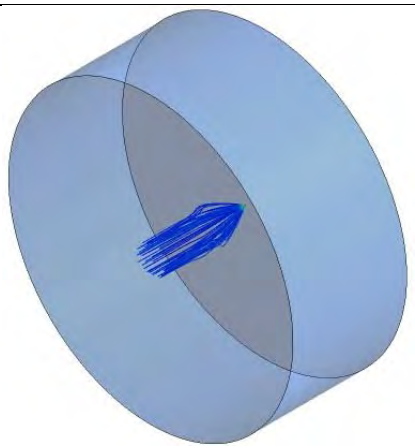

Table 3. 6, Case A: Droplet Mean Particle Diameter variation as droplets travels towards outlet boundary vs. Operative Pressure, Results based on Schmehl model

Schmehl model		
Pressure (MPa)	SIDE VIEW	ISO. VIEW
6	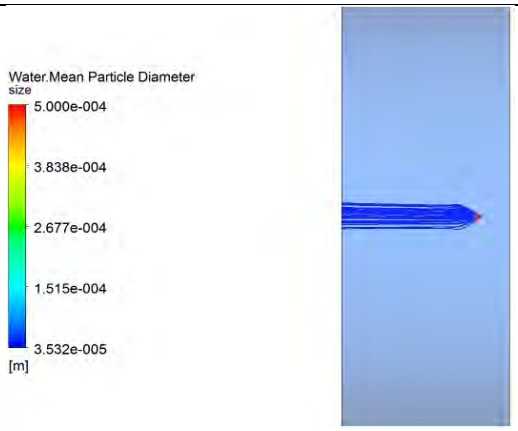	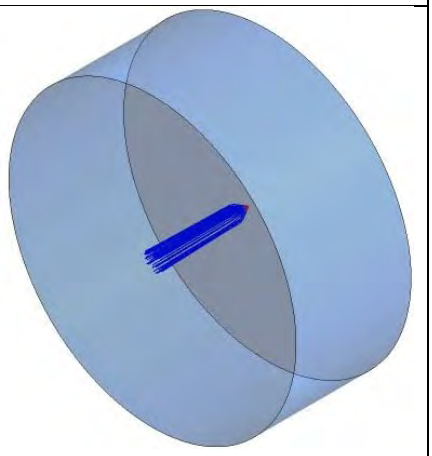
7	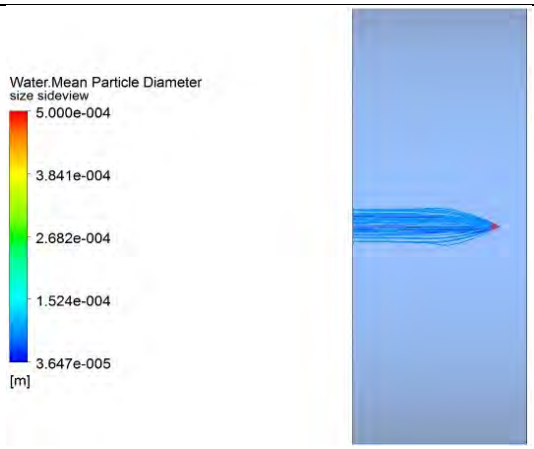	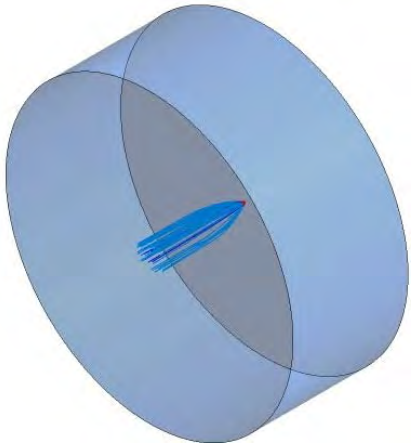
8	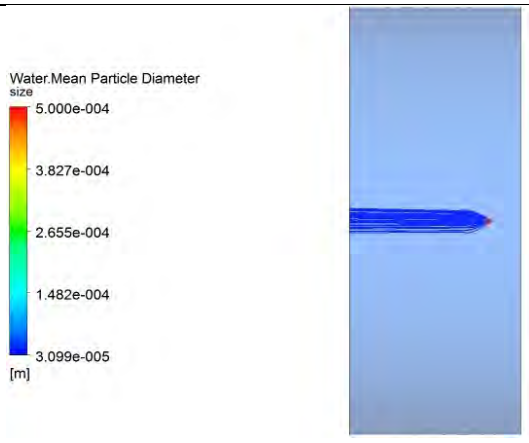	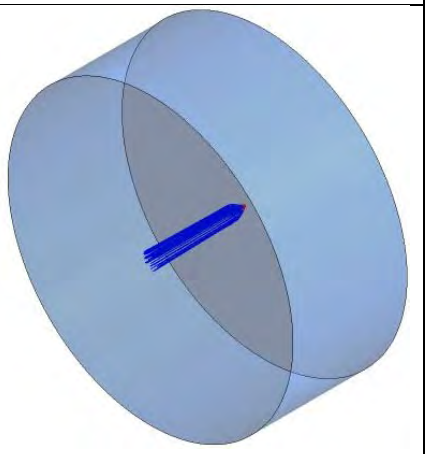

3.1.4. Errors analysis

Two sources of errors are expected for case A, the first source of errors comes from collecting data experimentally, and the second source of errors is obviously computational error. Malvern Spraytec Particle Sizer used to measure droplet size experimentally in this study is claimed to have range of inaccuracy lower than 1% for range of particle size 0.1-2000μm [22].

Absolute relative error of investigated breakup models in estimating SMD is reported in Figure 3.3 for the applied values of operative pressure. As clearly shown ETAB has the lowest absolute relative error with range of 3-26%, next comes TAB model with range of 11-32%, then Schmehl model with range of 48-54%, finally Reitz & Diwakar model and CAB models with ranges of 35-68% and 42-72% respectively.

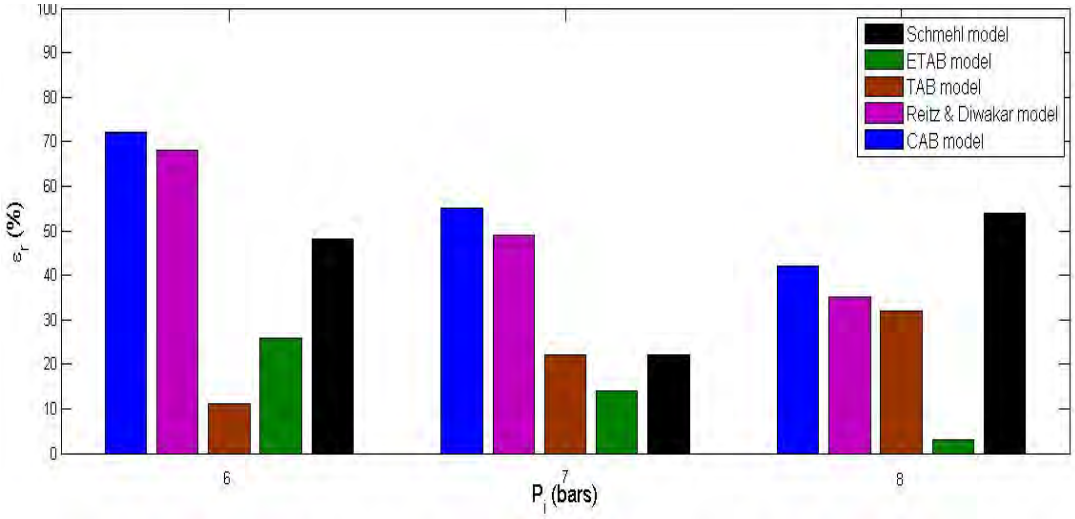

Figure 3. 3, Absolute relative error of breakup models in estimating SMD for Case A

To enable clearer approximation of each model error magnitude, an average value of absolute relative error for each model is summarized in Table 3.7 in ascending order.

Table 3. 7, Average absolute relative error of breakup models for Case A

Model	Average $\lvert\varepsilon_r\rvert$
ETAB model	14%
TAB model	22%
Schmehl model	41%
Reitz & Diwakar model	51%
CAB model	57%

3.2. Case B: Water jet injected into cross-flow air

The experimental data used in this case were reported for a study carried out by David Sedarsky [23]. A variety of Weber numbers, $21 \geq We \geq 122$ and momentum flux ratios, $37 \geq q \geq 153$ were investigated, the study analyzed the effect of air velocity, water velocity, and nozzle diameter on SMD. The reported results of this study are the characteristic droplet diameter, SMD, and the penetration length. The operative parameters for this study are presented in Table 3.8

Table 3. 8, [23], Operative parameters for David Sedarsky study

We	Case	d_i (mm)	U_i (m/s)	U_g (m/s)	Re_i	q
21	9	0.5	10.4	48	5.18×10^6	37
21	2	0.5	21	48	1.05×10^7	153
29	4	0.7	21	48	1.46×10^7	153
34	8	0.5	13.5	62	6.72×10^6	38
40	7	0.5	15	67	7.47×10^6	40
41	6	1	21	48	2.09×10^7	153
49	1	0.5	21	74	1.05×10^7	64
68	3	0.7	21	74	1.46×10^7	64
98	5	1	21	74	2.09×10^7	64
122	10	1.25	21	74	2.61×10^7	64

3.2.1. Experimental Setup

Figure 3.4 below presents the experimental facility used for this study. As it is shown injector is held perpendicular to the upper surface of the wind tunnel and its orifice kept level with the channel wall. Honeycomb is mounted at the entrance of wind tunnel to reduce any turbulent effects produced by the fan.

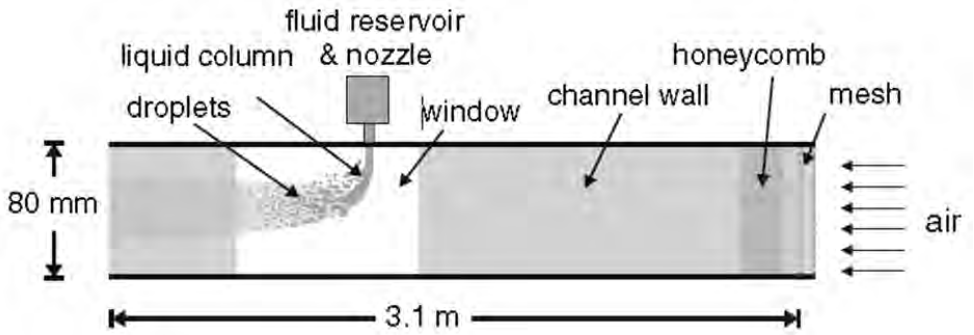

Figure 3. 4. [23], Experimental facility of David Sedarsky study

Nozzle design is represented in Figure 3.5; it has four interchangeable nozzle tips of varying exit diameter: 0.5, 0.7,1 and 1.25mm. The length to width ratio is 4 to get good flow distribution. Three optical techniques where used to characterize breakup processes: Particle Imaging Velocimetry, High-Speed Shadowgraph, and Ballistic Imaging.

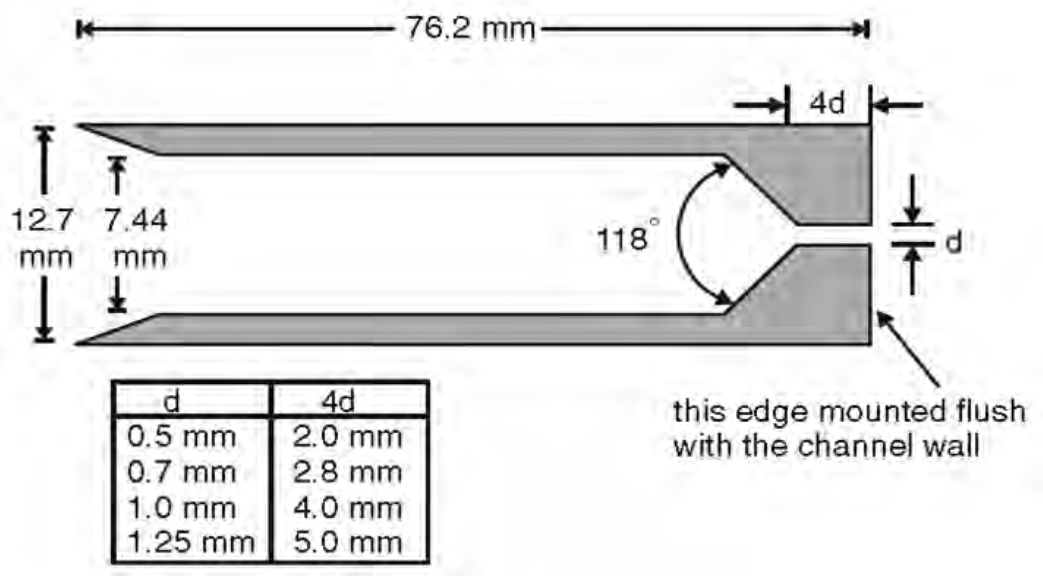

d	4d
0.5 mm	2.0 mm
0.7 mm	2.8 mm
1.0 mm	4.0 mm
1.25 mm	5.0 mm

Figure 3. 5. [23], Schematic of nozzle used in David Sedarsky study

3.2.2. Computational Setup

CFD simulations were performed using ANSYS 12.0 CFX package, the geometry of the computational domain was set identical to the test section geometry used in this work (Figure 3.4). The injection point was centered at upper boundary of the test section. Mesh used in this simulation was 3D mesh with approximately 300000 total numbers of elements, point spacing control around the injection point

was used with radius of influence equal to 20mm and expansion factor of 1.2, with this number of elements the results are mesh-independent.

Working fluids were assumed at 25℃ and the airflow at 100 kPa, the flow assumed to be turbulent and k-Epsilon method is used to characterize the turbulence effect. Boundary conditions for the sides of the test section were set to wall boundary condition type. Inputs for computational setup for all cases are listed in Table 3.8 above.

3.2.3. Results and discussions

Table 3.9 presents the reported experimental results [23] for SMD and results obtained from breakup models. Experimental data presented in Table 3.9 collected in the primary breakup region, however comparison with breakup models is possible since the breakup takes place in the initial zone near injector. Yet results reported of breakup models are collected in the initial region and any secondary breakup takes place downstream is not considered.

Table 3. 9, SMD for the different cases reported from David Sedarsky study compared to breakup models results

Case	We	q	SMD ($\boldsymbol{\mu m}$)					
			Exp.	TAB	Schemhl	ETAB	CAB	Reitz
9	21	37	160	173	158	181	385	343
2	21	153	292	181	156	331	441	379
4	29	153	272	180	191	297	353	313
8	34	38	179	146	144	199	312	259
7	40	40	165	133	138	116	286	229
6	41	153	357	273	248	356	480	382
1	49	64	289	116	117	260	227	179
3	68	64	222	105	149	257	202	188
5	98	64	217	157	71.2	242	285	239
10	122	64	150	109	69	123	324	247

Again ETAB model showed the best accuracy in estimating SMD for most of cases. Also for this case Schmehl model presented good accuracy for some of the cases. TAB model underestimates SMD values for most of the cases. Reitz & Diwakar and CAB models tend to overestimate droplet size for this case also. Since the experimental study focus on characterizing breakup regimes and the primary zone

is considered only, reporting the variation of droplet size for all cases is not significant., however one case is presented in Table 3.10 to enable a clear presentation of the performance of the different models. Table 3.10, present the breakup process and variation of droplet mean particle diameter as water particles travel away from injector for case 9. Experimentally the penetration length was reported to be 9mm. ETAB model showed the best accuracy penetration depth with 7mm, TAB model underestimated it with 3.4mm was measured for penetration depth. All other models overestimated the penetration depth.

Table 3. 10, Droplet mean particle diameter variation based on the investigated secondary breakup models for Case B

Case 9		
Model	SIDE VIEW	ISO. VIEW
Reitz & Diwakar	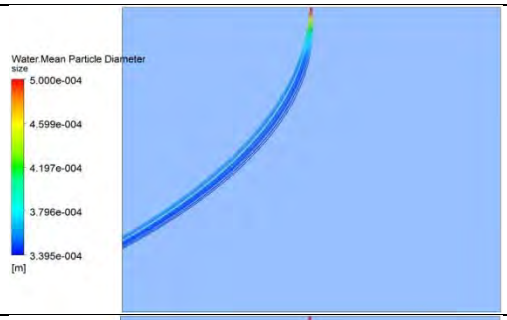	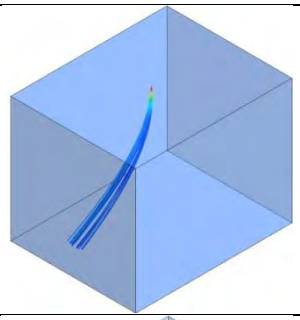
CAB	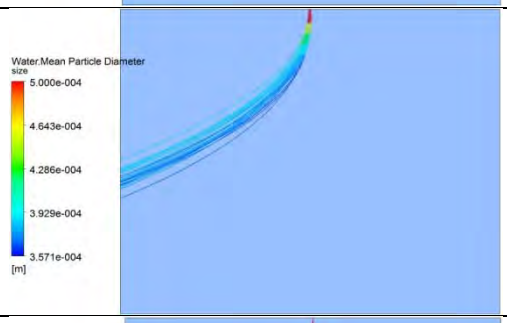	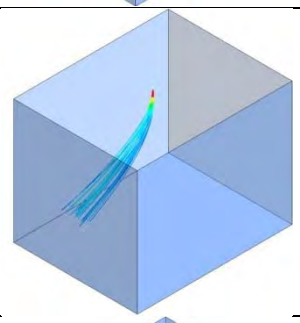
ETAB	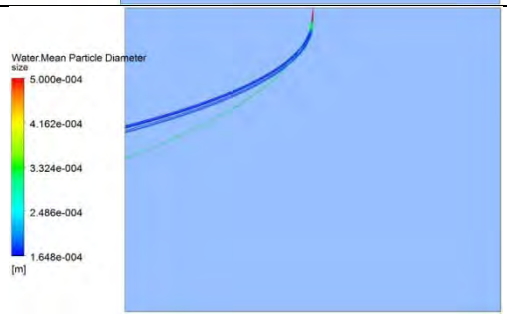	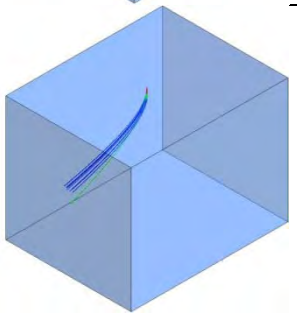
TAB	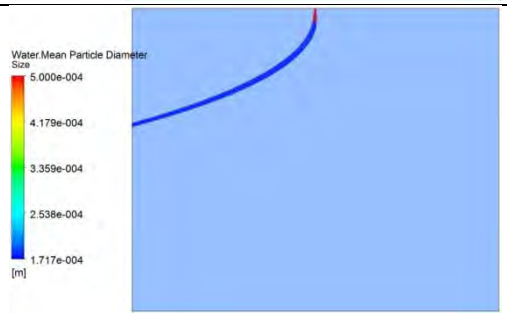	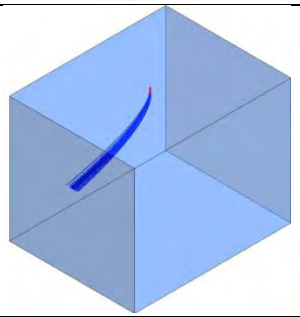
Schmehl	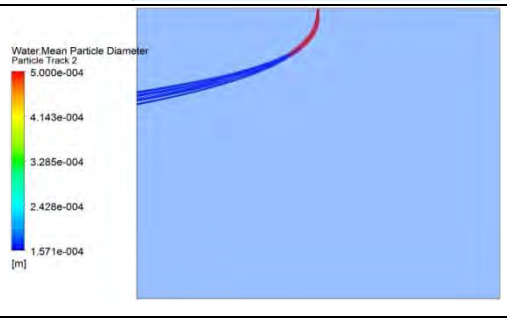	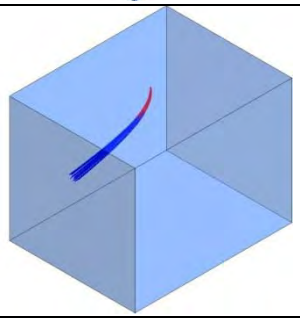

3.2.4. Error analysis

Regarding experimental results Sedarky [23] claimed that only droplet sizes less than $20\mu m$ in the wake of liquid column are not detected. As presented in Table 3.9, SMD are in the order of $200\mu m$ which is greater that the cutoff value, accordingly results should be very accurate.

Absolute relative error of investigated breakup models in estimating SMD is reported in Figure 3.3 for case B. ETAB has the lowest absolute relative error with range of 0.1-18% and only case 6 showed higher error of 30%, TAB model has a range of 8-60%, Schmehl model with range of 1-67%, Reitz & Diwakar model and CAB models with range of 7-114% and CAB mode with range of 9-141%.

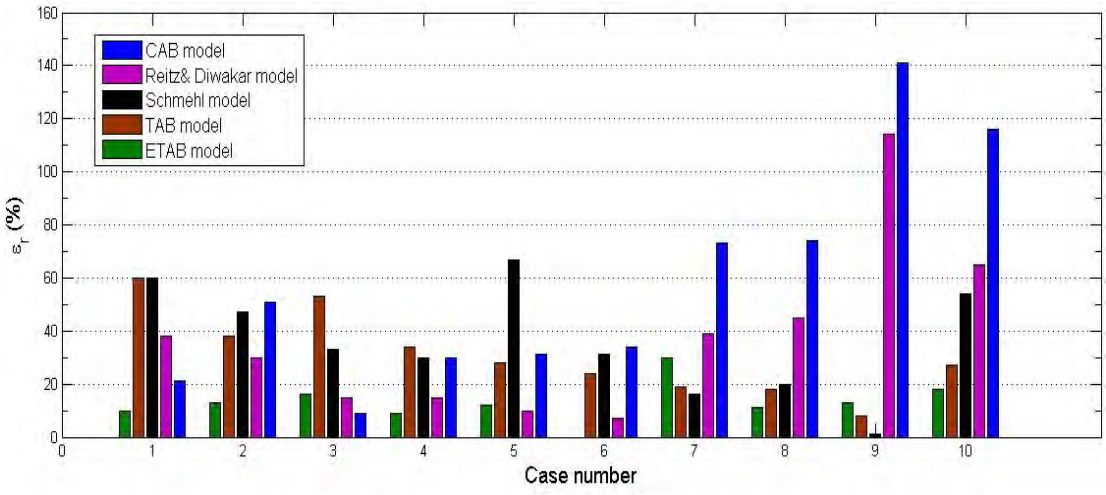

Figure 3. 6, Absolute relative error of breakup models in estimating SMD for Case B

Since the number of cases for this study is high the order of each model in term of accuracy is not obvious, to get a clear presentation of the accuracy of each model, an average value of absolute error is calculated and reported in Table 3.11, the order of breakup models is ascending in term of accuracy, ETAB model shows the best accuracy with 13% average relative error, followed by TAB model with 31%, Schmehl comes next with 36%, Reitz & Diwakar with 38%, and finally CAB model with 58%.

Table 3. 11, Average absolute relative error of breakup models

Model	Average $\|\boldsymbol{\varepsilon_r}\|$
ETAB model	13%
TAB model	31%
Schmehl model	36%
Reitz & Diwakar model	38%
CAB model	58%

3.3. Case C: Water jet injected into co-flow air

For case C two studies were investigated, one study was used to investigate the performance of breakup models in detecting the droplet size when water is injected in parallel direction to air, this study was carried out by Liu [24]. The second study used to investigate the performance of breakup model to characterize the change of water droplets velocity as it travels away from nozzle orifice, this study was carried out by M. Varga [49].

3.3.1. Case C.1: Droplet size estimation

The experimental data used in this case were reported for a study carried out by Liu [24]. In this study the effect of water jet diameter is investigated for co-axial airblast atomizer. Rage of water to air flux ratio of $0.137 < m < 15.6$. The reported results are SMD values for the mentioned range of water to air mass flux [24].

3.3.1.1. Experimental setup

Figure 3.7 presents a schematic of the airblast atomizer and the geometry of the set used in this study. Range of water injection diameter was used $d_l = \{2.00, 3.10, 5.00, 9.02, 16.98\} mm$. Malvern Spraytec Particle Sizer technique was used to measure the droplet size at an axial distance of 680mm away from the orifice.

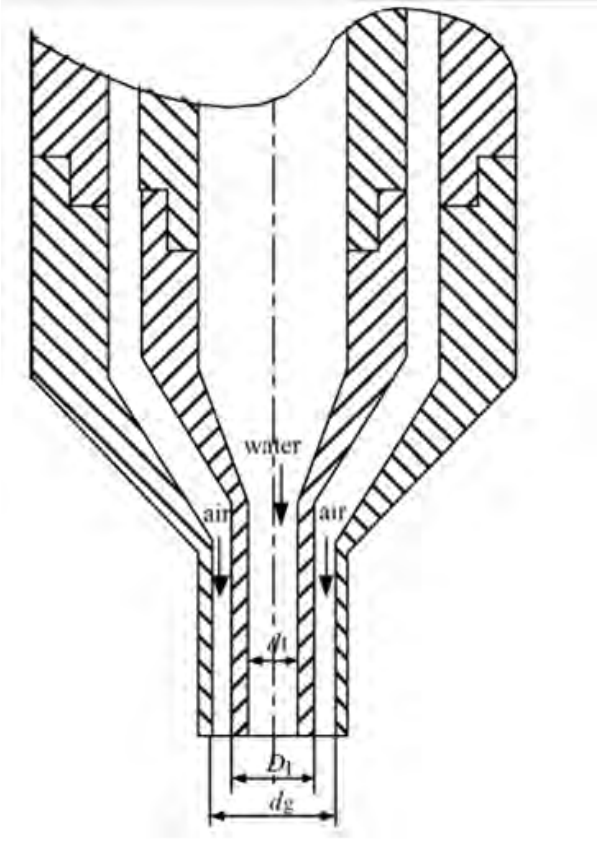

Figure 3. 7. [24], Schematic of Airblast atomizer used in Liu study

3.3.1.2. Computational setup of Case C.1

CFD simulations were performed using ANSYS CFX, the geometry of the domain was set as a cylinder with a diameter of 0.3m and 0.7m length. The injection point was placed at the center of the cylinder a distance of 20mm from the air inlet. Mesh used in this simulation was 3D mesh with approximately 260000 total numbers of elements, with this number of elements results are mesh-independent.

Working fluids were assumed at 25℃ and the airflow at 100 kPa, the flow assumed to be turbulent and k-Epsilon method is used to characterize the turbulence effect. Sides boundary was set to open boundary. Droplet size, SMD, data were collected at the outlet boundary.

3.3.1.3. Results and discussions

Results CFD simulation were performed for single value of water to air mass flux ratio $\boldsymbol{m = 1.64}$, this value falls in the middle of the investigated range in Liu study [24]. Four cases where investigated based on fixed water to air mass flux ratio. Table 3.12 presents these cases.

Table 3. 12, Operative parameters for Case C.1. For the four cases m=1.64

Case number	d_i (mm)	V_i (m/s)	V_a (m/s)
1	2.00	26.25	170
2	3.10	10.93	170
3	5.00	4.20	170
4	9.02	1.29	170

Figures 3.8 and 3.9 present the change of SMD with water injection diameter and water injection velocity respectively in constant water to air mass flux ratio (constant water mass flow rate) for experimental results and results of breakup models. Again for the current Case ETAB model shows a very good accuracy, while TAB model underestimates SMD values. Reitz & Diwakar and CAB models tend to exaggerate values of SMD for this case also. Schemehl model showed odd tendency and its results are not plotted. Variations of droplet size in the computational model are presented in Tables 3.13-17 for the investigated breakup models.

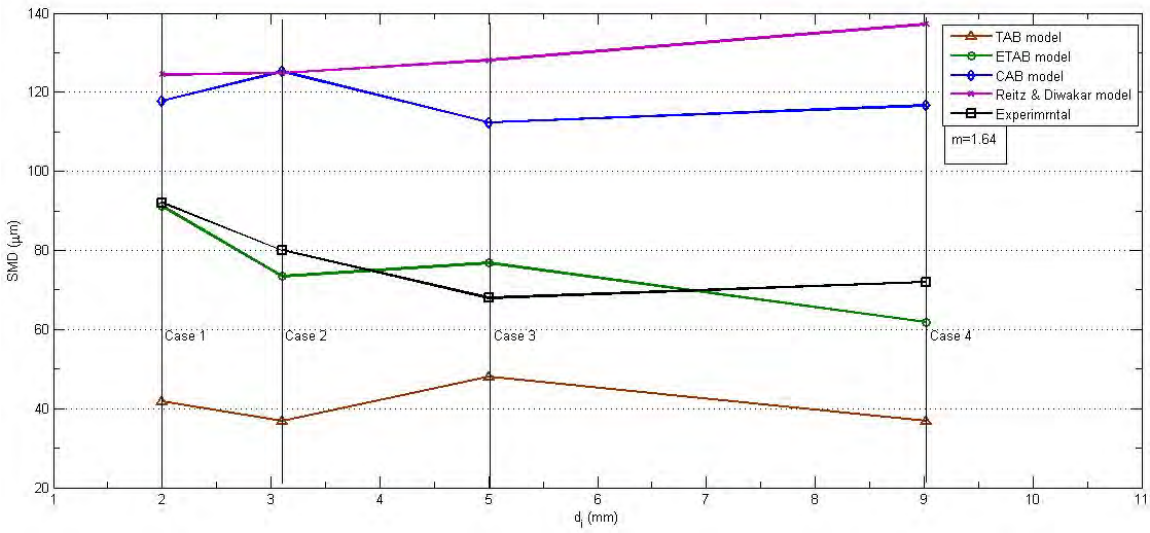

Figure 3. 8, Experimental results of Lui study [24] and breakup models results for SMD vs. water injection diameter constant water to air mass flux

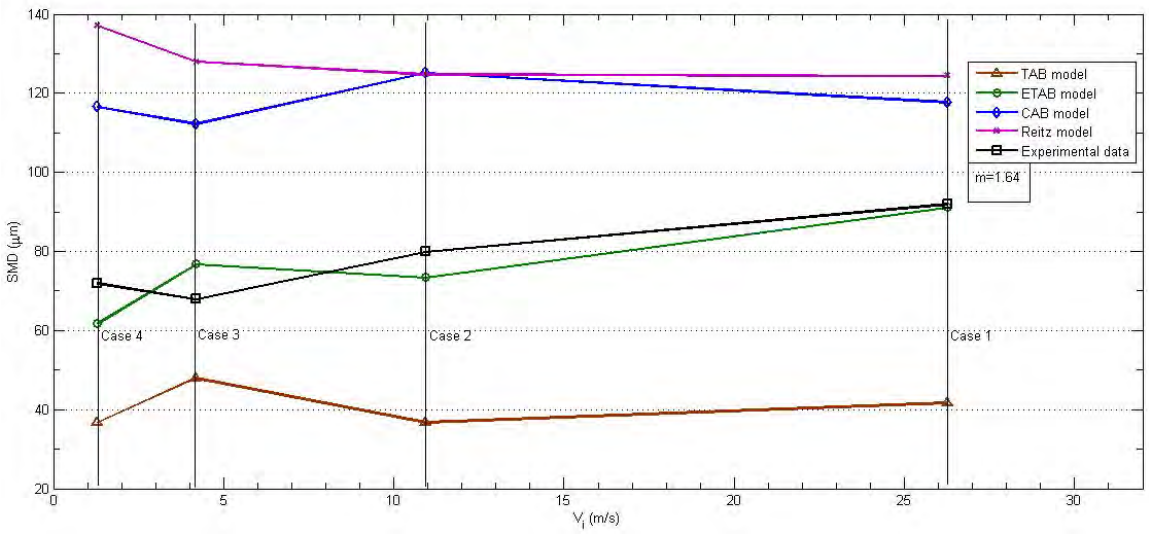

Figure 3. 9, Experimental results of Lui study [24] and breakup models results for SMD vs. water injection diameter constant water to air mass flux

Table 3. 13, Droplet mean diameter variation in the computational domain for Case C.1 based on Reitz & Diwakar model

Reitz & Diwakar model		
Case 1		Case 2
Side. View	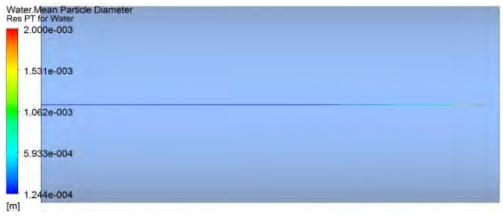	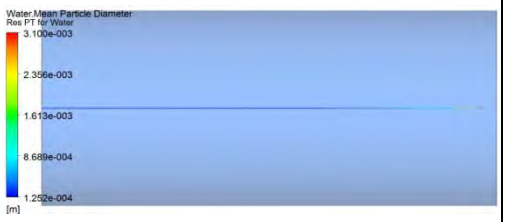
Iso. View	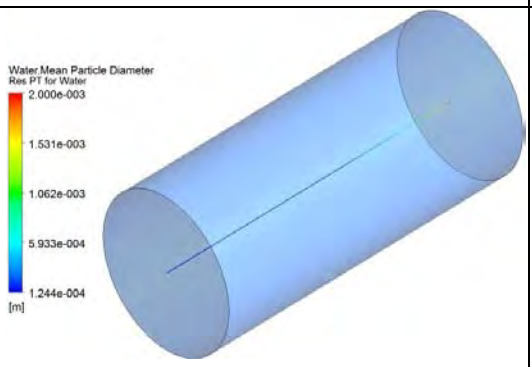	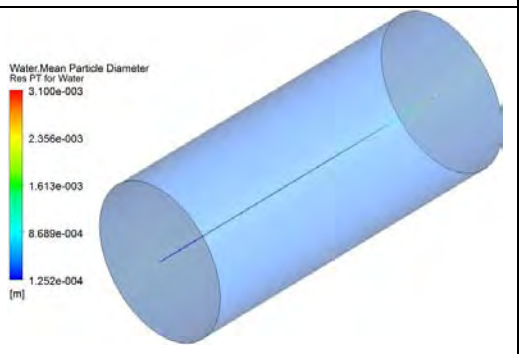
Case 3		Case 4
Side. View		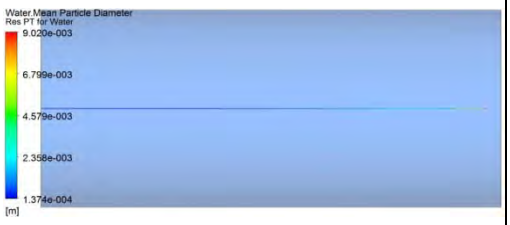
Iso. View	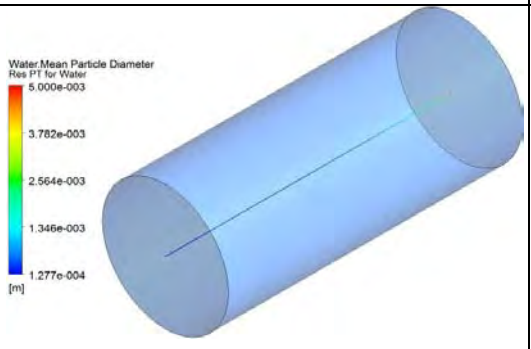	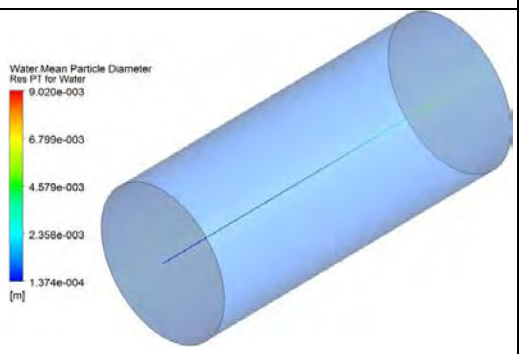

Table 3. 14, Droplet mean diameter variation in the computational domain for Case C.1 based on TAB model

TAB model		
Case 1		Case 2
Side. View	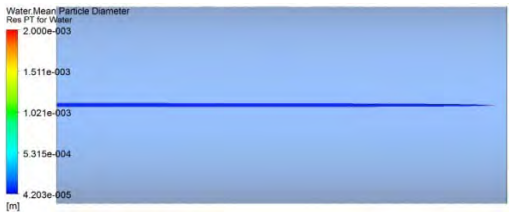	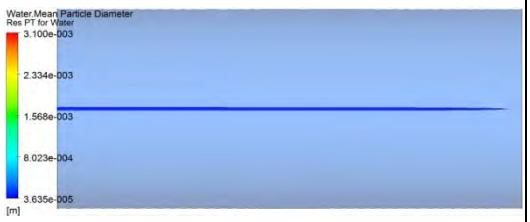
Iso. View	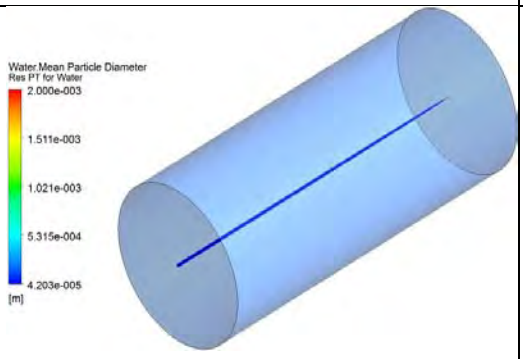	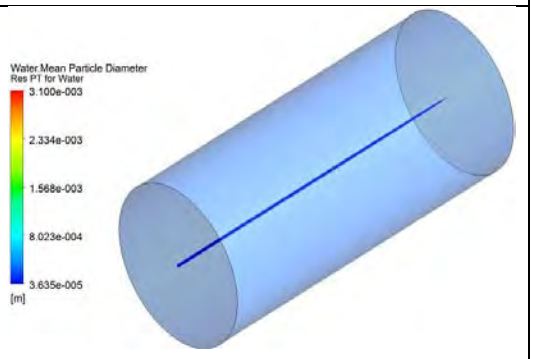
Case 3		Case 4
Side. View	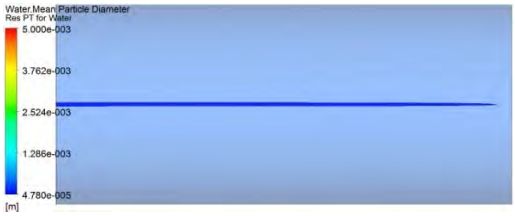	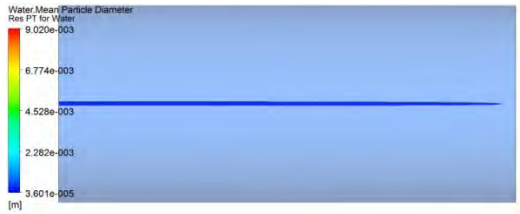
Iso. View	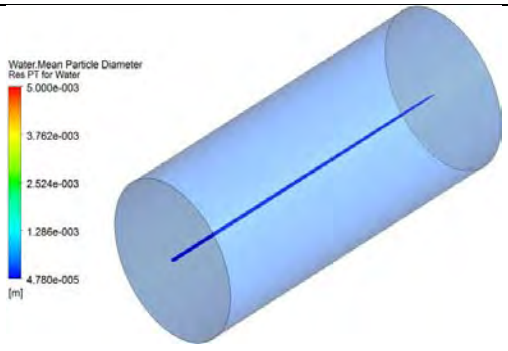	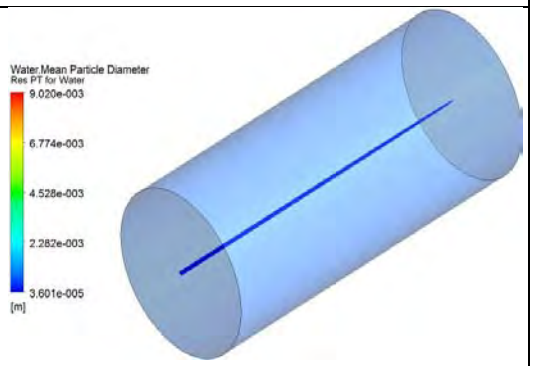

Table 3. 15, Droplet mean diameter variation in the computational domain for Case C.1 based on ETAB model

ETAB model		
Case 1		Case 2
Side. View	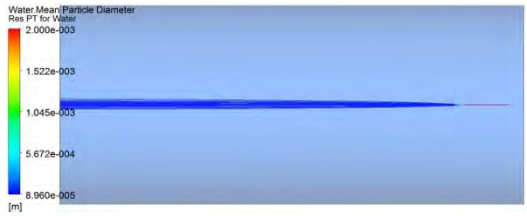	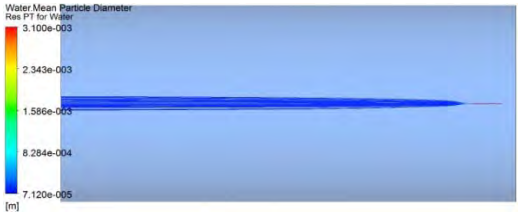
Iso. View	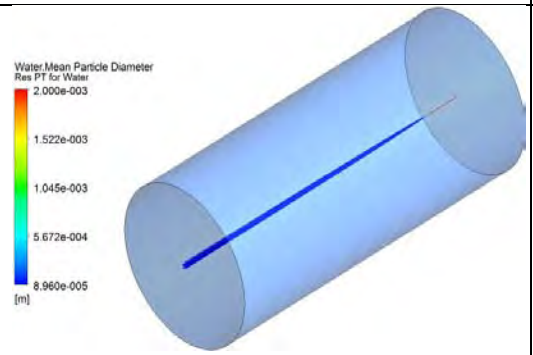	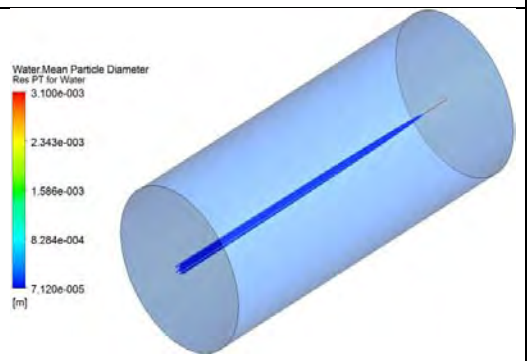
Case 3		Case 4
Side. View	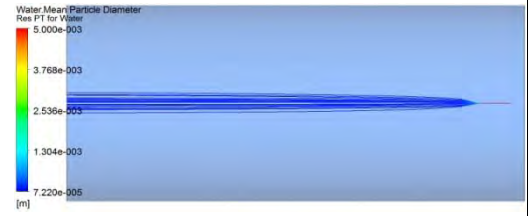	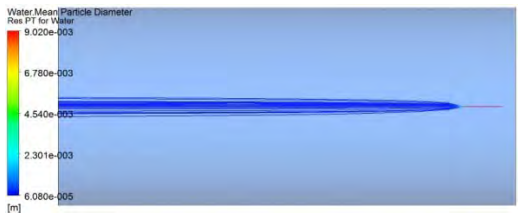
Iso. View	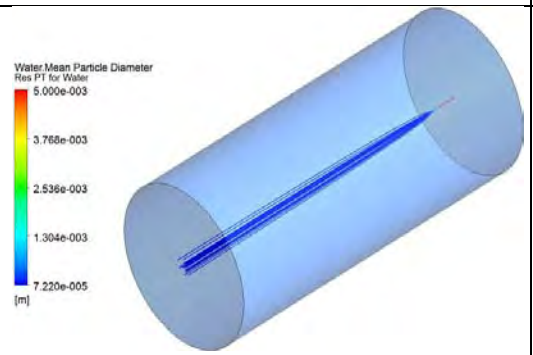	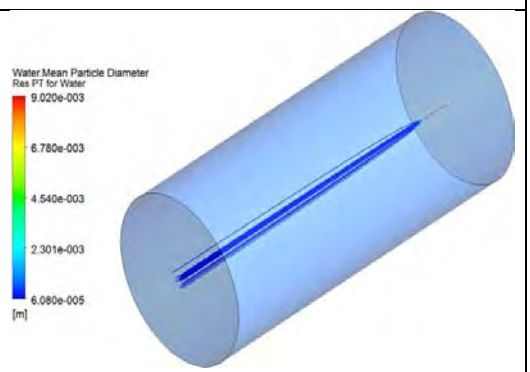

Table 3. 16, Droplet mean diameter variation in the computational domain for Case C.1 based on CAB model

CAB model		
Case 1		Case 2
Side. View	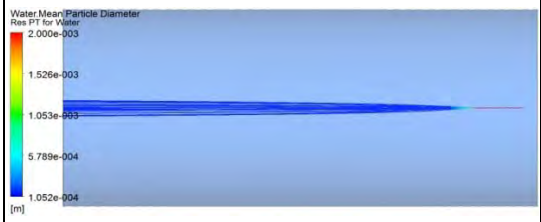	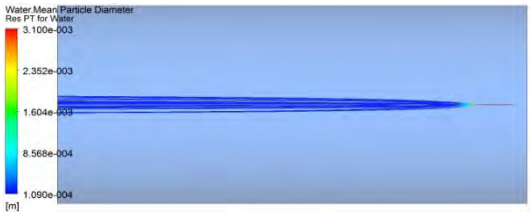
Iso. View	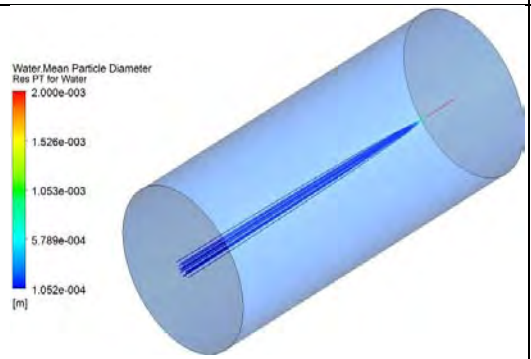	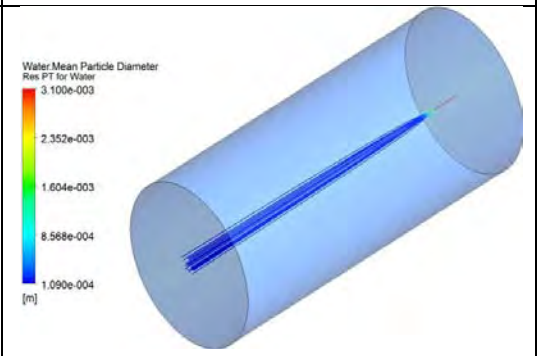
Case 3		Case 4
Side. View	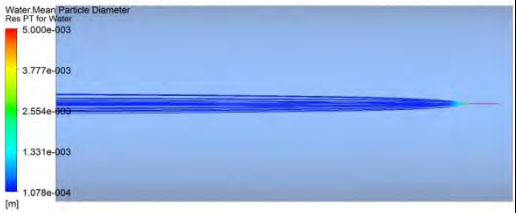	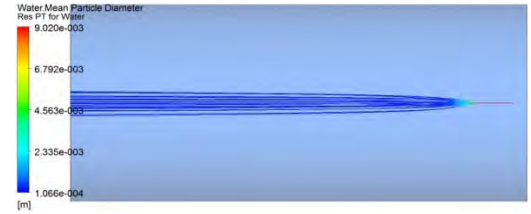
Iso. View	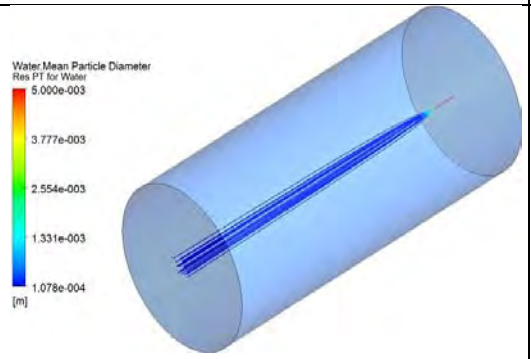	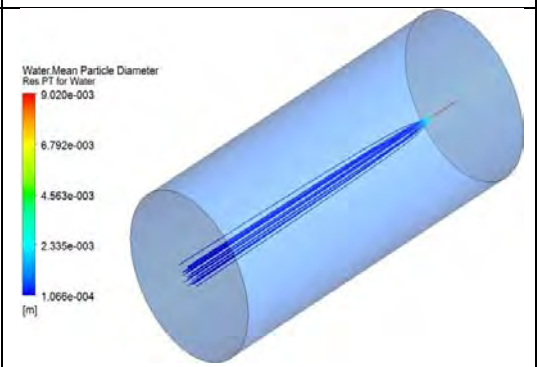

Table 3. 17, Droplet mean diameter variation in the computational domain for Case C.1 based on Schmehl model

Schmehl model		
	Case 1	Case 2
Side. View	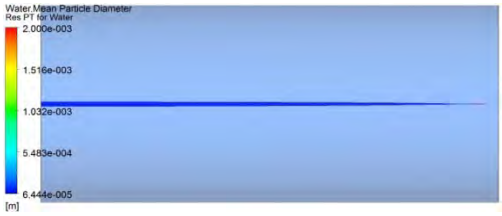	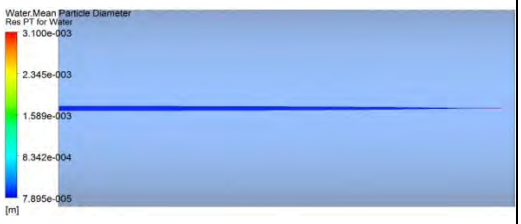
Iso. View	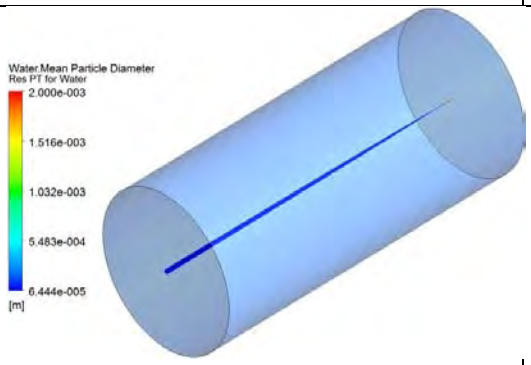	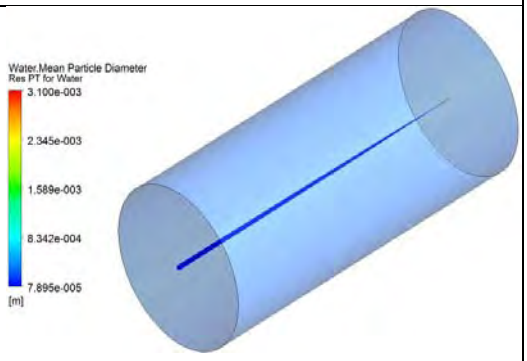
Case 3		Case 4
Side. View	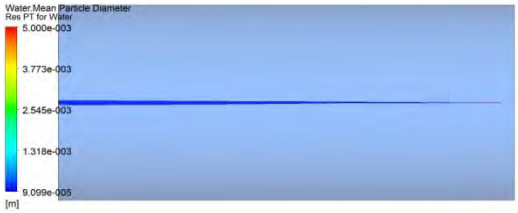	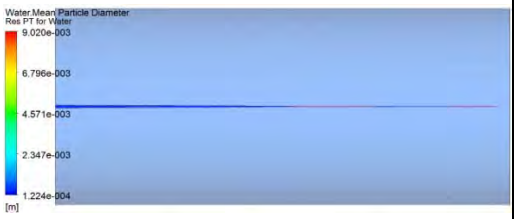
Iso. View	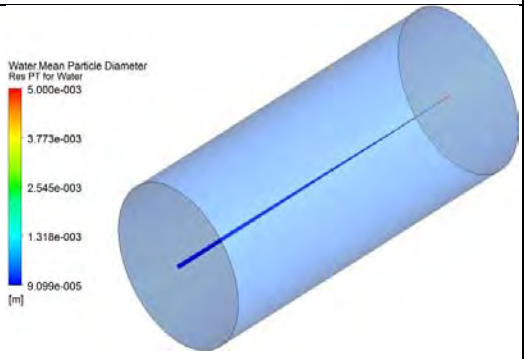	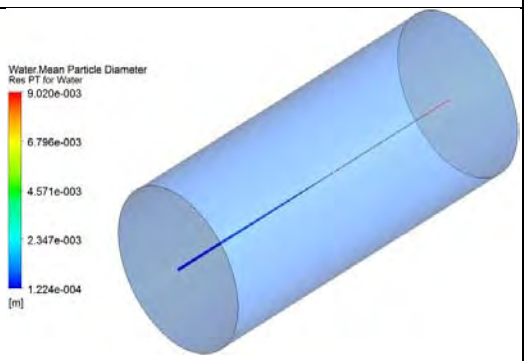

3.3.1.4. Errors analysis

Absolute relative error of investigated breakup models in estimating SMD is reported in Figure 3.10 for case C.1. ETAB presented the lowest absolute relative error with range of 1-33%, TAB model showed a range of 48-60%, Schmehl model showed a range of 10-37%, Reitz & Diwakar model showed a range of 35-49%, and CAB model showed a range of 22-36%.

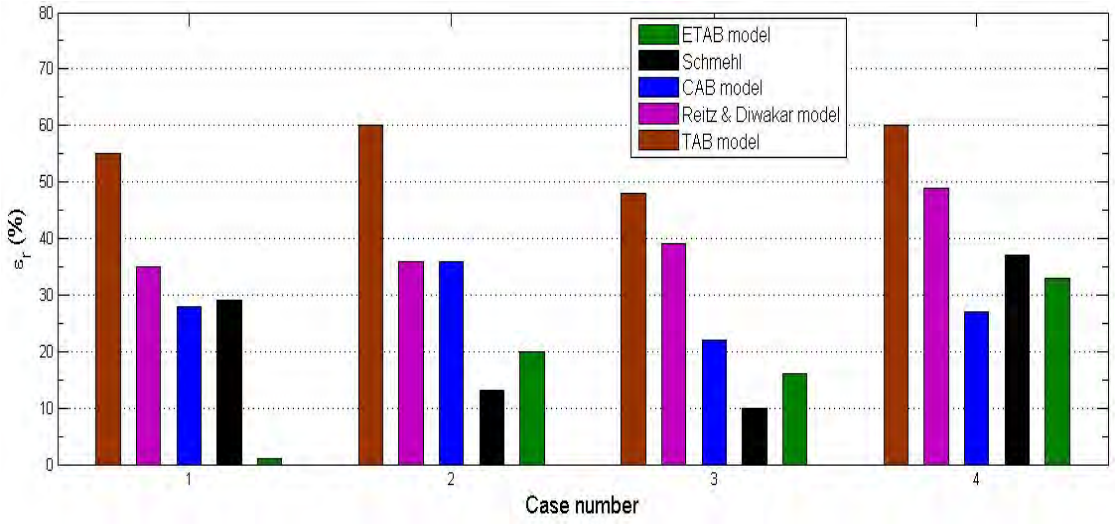

Figure 3. 10, Absolute relative error of breakup models in estimating SMD for Case C.1

Average absolute error for each model is reported in Table 3.18 below in ascending order. ETAB showed the best accuracy with 18% average absolute relative error, followed by Schmehl model with 22%, CAB model comes next with 28%, then Reitz & Diwakar model with 40%, and finally comes TAB model with 56%.

Table 3. 18, average absolute relative error of breakup models for Case C.1

Model	Average $\|\boldsymbol{\varepsilon_r}\|$
ETAB model	18%
Schmehl model	22%
CAB model	28%
Reitz & Diwakar model	40%
TAB model	56%

3.3.2. Case C.2: Droplets velocity variation

Until now all the validation cases were focused on the droplet size only, and no validation cases were performed to investigate the velocity of droplets downstream, although droplet velocity is an important parameter in the current work, this due to the assumption that droplets velocity reaches air velocity downstream the injector orifice after some distance. However, although droplets velocity reaches the continuous medium velocity eventually, it is important to investigate the distance at which droplets velocity reaches airstream velocity. Case C.2 is focused on investigating the behavior of water droplets velocity downstream injector orifice.

Experimental data used in this case were reported for a study carried out by M. Varga [49]. The breakup process of liquid jet in co-axial air flow was investigated in this study

3.3.2.1. Experimental setup

In this study large-area co-axial liquid jet was used, schematic of the nozzle is presented in figure 3.11. A round liquid jet surrounded by airstream, with 11.2 air-water aria ratio which allows for uniform and simple exit conditions. High speed video technique was used to investigate the change of water droplet velocity.

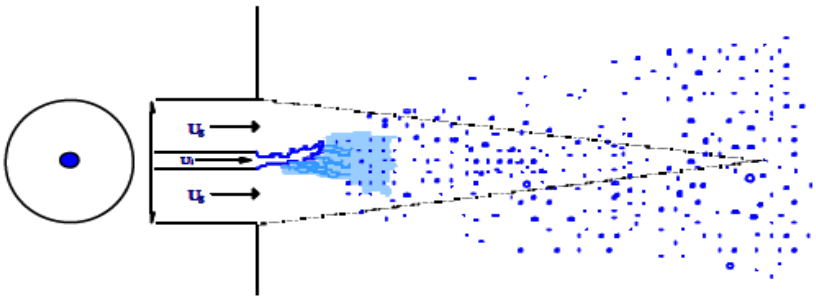

Figure 3. 11. [49], Schematic of nozzle used in M.Varga study

3.3.2.2. Computational setup

CFD simulations were performed using ANSYS CFX, the geometry of the domain was set as a cylinder with a diameter of 5 cm and 0.7 m length. Water inlet region was placed at the center of the cylinder a distance of 20mm from the air inlet region. Mesh used in this simulation was 3D mesh with approximately 170000 total numbers of elements, with this number of elements results are mesh-independent. Working fluid were assumed at 25℃ and the airflow at 100 kPa, the flow assumed to be turbulent and k-Epsilon method is used to characterize the turbulence effect.

3.3.2.3. Results and discussions

Result reported for mean slip velocity change in the axial distance away from nozzle in M.Varga [49] study along with computational results for breakup models are plotted in Figure 3.12. Water is injected at low speed ($V_l = 1.7\ m/s$), while air is at relatively high speed ($V_g = 165\ m/s$), for this reason initially mean slip velocity is negative, water speed starts to increase dramatically as it is injected to the high momentum airstream. Due to inertia, water speed exceeds air speed at some point resulting of mean slip velocity to reach an optimum value of approximately 20 m/s at a distance of 225mm $(x/D_g = 20)$, after that water speed start to decelerate to reach air velocity at a distance of 675mm $(x/D_g = 20)$. Reported experimental data of V.Vagra [49] where measured for only few points (10 points) for this reason turbulence effect is not shown, however computational results were reported for over 250 points and turbulence effect is clearly presented.

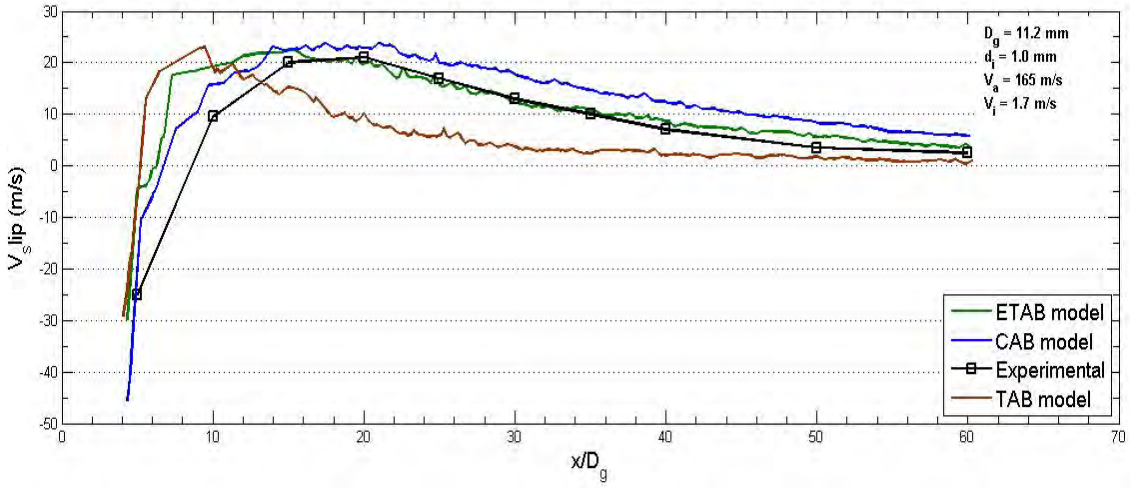

Figure 3. 12, Experimental results of V.Varga [49] and breakup models results of mean slip velocity change in the axial direction away from nozzle

ETAB model shows very good agreement with experimental data. TAB model shows good results but it underestimates the mean slip velocity while CAB model tend to slightly overestimate it. Reitz & Diwakar model greatly overestimated the value of mean slip velocity and Schemehl model showed odd results, later two models' results were not plotted. Results of mean slip velocity variations in the computational domain shown in Table 3.19 for investigated breakup models.

Table 3. 19, Mean slip velocity variation in the computational domain for Case C.2 for breakup models

Reitz & Diwakar	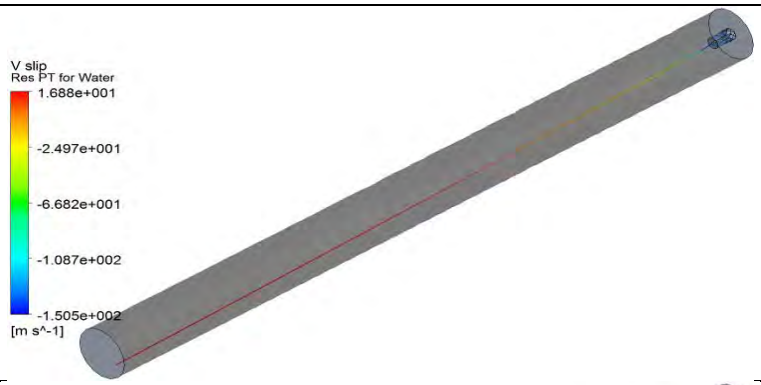
CAB	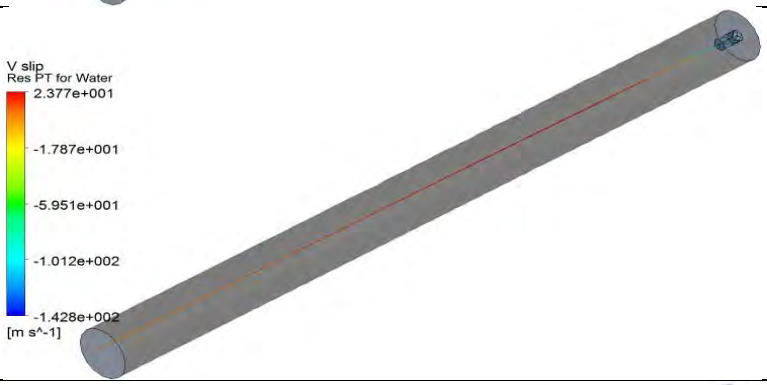
ETAB	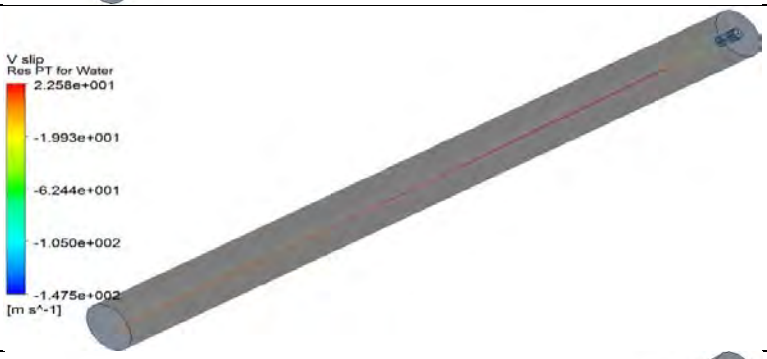
TAB	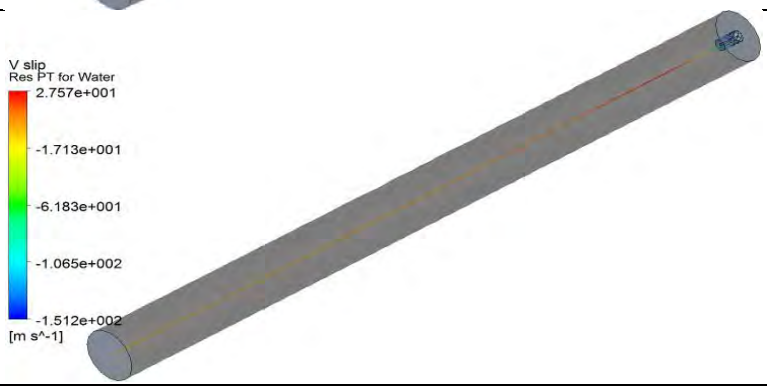

3.4. Conclusions

In this chapter reliability of different breakup models in estimating spray characteristics particularly droplet size was investigated, for three cases: Case A: water atomization in still air, Case B: water jet in cross-flow air, and Case C: water jet

in co-axial air. For each of the three cases breakup models performance was validated against experimental data, where experimental data were collected from literature for experimental studies with conditions similar to the mentioned cases conditions. Performance of five different secondary breakup models was investigated for the mentioned purpose. For all cases simulations were performed while breakup models' constants held to their default values.[1] The results of this work reflected a clear vision for the performance of each of the five breakup models in estimating characteristics mean droplet diameter, SMD, and other spray characteristics. Error analysis was carried out to enable a quantitative determination of error range for each breakup model in estimating SMD. Moreover, general tendency of each model in investigating spray characteristics was highlighted. A summary of key findings are summarized in Table 3.20

Table 3. 20, average absolute relative error and general tendency of breakup models for the investigated cases

Model	Case A: Water injected in still Air		Case B: Water injected in cross-flow air		Case C: Water injected in co-flow air	
	Average $\|\boldsymbol{\varepsilon_r}\|$	General Tendency	Average $\|\boldsymbol{\varepsilon_r}\|$	General Tendency	Average $\|\boldsymbol{\varepsilon_r}\|$	General Tendency
ETAB	14%	Slightly Overestimates Results	13%	Slightly Overestimates Results	18%	Non-monotonic Tendency
Schmehl	41%	Non-monotonic Tendency	36%	Underestimates Results	22%	Non-monotonic Tendency
CAB	57%	Significantly Overestimates Results	58%	Significantly Overestimates Results	28%	Significantly Overestimates Results
Reitz&Diwakar	51%	Significantly Overestimates Results	38%	Overestimates Results	40%	Significantly Overestimates Results
TAB	22%	Slightly Underestimate Results	31%	Underestimates Results	56%	Significantly Underestimates Results

As reported in Table 3.20 ETAB model showed the best accuracy for all cases with a maximum absolute relative error in the order of 18%, Accordingly ETAB model is the most reliable model among the investigated secondary breakup models. However one uses the results of this work should be aware that those results are valid for the

[1] Default values of constants for each secondary breakup model are reported in chapter 2

investigated problem nature and conditions, and not to be generalized for other type of problems such as atomization of fuel in high pressure air flow.

Injected water velocity change as droplets travel away from injector was investigated too in the current work to get a clear presentation of the distance it takes droplets velocity to reach air stream velocity, and it was shown that at an axial distance of approximately 675 mm, water droplet velocity reaches airstream velocity for a case with high initial velocity lag between the injected water and the airstream.

Chapter 4

Numerical Optimization of Online Washing System for Compressor

Efficiency of washing is measured by the ability of injected water to remove fouling accumulated on compressor blades without causing coating loss or mass loss of blades due to the impinging of high speed water droplets. An optimum design of online washing system requires controlling the water spray characteristics at the inlet to compressor first stage, i.e. just before impacting the blades. Controlling spray characteristics requires understanding the effect of nozzles geometries and type, operating parameters, and physical parameters on the water mass flow and droplet size distribution [26].

Droplets size must be controlled to ensure droplets size is big enough to allow efficient washing, yet not so big to cause blades erosion. Water-to-air ratio must be high enough to ensure efficient washing without the potential of erosion. Water particles speed must be kept lower than the acceptable range to avoid erosion. Nevertheless water distribution must be uniform and covers the entire cross-sectional area of the compressor to prevent erosion and not to affect the centrifugal forces on blades.

In this chapter an optimization procedures for online washing system of compressor are carried out based on numerical approach. ETAB breakup model, which showed the best reliability based on the results of chapter 3, is used for CFD simulations. The optimization procedures aim to propose a general methodology for optimizing the water flow characteristics to produce an efficient design of online washing system of compressor, optimizing steps are summarized as follow:

1. Introducing Geometry
2. Setting optimization criteria and constraints
3. Computational setup
4. Selecting the appropriate position of nozzles

5. Determining the optimum mass flow rate per nozzle for a practical range of nozzle diameters
6. Determining the proper number of nozzles
7. Determining the optimum cone angle of nozzles

CFD simulations are performed using ANSYS12.0 CFX package and linked to goal-driven-optimization tool, integrated in ANSYS12.0 CFX workbench, to set the limits and boundaries for operative and physical parameters.

4.1. Physical Domain

The optimization steps are performed for an approximate geometry of MS5002 gas turbine bell mouth (intake), an existing design of the online washing system for this type of gas turbine allows for comparisons with the present numerical-based design procedure. The MS5002 is a gas turbine specifically designed for mechanical drive applications such as gas boosting, gas injection/reinjection, oil & gas pipelines, LNG plants and gas storage. It has a broad operating speed range to meet the operating requirements of the most common driven equipment (centrifugal compressor and pumps) as well as the ability to burn large variety of gaseous and liquid fuels. An approximate geometry of MS5002 bell mouth is presented in Figure 4.1

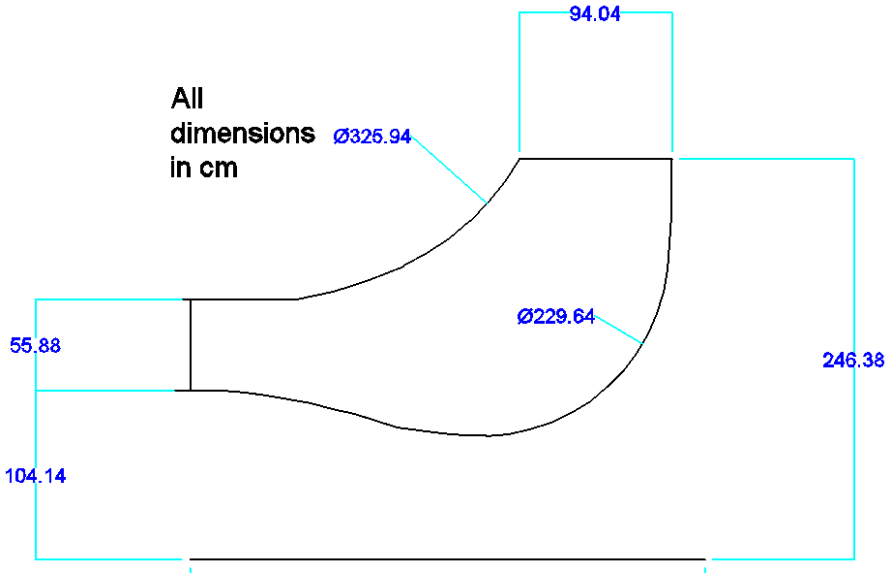

Figure 4. 1, Approximate geometry of MS5002 Gas turbine intake

4.2. Optimization criteria and constraints

Before starting the optimization procedures criteria and constraints must be assigned for spay characteristics. Constraints for droplet size, droplet velocity, water to air ratio, and water distribution is collected from literature and summarized in this section.

4.2.1. Droplet impact velocity and characteristics Sauter Mean Diameter, SMD.

Allowable range of droplet size and impact velocity downstream at the compressor first stage must be determined. Allowable ranges of droplet size depends significantly on the blades materials and coating used, blade geometry, and shaft rotational speed [50]. Accordingly, different types of gas turbine have different ranges for droplet size and threshold velocity. However, referring to literature, for efficient online washing there is a fair agreement that SMD should be kept in the range of $50 - 250\ \mu m$ [15,16], and threshold velocity must be less than $300\ m/s$ for stainless steel [51].

4.2.2. Water-to-air ratio range.

Water-to-air mass flow ratio is an important parameter to consider for an efficient design of online washing system. High water-to-air ratio can cause erosion due to the impacting of droplets with high frequency, however going for low water-to-air ratios with high intervals of time does not compensate for high water-to-air ratio for short intervals of time as fouling tends to accumulate at the aft of the gas turbine [53,54,56]. An adequate range of water-to-air ratio must be determined to ensure efficient cleaning without the potential of blades erosion.

Water-to-air ratio required for efficient washing varies with the amount of contaminants enters compressor and the power output of the gas turbine, however with reference to literature water-to-air ratio in the range of 0.2%-0.7% (in mass bases) is recommended for engines up to 50MW [6,17,18,19]. MS5002 gas turbine falling in the given range of power output.

Going for higher water-to-air rations plays a key role in enhancing the cleaning efficiency [17,18,20,21]. Online washing required for a certain gas turbine varies depending on the environment and application of gas turbine, however for the current work a high value of water-to-air ratio of 0.6% is used for the numerical-based optimization to ensure efficient washing.

4.2.3. Water distribution and water particle trajectory

It is important for injected water to cover the entire cross-sectional area of compressor instead on impacting small area with high water mass flow density to avoid erosion [14], for this reason an uniform distribution of water should be maintained.

Also impinging of water droplets for casing walls reduce the efficiency of washing, hence droplets trajectory should be tracked to ensure uniform distribution of water on the entire cross-sectional area of compressor and to ensure that water droplets are not impacting the casing of the bell mouth.

4.3. Computational setup

Creating the computer-aided design (CAD) model is the first step in the CFD simulation process. For the present study, the CAD model representing the bell mouth and the flow domain is shown in Figure 4.2.

Mesh used in this simulation was 3D mesh with approximately 2,080,0000 total numbers of elements, with this number of elements results are mesh-independent.

As shown in Figure 4.2, air enters the bell mouth at a speed of 36 m/s, the air inflow is represented by the radial arrows, while the air outflow is represented by the axial arrows. The rest of the domain represents solid walls.

ETAB secondary breakup model, which showed the best reliability based on the results of chapter 3, was used in the CFD simulation to characterize breakup process. Spray of hollow-cone pattern was selected to ensure wide angle distribution.

Working fluids were assumed at 25℃ and the airflow at 100 kPa, the flow assumed to be turbulent and k-Epsilon method is used to characterize the turbulence effect.

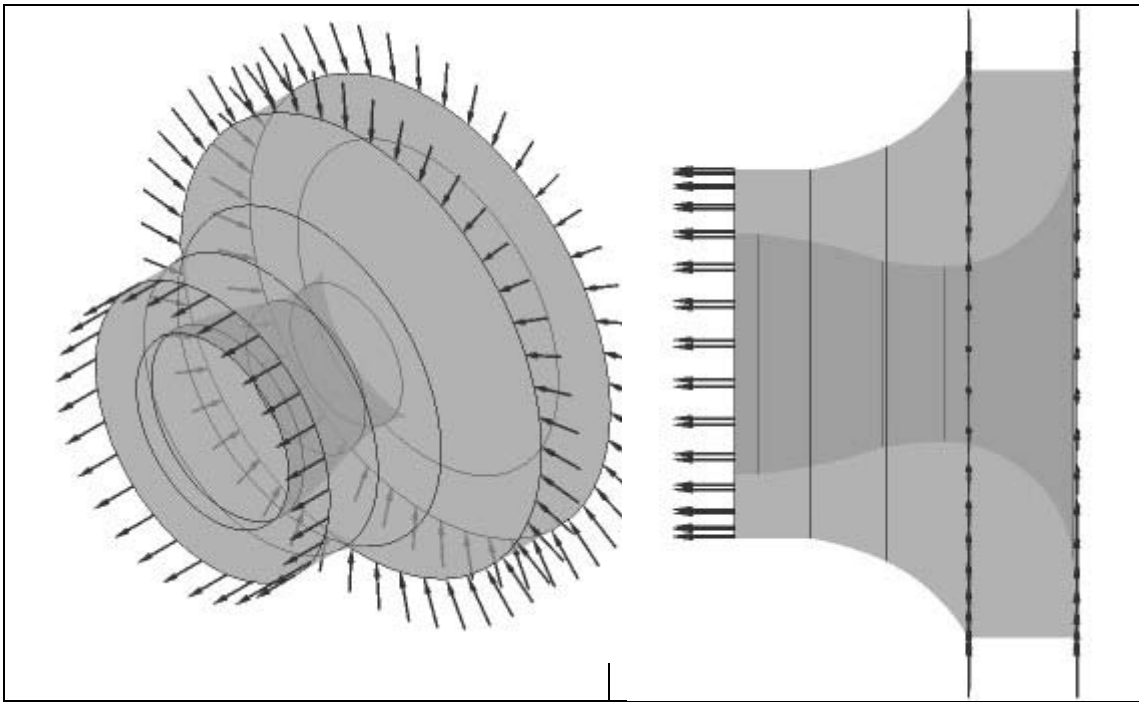

Figure 4. 2, CAD model of the bell mouth and flow domain for MS5002 gas turbine

4.4. Nozzles positions

Water nozzles can be located either inside mounted on the walls of the bell mouth or outside at the inlet to the bell mouth. However due to the big size of this engine, it requires big number of nozzles to wash compressor blades, and it is more practical to locate nozzles inside the casing. Position of nozzles inside the bell mouth must be selected such that initial velocity lag between the injected water and airflow is highest, due to two reasons: 1) To maximize the aerodynamic forces acting on the droplet surface and allow maximum droplet distortion which results in a minimum droplet spray size, were droplet spray size must be in micro level to avoid blade erosion. 2) To allow injected water to penetrate farther in the airstream, by making flux ratio q highest.

Water injected from nozzles at high speed, so highest initial velocity lag can be obtained by injecting water at regions where airflow speed is lowest. Figure 4.3 shows the stream lines of air inside the domain, as clearly shown airstream velocity is lowest at the initial region near the inlet. So to maximize velocity lag water must be injected in this region.

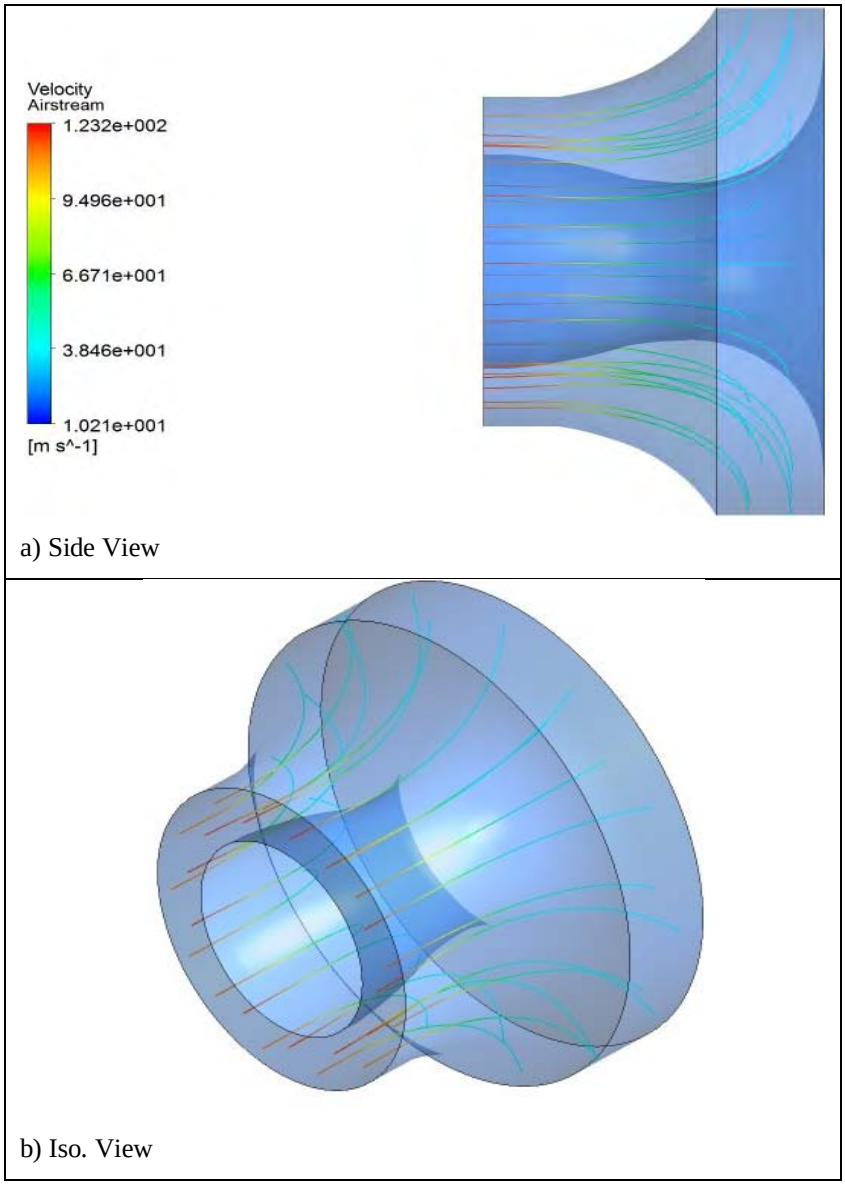

Figure 4. 3, Air streamlines for the air velocity inside the domain

Two positions for nozzles can be chosen, the first position: on the outer surface of the bell mouth near the inlet, and the injection direction is radial parallel to the airflow. The second position: on the inner wall of the bell mouth, and the injection direction is axial through the airflow. To enable comparison with practical existing design, nozzles are positioned approximately at similar positions of existing design, see Figure 4.4.

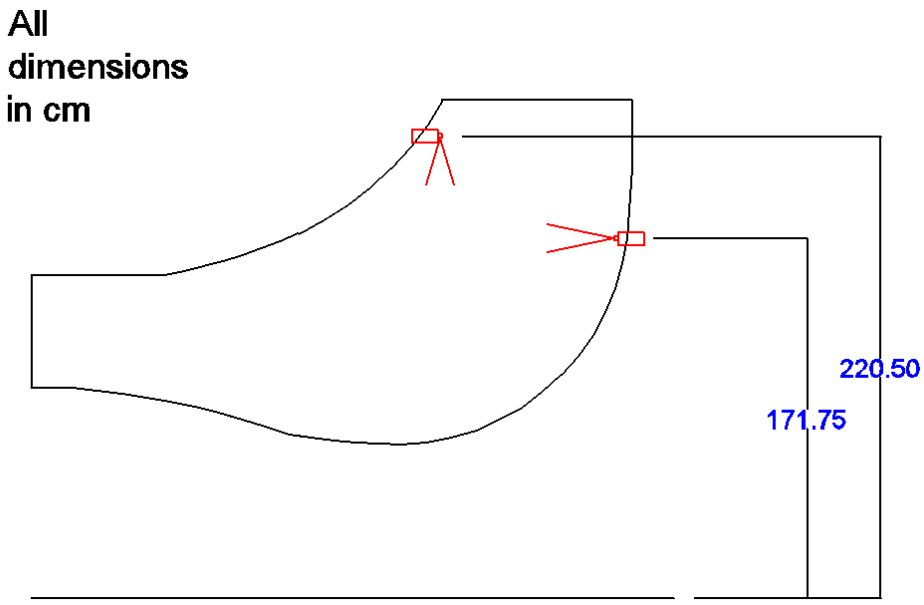

Figure 4. 4, Nozzles positioning

4.5. Optimum mass flow rate per nozzle

Operative mass flow rate, of nozzles controls the injection velocity V_i of water which characterizes the breakup process of water jet. Optimum mass flow rate of nozzle can be determined based on the constraints of SMD rage $50 - 250\ \mu m$, while water impact velocity is controlled by the air stream velocity based on results discussed in chapter 3 As shown in Figure 4.3, airstream velocity reaches $125\ m/s$ at the outlet boundary of bell mouth, water velocity is expected to reach this value.

4.5.1. Optimum mass flow rate for axial nozzle positions

Linking goal-driven-optimization tool to CFD simulations allows determining the range of mass flow rate based on the given limits of SMD. Figures 4.5 shows the upper and lower limits of mass flow rate per nozzle versus nozzle diameters for the axial nozzle. The upper boundary corresponds to SMD = $50\ \mu m$, and the lower boundary corresponds to SMD = $250\ \mu$m.

As clearly shown for constant nozzle diameter, higher mass flow rate values are required to produce smaller droplet size, this is because as water injection velocity increase, more distortion of droplets takes place due to the increased aerodynamic forces acting on the droplet surface resulting in lower droplets sizes. As nozzle diameter increases higher mass flow rate is required to produce the same droplet sizes since higher mass flow rate is required to produce the same injection velocity.

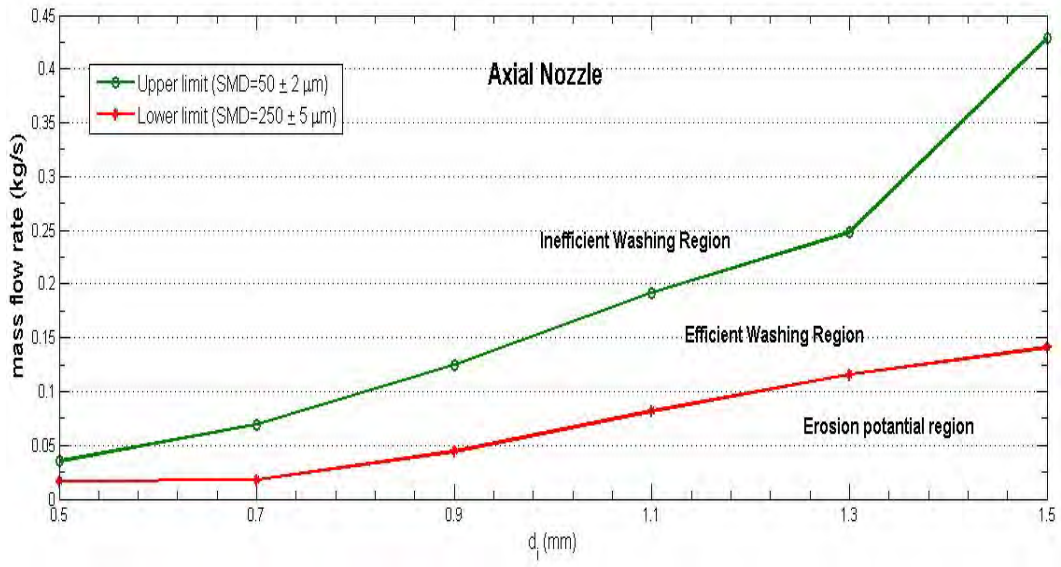

Figure 4. 5, Upper and lower limits of operating mass flow rates vs. nozzle diameter for axial position of nozzles

Based on the shown boundaries, three regions can be classified: Inefficient washing region, Efficient washing region, and Erosion potential region.

Exceeding the upper boundary results in SMD$< 50\mu m$, small droplet sizes can affect the efficiency of washing since small droplets are not capable of removing fouling efficiently and not capable to propagate to further compressor stages [5]. Efficient washing region corresponds to SMD range of $50 - 250\ \mu m$ which is the range of droplets sizes produces an efficient washing without the potential of erosion. Finally erosion potential regions corresponds to SMD$> 250\mu m$, the impinging of droplet with this size can results in coating loss and erosion of compressor blades.

4.5.2. Optimum mass flow rate for radial nozzle positions

. Figures 4.6 shows the upper and lower limits of mass flow rate per nozzle versus nozzle diameters for the radial nozzles. The upper boundary corresponds to SMD = $50\ \mu m$, and the lower boundary corresponds to SMD = $250\ \mu m$. Similar approach is performed to produce the mass flow rate boundaries for radial position.

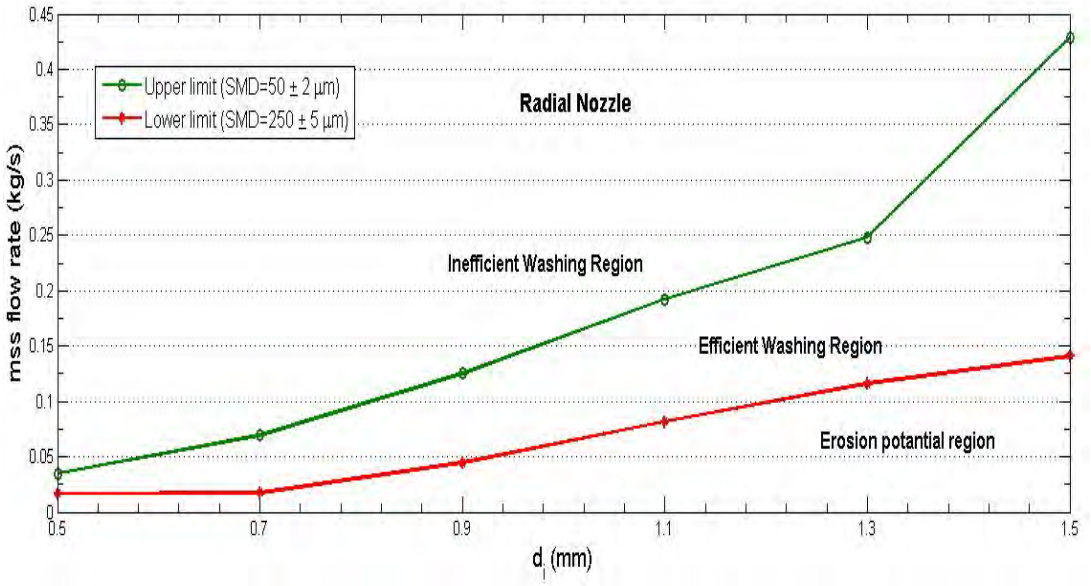

Figure 4. 6, Upper and lower limits of operating mass flow rates vs. nozzle diameter for radial position of nozzles

Axial nozzles inject water through the airflow while radial nozzles inject water parallel to the airflow (Figure 4.4), accordingly for same flow rate, initial velocity lag produced by axial nozzle is higher than initial velocity lag from radial nozzles. For this reason upper and lower boundaries of mass flow rates are slightly shifted up for radial positions as can be seen in Figure 4.7.

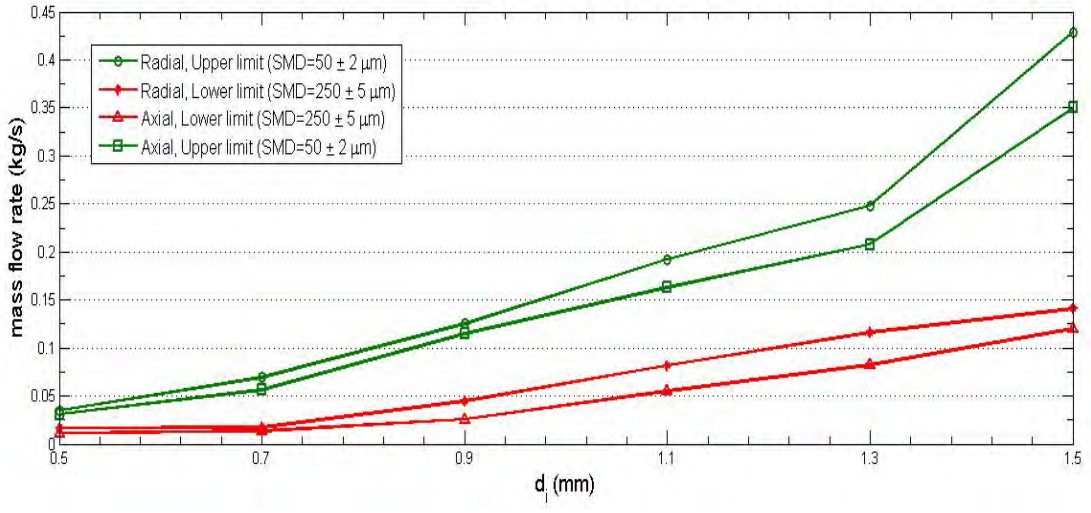

Figure 4. 7, Comparison of Upper and lower limits of operating mass flow rates vs. nozzle diameter for radial and axial positions of nozzles

4.6. Feasible range of nozzle number

A total air mass flow rate of 620.64 kg/s is entering the gas turbine, where this amount was measured at an inlet air velocity of 36 m/s and at temperature of 25°C

and pressure of 100 kPa. According to this amount of air and 0.6% water to air ratio, total water mass flow rate of 3.68 kg/s is required to wash compressor blades efficiently.

This total mass flow rate of water is injected from number of nozzles distributed in the axial and radial positions presented in Figure 4.4. It is assumed that radial nozzles are responsible on washing the outer cross-sectional area of compressor , while axial nozzles are responsible from the inner cross-sectional area of compressor, so total mass flow rate of water is divided equally between the axial nozzles and radial nozzles with 1.84 kg/s for each.

Next step of optimization pressures are to determine the range of nozzles number in both the axial and radial positions that cover the total required mass flow of water within the limits of SMD for efficient washing.

4.6.1. Number of axial nozzles

As mentioned above total water mass flow rate of 1.84 kg/s is required from the axial nozzles. Figure 4.8 shows the intersection between lines of constant water mass flow rate per nozzle and the three regions for axial nozzles presented in section 4.4.

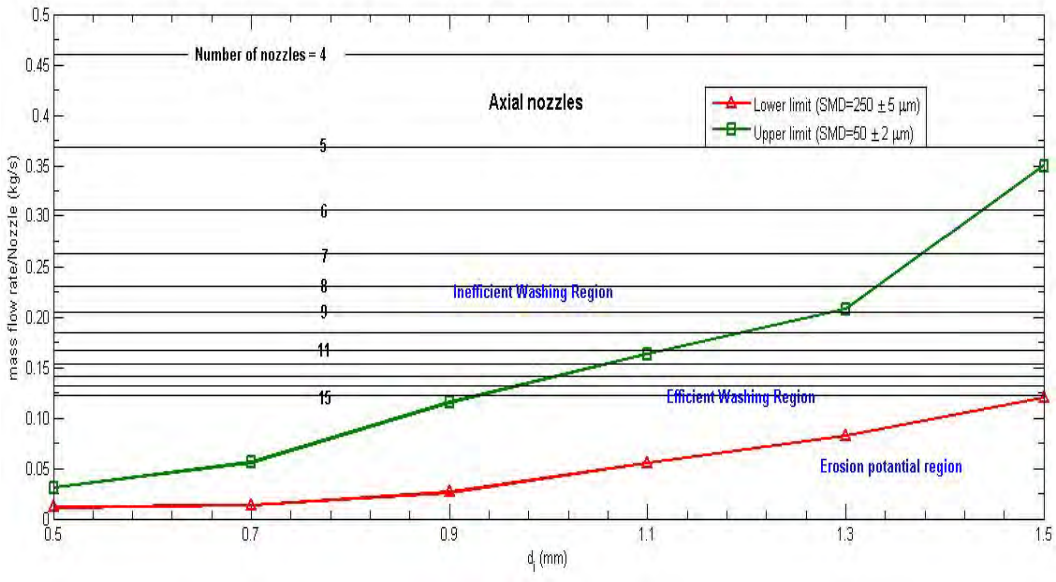

Figure 4. 8, Intersection between lines of constant water mass flow rate per nozzle and classified regions for axial nozzles based on 6% water-to-air ratio

Straight lines present the required number of nozzles for a certain water mass flow rate per nozzle to deliver the required total mass flow rate of water, these lines

are produced by dividing the total mass flow rate of water required from the axial nozzles by the number of nozzles. It is not practical to go for high number of nozzles for two reasons: 1) Going for high number of nozzles tends to complicate the system. 2) The amount of mass flow rate per nozzle for number of nozzles higher than 12 nozzles do not differ sufficiently. therefore selection of number of nozzles is limited to maximum number of 12. Also selecting number of nozzles limited to those exists in the efficient washing region.

For different nozzle diameters, different ranges of nozzles number exist, as clearly shown in Figure 4.8 higher ranges of nozzles numbers is possible for higher diameters, Table 4.1 summaries the feasible ranges for the given diameters.

Table 4. 1, Feasible rages of axial nozzles number

Diameter (mm)	Feasible range of axial nozzles number
0.5	Out of range
0.7	Out of range
0.9	Out of range
1.1	12
1.3	$\{9, 10, 11, 12\}$
1.5	$\{6,7,8,9, 10, 11, 12\}$

As shown in Table 4.1, only for diameters of 1.3 and 1.5 mm considerable range of nozzles numbers can be selected from.

4.6.2. Number of radial nozzles

Figure 4.9 shows the intersection between lines of constant water mass flow rate per nozzle and the three regions for radial nozzles

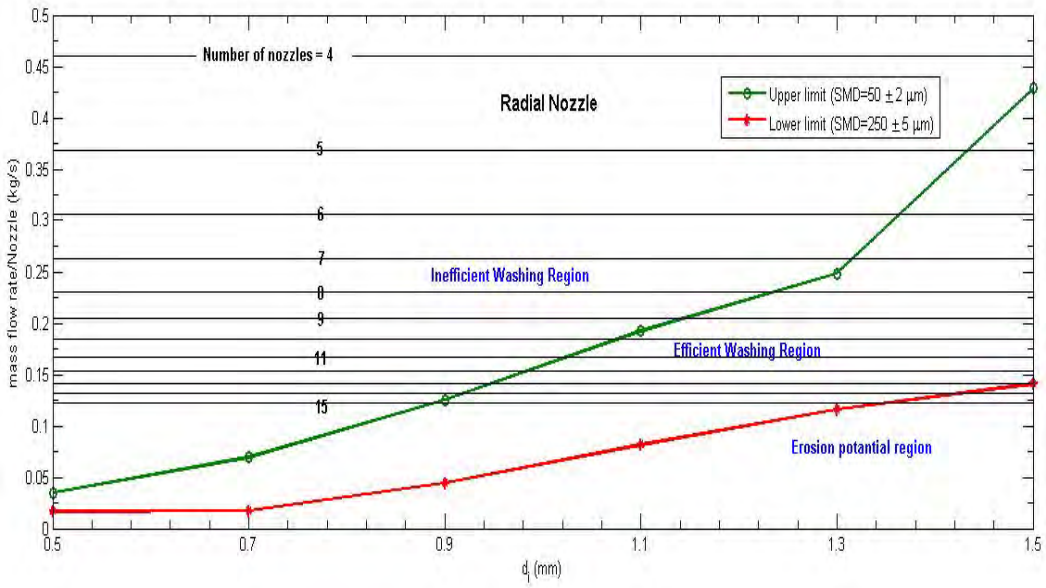

Figure 4. 9, Intersection between lines of constant water mass flow rate per nozzle and classified regions for radial nozzles based on 6% water-to-air ratio

As shown in Figure 4.9 higher ranges of nozzles number are possible for the radial position. Table 4.2 summaries the feasible ranges for the given diameters.

Table 4. 2, Feasible rages of radial nozzles number

Diameter (mm)	Feasible range of axial nozzles number
0.5	Out of range
0.7	Out of range
0.9	Out of range
1.1	{10, 11, 12}
1.3	{8,9, 10, 11, 12}
1.5	{5,6,7,8,9, 10, 11, 12}

As shown in Table 4.2, for the radial case for diameters of 1.1, 1.3, and 1.5 mm considerable range of nozzles numbers can be selected from.

4.7. Optimum cone angle

Optimum cone angle of nozzles is the angle at which the injected water would cover the entire cross-sectional area of compressor without water droplets impacting the compressor casing. To ensure wide and uniform coverage of water on the

compressor cross-sectional area, nozzles with hollow cone angles are used in the optimization procedures since this type of nozzles can operate at wide cone angles.

In the previous section the selection of nozzle diameters was narrowed down to two options for axial nozzles: 1.3 and 1.5mm, and three options for radial nozzles: 1.1, 1.3, and 1.5mm. In this section an optimum cone angle for each option will be determined if possible by tracking the trajectory of water droplets and ensuring minimum number of droplets impacting the casing walls and water covers the entire outlet area.

4.7.1. Optimum cone angle for axial nozzles

Goal-driven-optimization tool is used to determine the optimum cone angle, the constraints applied are: zero or minimum wall stress caused by water droplets on the casing walls, and covering the required angular area per nozzle of the compressor cross section, this angular area is characterized by influence angle θ (Figure 4.10).

The parameter to optimize is cone angle, the optimization is performed to maximize influence angle θ under the given constraints.

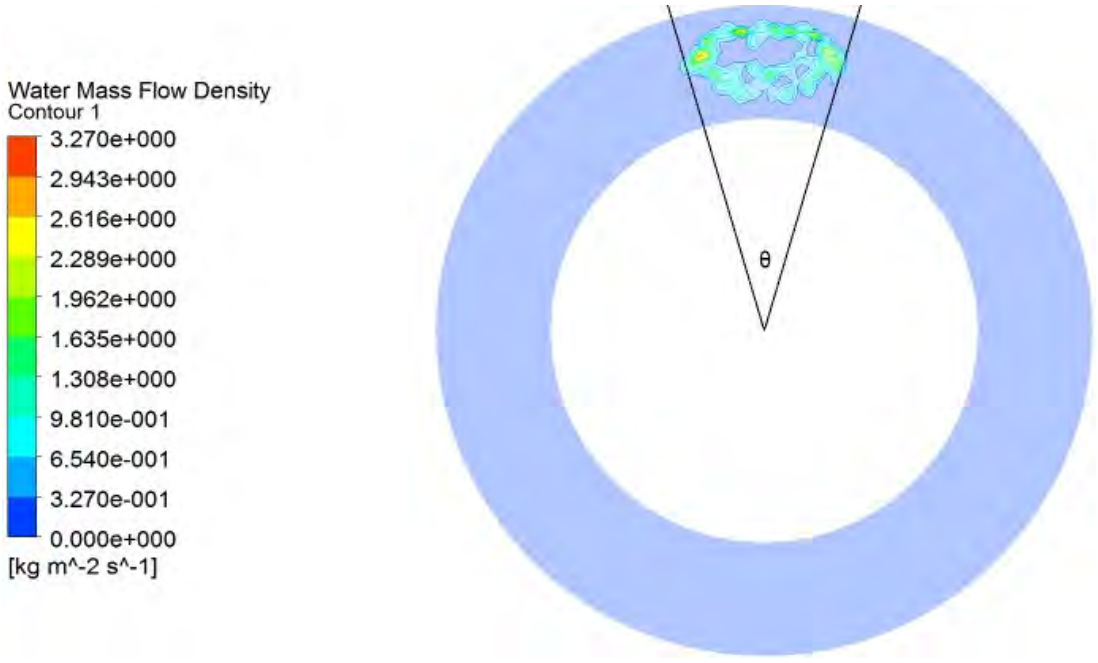

Figure 4. 10, Influence angle $\boldsymbol{\theta}$ on the outlet boundary of the intake (inlet to compressor section)

For axial nozzles two options of nozzles diameters are possible: 1.3 and 1.5mm. For each option, single nozzle is used to determine the optimum cone angle and only for feasible ranges of nozzles number presented in Table 4.1. The optimum

cone angle and associated maximum influence angle θ_m for nozzle diameter of 1.3 mm is presented in Table 4.3 below.

Table 4. 3, Optimum cone angle and influence angle θ for axial nozzles and diameter of 1.3 mm

No. of nozzles	Mass flow rate per nozzle (kg/s)	Optimum half-cone angle (degrees)	Maximum influence angle, θ_m (degrees)
9	0.2044	35.0	30.3
10	0.1839	32.0	29.7
11	0.1672	31.0	29.0
12	0.1533	13.0	25.8

Table 4.4 presents the optimum cone angle and associated maximum influence angle θ_m for nozzle diameter of 1.5 mm.

Table 4. 4, Optimum cone angle and influence angle θ for axial nozzles and diameter of 1.5 mm

No. of nozzles	Mass flow rate per nozzle (kg/s)	Optimum half-cone angle (degrees)	Maximum influence angle, θ_m (degrees)
6	0.3066	41.0	34.0
7	0.2628	40.0	40.1
8	0.2299	35.0	38.3
9	0.2044	26.0	34.6
10	0.1839	19.0	32.8
11	0.1672	15.0	31.5
12	0.1533	13.0	25.6

Required influence angle $\theta_{req.}$ is calculated based on the number of nozzles used. Axial nozzles are required to cover 360°, accordingly required influence angle can be determined by dividing 360° by the number of nozzles. Table 4.5 represents the required influence angle for different nozzles numbers.

Table 4. 5, Required influence angle for different nozzles number

No. of nozzles	Mass flow rate per nozzle (kg/s)	Required influence angle, $\theta_{req.}$ (degrees)
5	0.3679	72.0
6	0.3066	60.0

7	0.2628	51.4
8	0.2299	45.0
9	0.2044	40.0
10	0.1839	36.0
11	0.1672	32.7
12	0.1533	30.0

The next step of optimization is to compare the maximum influence angle θ_m presented in Table 4.3 and 4.5 with the required influence angle θ_{req} presented in Table 4.5, the optimum choice for each nozzle diameter is when the injected water almost covers the entire angular area of the compressor section, this can be achieved when the value of maximum influence angle θ_m is near the value of $\theta_{req.}$.

For nozzle diameter of 1.3mm, the mentioned above criteria is not valid for the feasible range of nozzles number. For nozzle diameter of 1.5, the selection criteria are met for nozzles number of 11. For this number of nozzles, $\theta_{req.} = 32.7$ and $\theta_m = 31.5$. As a result to what mentioned above, the optimum selection for operative and physical parameters is shown in table 4.6 below.

Table 4. 6, Optimum operative and physical parameters for axial nozzles

Nozzle diameter (mm)	1.5
Mass flow rate per nozzle (kg/s)	0.1672
Half-cone angle (degrees)	15
Number of nozzles	11
Distribution of nozzles	Equally spaced

With these parameters an optimized design of axial nozzles is achieved. Water flow characteristics for the optimum operation of axial nozzles are shown in Figure 4.11.

Variation of mean droplet diameter in the domain is shown in Figure 4.11.a, as clearly can be seen at the outlet boundary droplets diameters are in the acceptable range for SMD values. Figure 4.11.b shows the variation of water velocity in the domain and as was expected water velocity reaches the airstream velocity at the outlet

boundary, where airstream velocity reaches 125m/s as shown in Figure 4.3, and water flow velocity reaches 110 m/s at the outlet boundary as shown in Figure 4.11.b.

As presented in Figure 4.11.c wall stress caused by the impact of water droplets is very small and can be neglected with a maximum value of 7 Pascal, which indicates that only few droplets are impacting the casing walls.

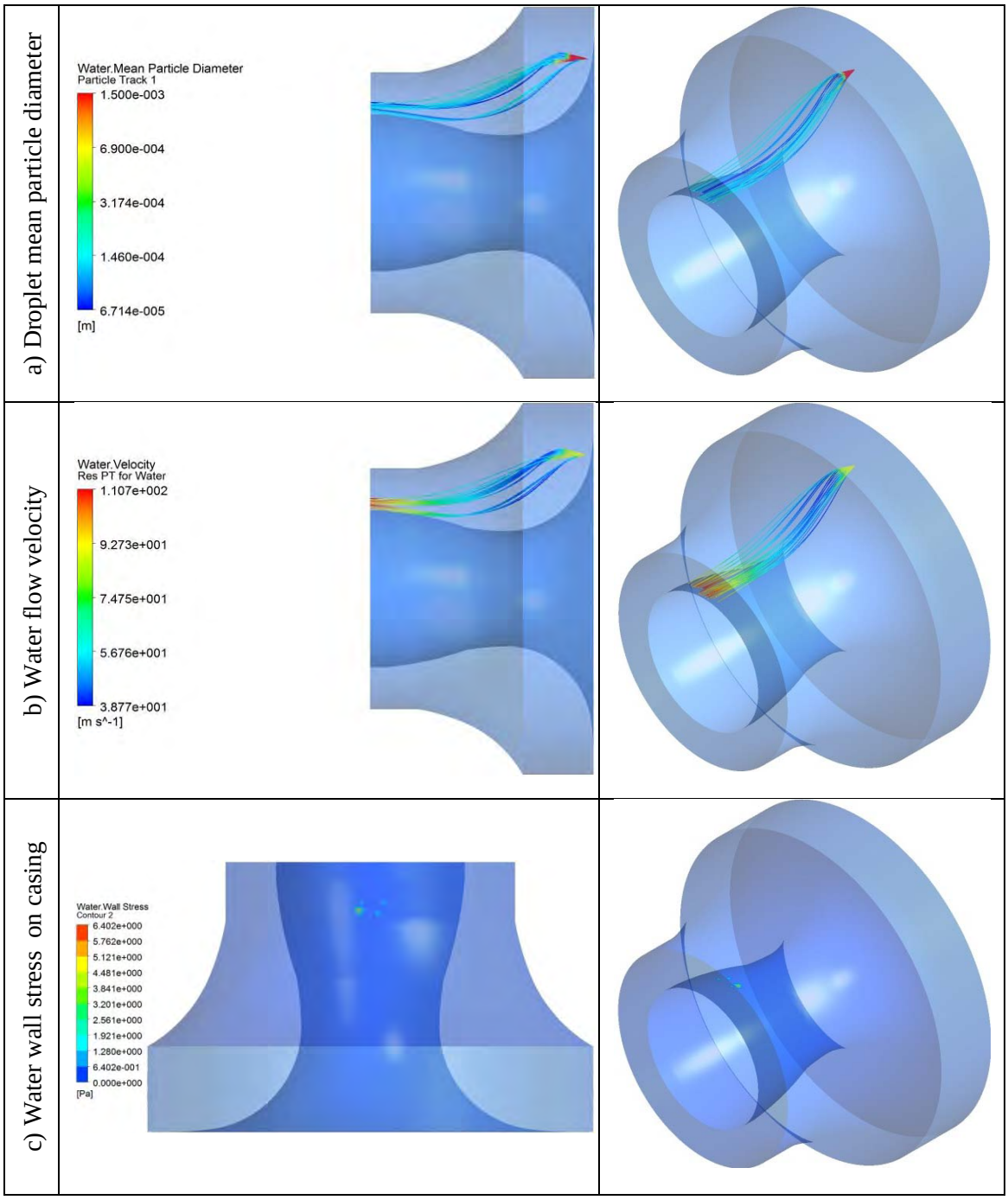

Figure 4. 11, Water flow characteristics for optimum operation of axial nozzle and nozzle diameter of 1.5mm

Figure 4.12 shows the water mass flow density on the outlet boundary, as clearly shown water tends to cover the lower area near the lower wall as expected for axial nozzles, and the influence angle is 31.5 as shown in Table 4.4 which ensures water covers the entire cross-sectional area of compressor when 11 axial nozzles are used.

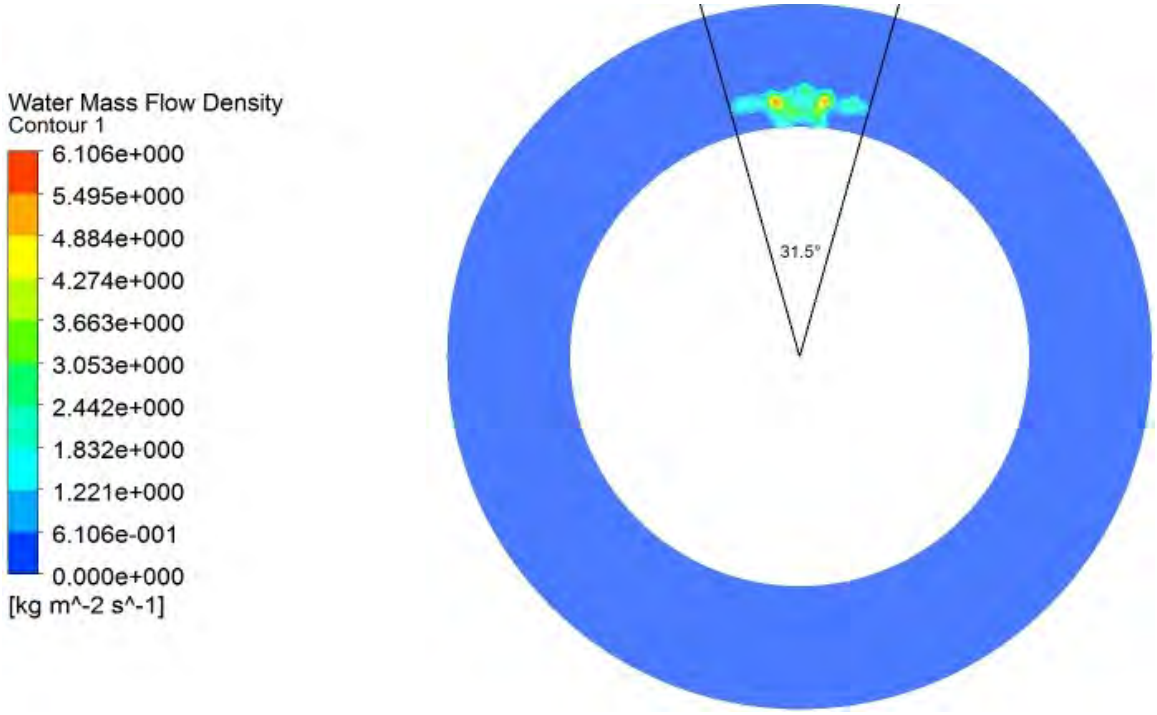

Figure 4. 12, Water mass flow density and influence angle at the outlet boundary for optimum operation of axial nozzle and nozzle diameter of 1.5mm

4.7.2. Optimum cone angle for radial nozzles

Similar approach used to determine the optimum cone angle for radial nozzles, however the optimization was performed for three options of nozzle diameters: 1.1, 1.3, and 1.5mm.

The optimum cone angle and associated maximum influence angle θ_m for nozzle diameter of 1.1, 1.3 and 1.5 mm is presented in Tables 4.7, 4.8, and 4.9 respectively.

Table 4. 7, Optimum cone angle and influence angle θ for radial nozzles and diameter of 1.1 mm

No. of nozzles	Mass flow rate per nozzle (kg/s)	Optimum half-cone angle (degrees)	Maximum influence angle, θ_m (degrees)
10	0.1839	54.0	24.6

11	0.1672	54.0	27.8
12	0.1533	54.0	29.6

Table 4. 8, Optimum cone angle and influence angle θ for radial nozzles and diameter of 1.3 mm

No. of nozzles	Mass flow rate per nozzle (kg/s)	Optimum half-cone angle (degrees)	Maximum influence angle, θ_m (degrees)
8	0.2299	54.0	28.4
9	0.2044	54.0	32.2
10	0.1839	54.0	32.8
11	0.1672	54.0	34.6
12	0.1533	54.0	35.6

Table 4. 9, Optimum cone angle and influence angle θ for radial nozzles and diameter of 1.5 mm

No. of nozzles	Mass flow rate per nozzle (kg/s)	Optimum half-cone angle (degrees)	Maximum influence angle, θ_m (degrees)
5	0.3679	54.0	26.5
6	0.3066	53.0	30.0
7	0.2628	54.0	34.0
8	0.2299	54.0	35.3
9	0.2044	54.5	39.8
10	0.1839	55.0	41.3
11	0.1672	51.0	44.2
12	0.1533	53.0	48.7

As clearly shown higher half-cone angle values are possible for radial nozzles comparing to axial nozzles, this is because the radial location is away from the walls. Also one can notice that lower maximum influence angles θ_m can be noticed for radial nozzles that axial nozzles despite the high value of half-cone angles, this is because axial nozzles inject water through the airstream while radial nozzles are injecting parallel to airstream.

By comparing the maximum influence angle θ_m presented in Tables 4.7, 4.8, and 4.9 with the required influence θ_{req} angle presented in Table 4.5, optimum half-cone angle can be found for each nozzle diameter. Optimum physical and operative parameters for each nozzle diameter are presented in Table 4.10 below.

Table 4. 10, Optimum operative and physical parameters for radial nozzles

	Nozzle diameter (mm)		
Parameter	1.1	1.3	1.5
Mass flow rate per nozzle (kg/s)	0.1533	0.1672	0.2044
Half-cone angle (degrees)	54.0	54.0	54.5
Number of nozzles	12	11	9
Distribution of nozzles	Equally spaced		

As Table 4.10 shows the optimization procedures limited the operative and physical parameters to three sets, and all of these sets meet the optimization constraints and criteria. One can select one of these sets based on the number of required nozzle to avoid complicating the system or to minimize cost, however the current work is concerned with the water flow characteristics and distribution. Accordingly a comparison of water flow distribution on the outlet boundary enables selecting the best choice. Figure 4.13, shows the water mass flow density distribution on the outlet boundary for the three choices represented in Table 4.10.

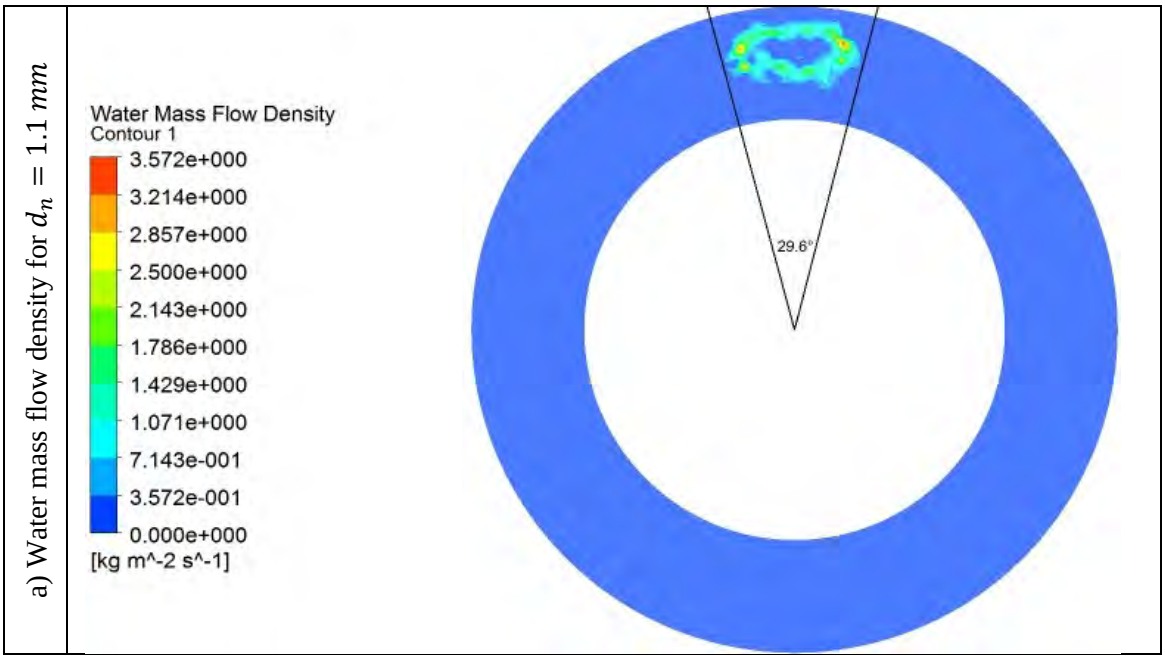

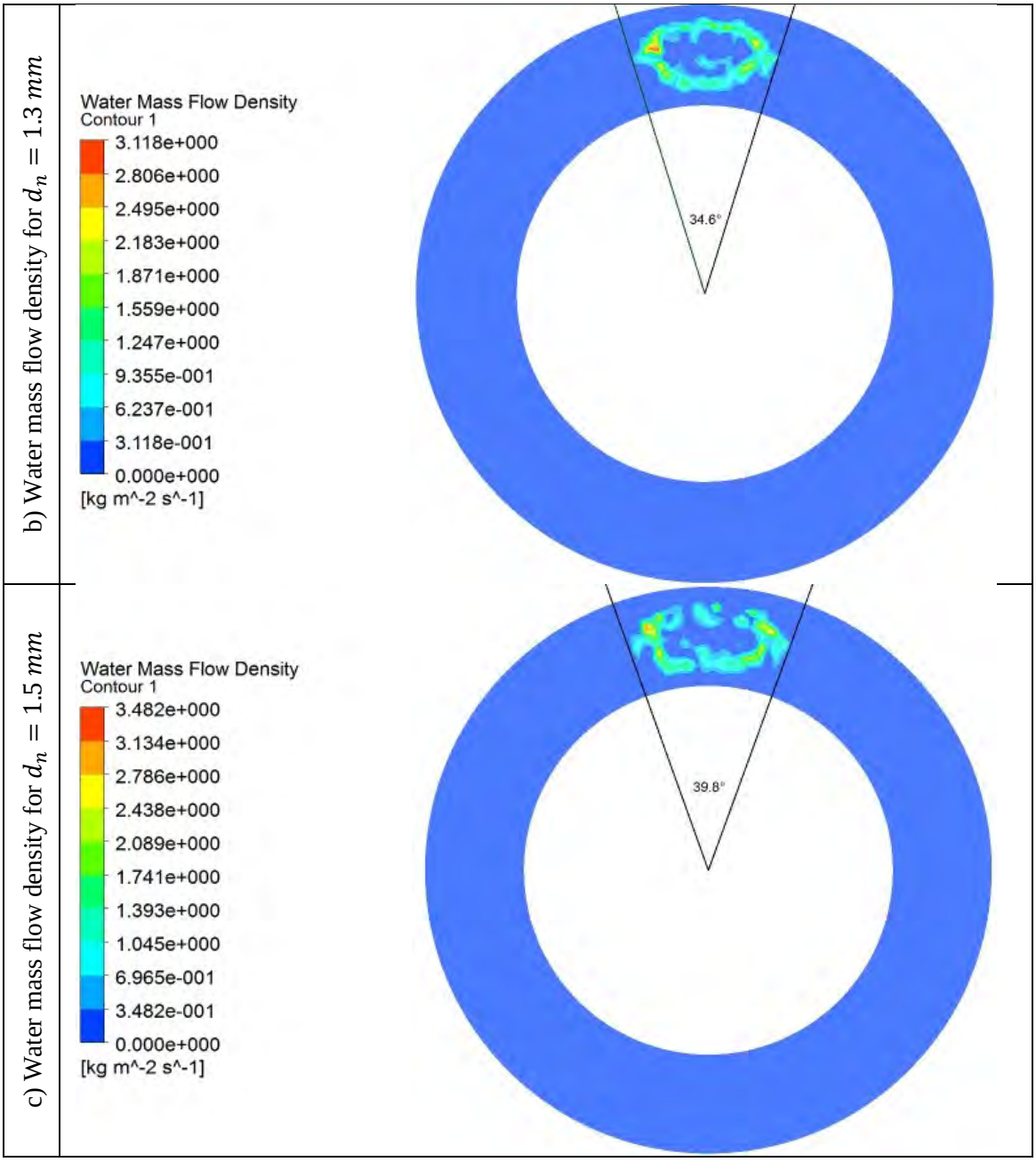

Figure 4. 13, Water mass flow density and influence angle at the outlet boundary for optimum operation of radial nozzles

Since radial nozzles are assumed to cover the outer cross-sectional area of the compressor, choice of $d_n = 1.1\ mm$ is the best since injected water is concentrated in the outer area. With this selection of physical and operative parameters for radial nozzles an efficient washing is ensured. Figure 4.14 shows flow characteristics for the optimum operation of radial nozzles of $d_n = 1.1\ mm$.

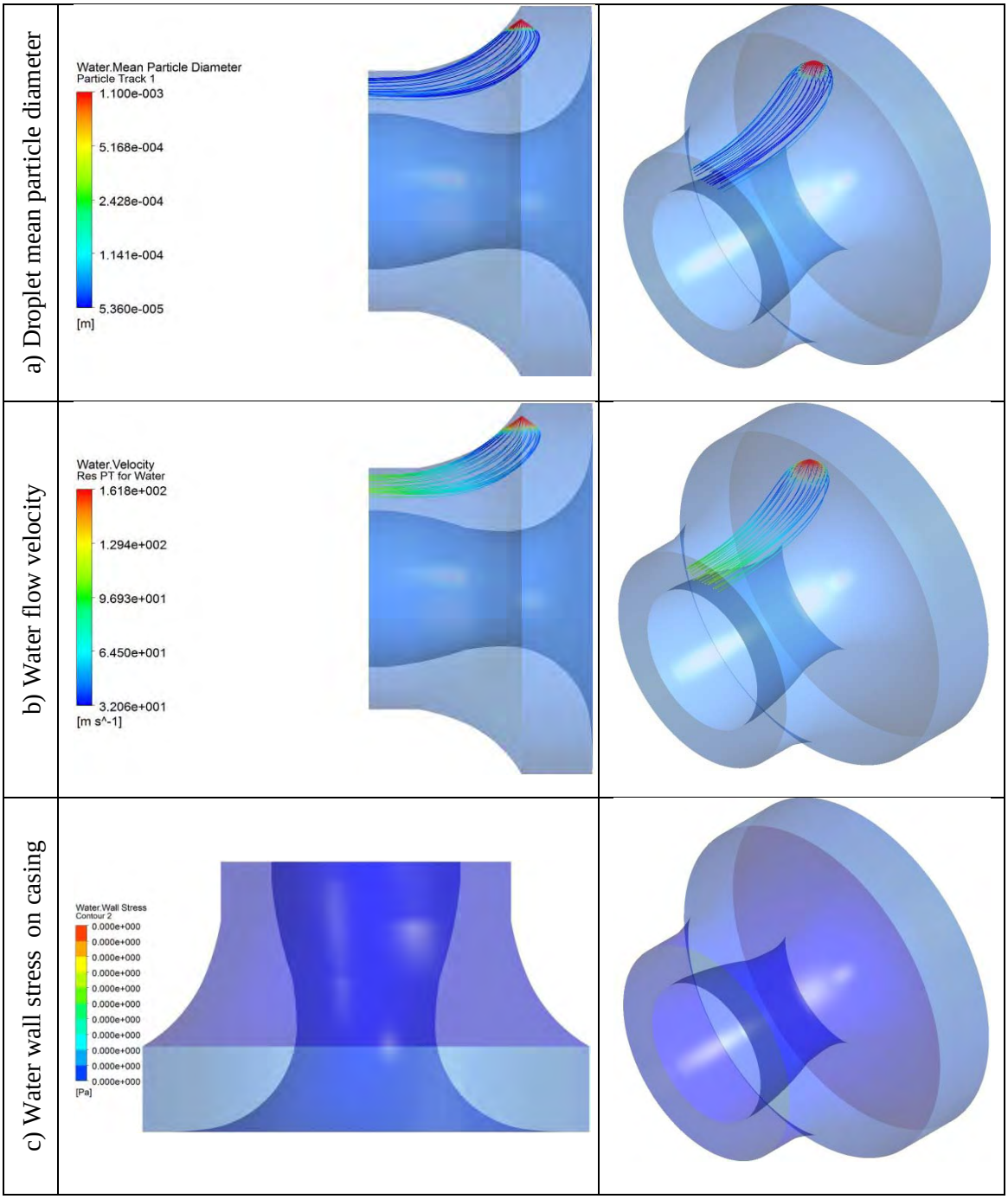

Figure 4. 14, Water flow characteristics for optimum operation of radial nozzle and nozzle diameter of 1.1mm

As Figure 4.14.a shows droplet size variation in the domain, as shown at the outlet boundary droplets diameters are in the acceptable range for SMD values. Figure 4.14.b shows water velocity variation in the domain, water velocity reaches the airstream velocity at the outlet boundary to reach approximately 111 m/s. Figure 4.14.c shows a zero stress of water on the casing which indicates that no water droplets are impacting the casing.

4.8. Conclusions

In this chapter numerical-based optimization procedures were performed for the purpose of optimization of online washing system of compressor for an approximate geometry for MS5002 gas turbine. The optimization procedures were focused on controlling water flow and spray characteristics to meet the desired criteria and constraints, ETAB breakup model was used to characterize the breakup process and hollow-cone spray paten was used to ensure wide angle spray. Constraints for SMD $(50 - 250\,\mu m)$, threshold velocity $(< 300\,m/s)$, water-to-air ratio (0.6%) were set to ensure efficient washing. And water droplet trajectory was tracked to prevent or minimize number of water droplets impacting the casing and to ensure water covers the entire cross-sectional area of compressor uniformly.

Two positions for nozzles were selected inside the bell mouth near the inlet region: axial and radial positions. Axial nozzles are responsible to cover the inner area of the bell mouth outlet boundary while radial nozzles are responsible on covering the outer area of the outlet boundary. An optimum values for operative and physical parameters were produced for axial and radial nozzles based on the given criteria and constraints. Results of optimum operative and physical parameters are summarized in Table 4.11 below

Table 4. 11, Optimum operative and physical parameter for optimized online

Parameter	Position	
	Axial	Radial
Nozzle diameter d_n (mm)	1.5	1.1
Mass flow rate per nozzle (kg/s)	0.1672	0.1533
Half-cone angle (degrees)	15.0	54.0
Number of nozzles	11	12
Distribution of nozzles	Equally spaced	

Chapter 5

Numerical-Based Optimized System versus Existing Design of Online Washing System of MS5002 Gas Turbine Compressor

In chapter four, numerical-based optimization procedures were performed to determine the optimum operation of online washing system for an approximate geometry of MS5002 gas turbine bell mouth. Optimization steps were carried out for single nozzle in the axial position and single position in radial position and it was assumed to be generalized for 11 nozzles in the axial position and the12 nozzles in the radial position respectively. To check the validity of this assumption, it is important to simulate the entire nozzles system of 23 nozzles with the optimum operative parameters and analyze the water spray characteristics for the entire system and verify that optimization constraints and criteria are met, which is the first objective of the current chapter.

The second objective is to analyze the operation of existing online washing system for MS5002 compressor numerically and compare the results with the optimized online washing system. Since there are no enough data about the operative cone angle of the existing design, the comparison is limited to water-to-air ratio, mass flow rates, and nozzle diameters. The comparison aims to: 1) ensure that optimum operative parameters are within the practical range for existing designs. 2) check the efficiency of the existing system by comparing its spray characteristics against the criteria for efficient online washing system.

For both objective ANSYS 12.0 CFX package is used, and ETAB breakup model is used to characterize the breakup process. Same geometry introduced in chapter 4 is used for both objectives. Both designs (optimized and existing) have the same axial and radial positions.

Mesh used in this simulation was 3D mesh with approximately 2,080,0000 total numbers of elements, with this number of elements results are mesh-independent.

Airstream velocity at the inlet boundary is 36 m/s. The rest of the domain represents solid walls. Working fluids were assumed at 25℃ and the airflow at 100 kPa, the flow assumed to be turbulent and k-Epsilon method is used to characterize the turbulence effect.

5.1. Optimized online washing system for MS5002 compressor: The entire system

Figure 5.1 presents the entire system of nozzle, 11 nozzles in the axial position and 12 in the radial position. As shown nozzles are equally spaced distributed in the axial and radial direction. Operative parameters for both axial and radial nozzles are presented in Table 5.1 below.

Table 5. 1, Operative parameters for axial and radial nozzles of the optimized system

Parameter	Position	
	Axial	Radial
Nozzle diameter d_n (mm)	1.5	1.1
Mass flow rate per nozzle (kg/s)	0.1672	0.1533
Half-cone angle (degrees)	15.0	54.0

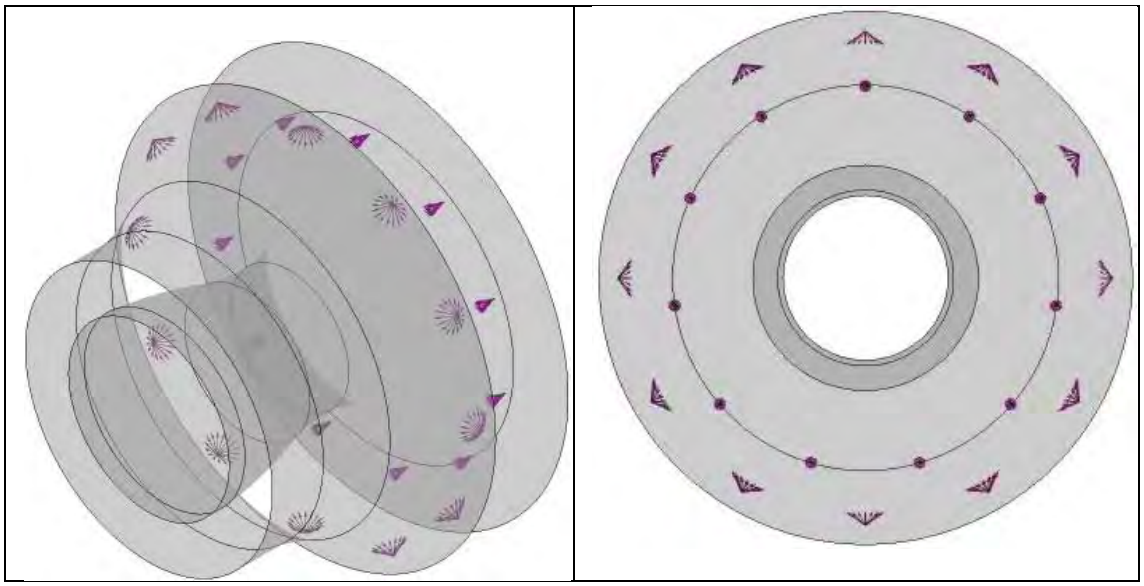

Figure 5. 1, Axial and radial nozzles positions of the optimized system

As shown in Figure 5.1 radial and axial nozzles are distributed equally spaced. Radial nozzles injection direction is parallel to airflow while injection direction for

axial nozzles is through the airflow. For this nozzles system water injected with a total mass flow rate of 3.68 kg/s, divided equally between radial and axial nozzles with operative mass flow rates presented in Table 5.1. With this total water mass flow rate, 0.6% water-to-air ratio is used.

Figure 5.2 presents the water spray characteristic in the domain. Variation of mean droplet diameter in the domain is shown in Figure 5.2.a, as can be seen at the outlet boundary droplets diameters in the range of $55 - 150\mu m$ which is in range for allowable SMD ($50 - 250\mu m$) and uniform droplet size distribution can be noticed in the domain for axial and radial nozzles.

Figure 5.2.b shows the variation of water velocity in the domain and as was expected water velocity reaches the airstream velocity at the outlet boundary, where airstream velocity reaches 125m/s as shown in Figure 4.3, and water flow velocity reaches 110-113 m/s at the outlet boundary as shown in Figure 4.11.b.

As presented in Figure 5.2.c wall stress caused by the impact of water droplets is very small and can be neglected with a maximum value of 12 Pascal, which indicates that only few droplets are impacting the casing walls, also uniform distribution can be seen.

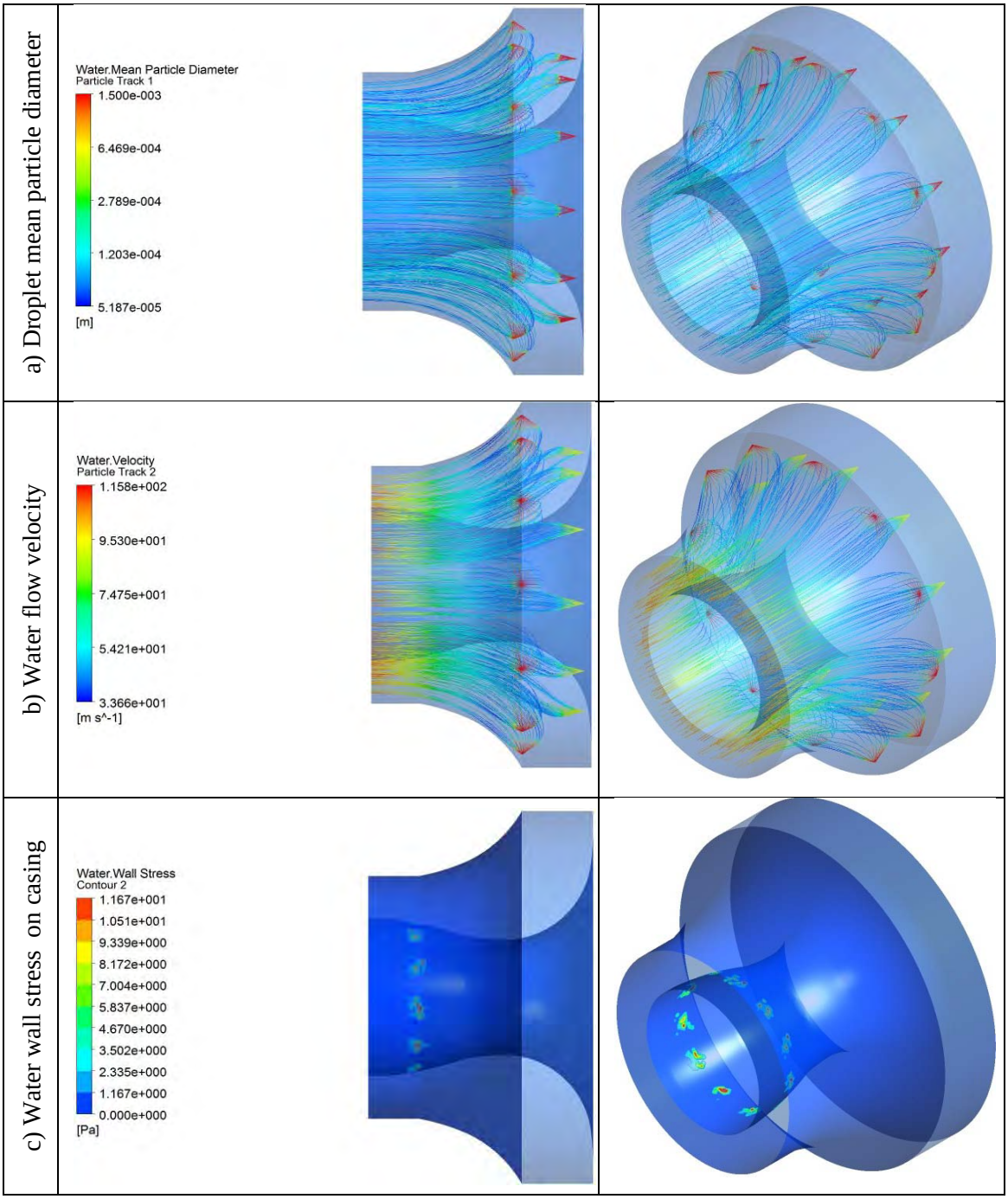

Figure 5. 2, Water flow characteristics for optimum radial nozzle ($\boldsymbol{d_n = 1.1mm}$) and axial nozzles ($\boldsymbol{d_n = 1.5mm}$)

Figure 5.3 shows the water mass flow density on the outlet boundary, as shown water covers the entire outlet boundary when the entire nozzles system is simulated for the optimized design. Despite high water mass flow density is presented in the inner region, water is distributed uniformly on the angular area.

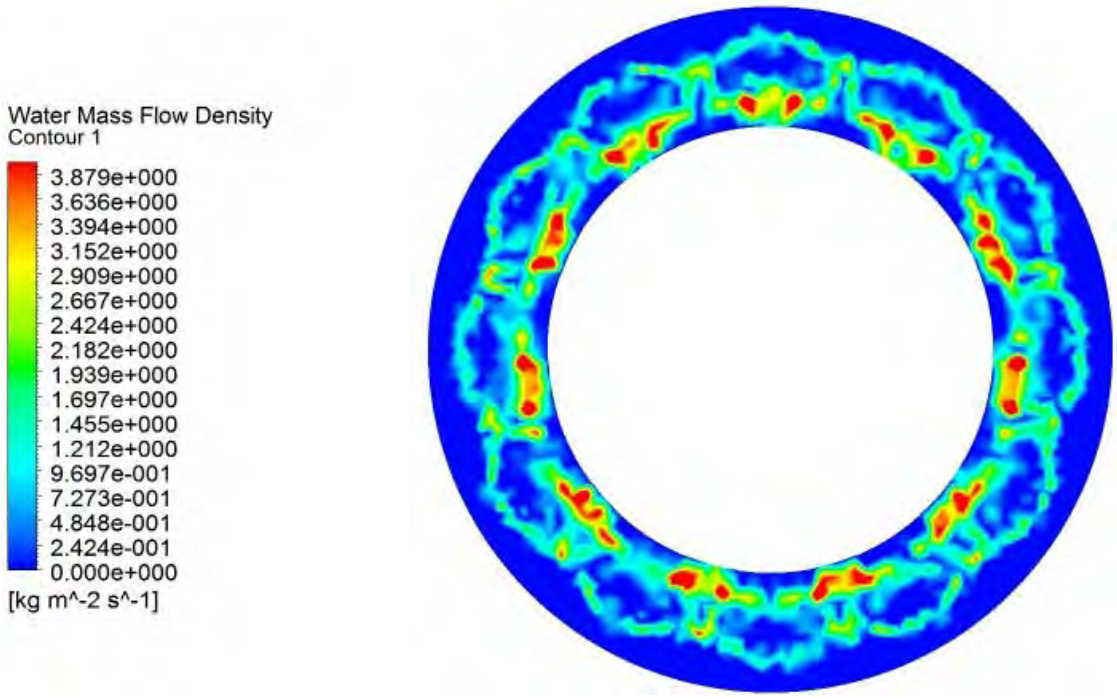

Figure 5. 3, Water mass flow density at the outlet boundary for optimum radial nozzle ($\boldsymbol{d_n = 1.1mm}$) and axial nozzles ($\boldsymbol{d_n = 1.5mm}$)

5.2. Existing design of online washing system for MS5002 compressor

The existing design consists of 14 total numbers of nozzles distributed uniformly, 7 nozzles in the axial position and 7 nozzles in the radial position. Figure 5.4 present the nozzle distribution in the bell mouth of the gas turbine.

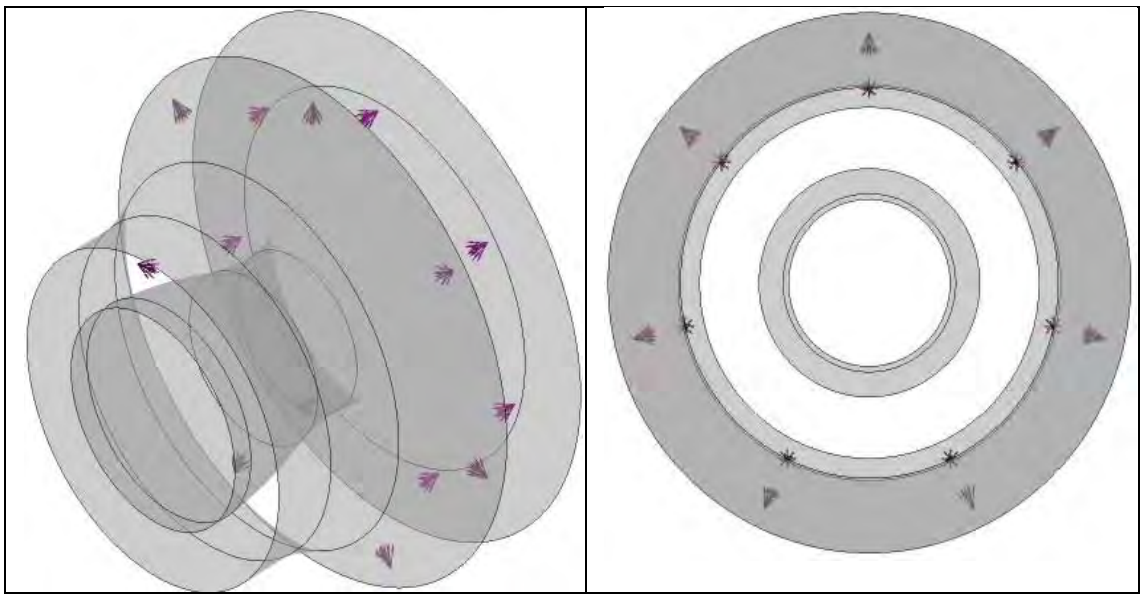

Figure 5. 4, Axial and radial nozzles positions of the Existing system

Mass flow rate and nozzle diameters for both axial and radial nozzles are presented in Table 5.2 below.

Table 5. 2, Operative parameters for axial and radial nozzles of existing system

Nozzle No.	Axial Nozzles		Radial Nozzles	
	d_n (mm)	Mass flow rate (kg/s)	d_n (mm)	Mass flow rate (kg/s)
1	0.787	0.06	0.584	0.15
2	0.787	0.10	0.584	0.45
3	0.787	0.25	0.584	0.93
4	0.787	0.56	0.584	0.41
5	0.787	0.33	0.584	0.12
6	0.787	0.13	0.584	0.07
7	0.787	0.06	0.584	0.07

Figure 5.5 shows the variation of droplet mean diameter in the domain, due to the lack of information about the operative cone angle, one droplet trajectory for each nozzle is shown. Droplet diameters at the outlet boundary are within the range of $25 - 90\ \mu m$

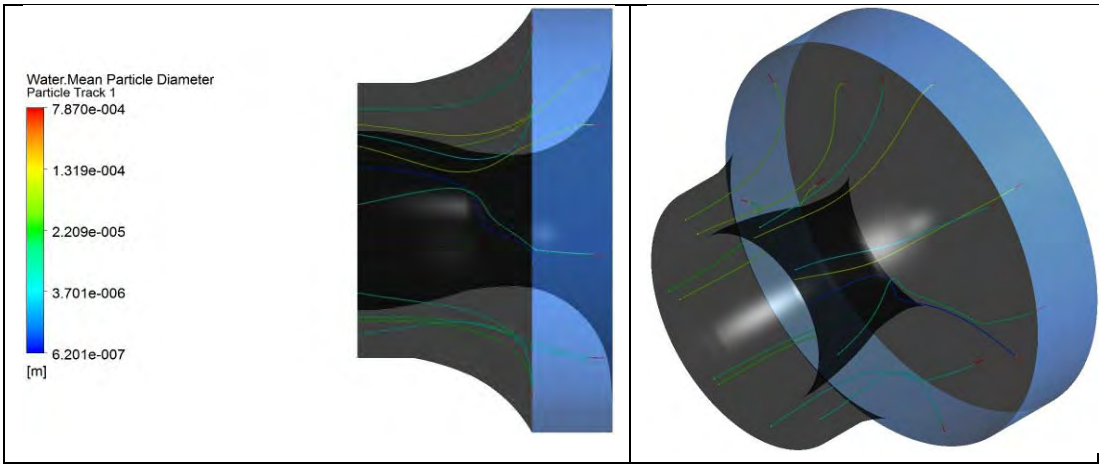

Figure 5. 5, Water mean particle diameter in the domain for existing design

5.3. Comparison of operative parameters for optimized design and existing design

After simulating both optimized and existing system of MS5002 gas turbine, comparison between operative and physical parameters of both designs is possible. Comparison of water-to-air ratio, mass flow rates per nozzle, and nozzle diameter is possible based on the available data of the existing design.

5.3.1. Water-to-air ratio: Optimized design versus existing design

Referring to literature water-to-air ratio in the range of 0.2%-0.7% (in mass bases) is recommended for engines up to 50MW [44,53,54,57]. Also it is recommended to go for high water-to-air ratio for efficient online washing [53,54,55,56], for this reason water to air ration of 0.6% was selected for the optimized design.

For existing design based on the mass flow rate values reported in Table 3.2, a total water mass flow rate of 3.69 kg/s is presented. Total air mass flow rate of 620.64 kg/s enters the bell mouth, accordingly water-to-air ratio of 0.595% is used for the existing design, based on this results water-to-air ratios for optimized design and existing design are approximately equal and agree with the reported ranges collected from literature.

5.3.2. Nozzles operative parameters: Optimized design versus existing design

For optimized design, nozzle diameters for axial and radial nozzles of 1.5 and 1.1mm respectively and mass flow rates per nozzle for axial and radial nozzles of 0.1672 and 0.1533 kg/s respectively were found to be the optimum values to allow droplet sizes to be in the efficient washing region where SMD in the range of 50-250 μm, based on the numerical results droplet sizes were in the range of 55-150 μm.

For existing design, nozzle diameters for axial and radial nozzles of 0.787 and 0.584mm respectively, which is smaller than the optimized design. Nevertheless high mass flow rates per nozzle are used for the existing design, which results in very high injection velocity and smaller droplet sizes. As reported in section 5.2 droplet mean diameters are within the range of 25-90 μm which means that some nozzles are operating inside the efficient washing region and other within the inefficient washing region.

Chapter 6

Conclusions and Recommendations

6.1. Summary and Conclusions

The current work aimed to propose a generalized structured methodology for optimizing gas turbine online washing system based on numerical approach. ANSYS 12.0 CFX package was used for this purpose. The work was divided into three parts: 1) Selecting the most reliable numerical breakup model to use for the optimization procedures. 2) Performing the numerical optimization procedures 3) Comparing the optimized design with existing online wash system.

Part one included validating cases against experimental studies, the tested CFD breakup models are: Reitz & Diwakar Breakup Model, Taylor Analogy Breakup (TAB) model, Enhanced Taylor Analogy Breakup (ETAB model), Cascade Atomization and Breakup (CAB) model, and Schmehl Breakup model. Reliability of mentioned breakup models in estimating spray characteristics particularly droplet size was investigated, for three cases: case A: water atomization in still air, case B: water jet in cross-flow air, and case C: water jet in co-axial air. For all cases simulations were performed while breakup models' constants held to their default values.

The results of part one included error analysis for each model in estimating SMD values, error analysis allowed for clear presentation of the performance each breakup model in estimating droplet size and other spray characteristics. General tendency and average relative error for each breakup model is presented in Table 3.20. Based on the error analysis it was found that ETAB model showed the best accuracy with Average absolute error of 14%, 13%, and 18% for Cases A, B, and C respectively. And with general tendency to slightly over estimating SMD values for cases A and B while it showed a non-monotonic tendency for case C.

Also ETAB model showed the best accuracy in estimating the water velocity change as droplets travel away from injector. And it was found that at an axial distance of approximately 675 mm, water droplet velocity reaches airstream velocity for a case with high initial velocity lag between the injected water and the airstream.

For part 2, numerical-based optimization procedures were performed where ETAB breakup model was used for CFD simulations. The optimization procedures aimed to propose a general methodology for optimizing the water flow characteristics to produce an efficient design of online washing system of compressor. Goal-Driven-Optimization tool was used for the optimization procedures. The optimization steps are summarized as follow:

1. Introducing Geometry
2. Setting optimization criteria and constraints
3. Computational setup
4. Selecting the appropriate position of nozzles
5. Determining the optimum mass flow rate per nozzle for a practical range of nozzle diameters
6. Determining the proper number of nozzles
7. Determining the optimum cone angle of nozzles

An approximate geometry of MS5002 gas turbine was introduced for the optimization procedures. Constraints and criteria were collected from literature and set for the optimization procedures to ensure efficient washing without the potential of blades erosion. These constraints summarized as follow: SMD range of $50 - 250\ \mu m$, threshold velocity (Maximum impact velocity) of 1000 m/s, water-to-air ratio of 0.6%, minimum number of water droplets impinging the compressor casing, and injected water covers the entire cross-sectional area of compressor.

Two positions of nozzle were selected: axial and radial nozzles, the position of nozzles were selected such that water is injected in regions with low airstream velocity inside the bell mouth to allow maximum droplet distortion and to allow water to propagate in the airstream. Axial nozzles inject water through airflow while radial nozzles inject water parallel to the airflow.

It was found that an optimum design of online washing system for MS5002 compressor is feasible for the following nozzles system: 23 nozzles, 11 axial nozzles and 12 radial nozzles, equally spaces and with operative and physical parameters of $d_n = 1.5\ mm$, mass flow rate of 0.1672 kg/s, and half-cone angle of 15° for axial nozzles. And for radial nozzles of $d_n = 1.1\ mm$, mass flow rate of 0.1533 kg/s, and half-cone angle of 54°. With this nozzles system all criteria and constraints were met. Droplet size in the range of $55 - 150 \mu m$,

impact velocity of 110-113 m/s, and water covers the entire outlet boundary of bell mouth uniformly.

For part 3, comparison between the optimized system and existing system of online washing for MS5002 compressor was presented. The comparison is limited to water-to-air ratio used and nozzle operative parameters. The comparison aimed to ensure that optimum operative parameters are within the practical range for existing designs and to check the efficiency of the existing system by comparing its spray characteristics against the introduced constraints for efficient online washing system.

Existing system consists of 14 nozzles distributed uniformly, 7 nozzles in the axial position and 7 nozzles in the radial position. Both systems used the same axial and radial nozzle positions to allow comparison. Comparison of water-to-air ratio showed a very good agreement with 0.6% and 0.595% for optimized design and existing system respectively. For nozzles diameters existing design has lower values of nozzle diameters of 0.787 and 0.584 mm for axial and radial nozzles respectively, while optimized design has nozzle diameters values of 1.5 and 1.1 mm for axial and radial nozzles respectively. For mass flow rates existing design has higher values of operative mass flow rates.

Droplet mean diameter values for existing design were in the range of 25-90 μm which is lower than the range of droplet diameters reported for the optimized design. According to the droplet size for existing design it was found that most of nozzles are operating in the inefficient washing region.

6.2. Recommendations

- For optimum design of online washing system, extensive numerical analysis is required to determine the optimum operative and physical parameters.
- Setting the optimization constraints accurately results in optimized design of online washing system.
- ETAB breakup model shows very good accuracy in estimating droplet size and other spray characteristics for similar problem and it is recommended for the use of similar studies.
- Reliability of breakup models model investigated in this work is based on the current problem conditions and not necessarily to reflect similar results for other problems with different conditions.

- The proposed numerical-based methodology is structured and can be applied for other geometries.

6.3. Recommended future work

Water stress distribution on the compressor blades can be reviewed and analyzed based on CFD study, investigating the water stress distribution on blades allows for understanding the parameters affect liquid droplets-solid erosion phenomenon.

A well understanding of the parameters affect this phenomenon enable one to set more precise approximation of threshold velocity and maximum allowable droplet size for erosion.

REFERENCES LIST

[1] Scheper, G. W., Mayoral, A. J., Hipp, & E. J., "Maintaining Gas Turbine Compressors for High Efficiency", *Power Eng., 82_8_, pp. 54–57,* 1978.

[2] Birol, F., "World energy prospects to 2030" [online], *Energy Book, Issue 1: Autumn 2005*, London, UK, 2005.

[3] World Energy Council, "Performance of Generating Plant: New Realities, New Needs", *World Energy Council, London,* UK, 2004.

[4] Pignone S.p.A., "Axial Compressor On/Off-line Washing"

[5] C. Mund & Pilidis "Gas turbine compressor washing: historical developments, trends and main design parameters for online systems", *Journal of Engineering for Gas Turbines and Power, Vol. 128,* 2006.

[6] Faddegon & C. J., "Effective Compressor Cleaning as a Result of Scientific Testing and Field Experience", 1999.

[7] Engine Cleaning Technology, "Engine Cleaning Technology", *ECT Online*, USA, 2007

[8] O'Rourke and Amsdem, "The TAB Method for Numerical Calculation of Spray Droplet Breakup", "*SAE Technical Paper, 872089*', 1987.

[9] R.D. Reitz and R. Diwakar, "Structure of High-Pressure Fuel Sprays", *SAE Technical Paper, 870598*, 1987.

[10] VGB, " Reinigungsverfahren für Verdichter-und Turbinenbeschaufelungen an Gasturbinen im offenen Prozess", *VGB Merkblatt 106, 2nd Edition,* Germany, 1999.

[11] Elser & W., "Betriebserfahrungen beim Reinigen der Verdichter von Rolls-Royce Strahltriebwerken,", *Brennst.-Waerme-Kraft, 25_9_, pp. 347–348* 1973.

[12] Thames, J. M., Stegmaier, J. W., and Ford, J. J., Jr., "On-Line Compressor Washing Practices and Benefits,", *ASME Paper No. 89-GT-91,* 1989.

[13] McDermott, P., "Method and Apparatus for Cleaning a Gas Turbine Engine,,", "*U.S. Patent No. 5,011,540*" 1991.

[14] Becker, B., and Bohn, D., "Operating Experience With Compressors of Large Heavy-Duty Gas Turbines,", "*ASME Paper No. 84-GT-133*" 1984

[15] Jeffs, E., "No more compressor was day blues,", *Power Engineering International, 15*, 2007.

[16] Meher -Homji, C.B. and Bromley, A.F., "Gas Turbine Axial Compressor Fouling and Washing ", *Proceedings of the 33rd Turbomachinery Symposium* , 2004

[17] Syverud, E., Bakken, L.E., Langnes, K. and Bjørnås, F., "Gas turbine operation offshore; online compressor wash at peak load,", *ASME Paper No. 2003-GT-30871* , USA, 2003.

[18] Syverud, E., Bakken, L.E., "Online water wash test of GE J85-13",J. of Turbomachinery, Vol.129, No.1, pp. 136-142, USA, 2007.

[19] Foss, G., "On-line water wash test,", *Kværner Energy a.s., Test Cell, Report No. 690280*, 1999.

[20] Syverud, E., Bakken, L.E.," The impact of surface roughness on axial compressor performance deterioration,", *ASME Paper No. GT2006-90004, 2006*, 2007.

[21] Syverud, E., Bakken, L.E., "Axial compressor deterioration caused by saltwater ingestion,", *J. of Turbomachinery, Vol.129, No.1, pp. 119-126*, USA, 2007.

[22] E. Santagelo, "Characterization of high-pressure water-mist sprays: Experimental analysis of droplet size and dispersion", *Experimental Thermal and Fluid Science 34(2010) 1353-1366*, June 2010.

[23] Sedarsky, Paciaroni, Berrocal, Petterson, Zelina, Gord, & Linne, "Model validation image data for breakup of liquid jet in crossflow: part I", *Exp. Fluids (2010) 49:391-408*, January 2010.

[24] Liu, Li, "Effect of liquid jet diameter on performance of coaxial two-fluid airblast atomizers,", *Chemical Engineering and Processing 45 (2006) 240–245*, 2005.

[25] Park, Kim, and Lee "Breakup and atomization characteristics of mono-dispersed diesel droplets in cross-flow air stream", *International Journal of Multiphase Flow 32 (2006) 807-822*, February 2006.

[26] Zhou, Zhang, Yu, Xian Zhu, and Peng, "Experimental investigation and model improvement on the atomization performance of single-hole Y-jet nozzle with high liquid flow rate", *Powder Technology 199 (2010) 248-255*, January 2010

[27] C.-L. Ng, R. Sankarakrishnan, K.A. Sallam, "Bag breakup of non-turbulent liquid jets in cross-flow", *" International Journal of Multiphase Flow 34 (2008) 241–259*", USA, June 2007.

[28] J. C. Lasherase, E. Villermaux, and E. J. Hopfinger, "Break-up and atomization of a round water jet by a high-speed annular air jet", *J. Fluid Mech. (1998), .ol. 357, pp. 351±379*, USA, March 1998.

[29] Zhang, S. Ziada, "PDA measurements of droplet size and mass flux in the three-dimensional atomization region of water jet in air cross-flow", *Experiments in Fluids 28 (2000) 29Ð35*, 2000.

[30] R. Ragucci, A. Picarelli, G. Sorrentino, P. di Martino, "Validation of Droplets Behavior Model by Means of PIV Measurements in a Cross-flow Atomizing System", *32nd Meeting on Combustion*, 2009.

[31] A.Cavaliere, R.Ragucci and C. Noviello, "Bending and break-up of liquid jet in a high pressure airflow", *Experimental Thermal and Fluid Science Volume27, Issue 4*, April 2004.

[32] Wu, A. Kirkendall, P. Fuller, "Breakup Process of Liquid Jets in Subsonic Crossflow", *AIAA Journal-96-3024*, USA, 1999.

[33] K. A. Sallam, C. Aalburg and G. M. Faeth, "Breakup of Round Nonturbulent Liquid Jets in Gaseous Crossflow", *AIAA Journal Vol. 42*, USA, 2004.

[34] K. A. Sallam, Z.Dai and G. M. Faeth, "Liquid breakup at the surface of turbulent round liquid jets in still gases", *International Journal of Multiphase Flow Volume28, Issue 3*, USA, March 2002.

[35] Z.Liu and R. D. Reitz, "An Analysis of the Distortion and Breakup Mechanisms of High Speed Liquid Drops", *Int. J. Multiphase Flow Vol. 23*, USA, 1997.

[36] Miller A. and Gidaspow D , *AIChE Journal, Vol. 38, No. 11, p. 1811*, USA, 1992.

[37] S.V. Apte a, M. Gorokhovski, P. Moin, "LES of atomizing spray with stochastic modeling of secondary breakup", *International Journal of Multiphase Flow 29 (2003) 1503–1522*, USA, June 2003.

[38] R. Schmehl, G. Maier and S. Wittig, "CFD Analysis of Fuel Atomization, Secondary Droplet Breakup and Spray Dispersion in the Premix Duct of a LPP Combustor ", *Proc. of 8th Int. Conf. on Liquid Atomization and Spray Systems*, USA, 2000.

[39] K. M. Bade, W. Kalata, and R. J. Schick, "Spray Plume Characteristics at multiple Cross-Flow Angles, Experimental and Computational Assessments", *Spray Analysis and Research Survices From Spray Systems Co.*, Wheaton, USA, 2009.

[40] F.X. Tanner, "Liquid Jet Atomization and Droplet Breakup Modeling of Non-Evaporating Diesel Fuel Sprays", *SAE Technical Paper Series, 970050*, Detroit, USA, Febrauary 1997.

[41] Paolo E. Santangelo, Tartarini, Pulvirenti and Valdiserri, " Discharge and Dispersion in Water-Mist Sprays: Experimental and Numerical Analysis", *11th Triennial International Annual Conference on Liquid Atomization and Spray Systems, Vail, Colorado USA, July 2009*, July 2007.

[42] A. J. Yule and I. R. Widger, "Swirl atomizers operating at high water pressure", U.K., 1994.

[44] G. Batchelor, An Introduction to Fluid Dynamics. Cambridge, UK: Cambridge University Press, 1967.

[45] S. Pope, Turbulent Flows. Cambridge, UK: Cambridge University Press, 2003.

[46] K. L. WERT, "A Rationally-based Correlation of Mean Fragment Size For Drop Secondary Breakup, *b~t. J. Muhiphase Flow Vol. 21, No. 6, pp. 1063-1071*, USA, 1995.

[47] B. E. Gelfand, "Droplet breakup phenomena in flow with velocity lag", *Prog. Energy Combust. Sci. Vol. 22. pp. 201-265*, 1996.

[48] L.P. Hsiang and G.M. Faeth , "Near-Limit Drop Deformation and Secondary Breakup", *International Journal of Multiphase Flow, Vol. 18, No. 5, pp. 635-652*, 1992.

[49] Christopher M. Varga, Juan C. Lasheras, "Atomization of a small-diameter liquid jet by a high-speed gas stream,", "*LEGI-CNRS/UJF/INPG, BP 53, 38041 Grenoble Cedex*", California, USA.

[50] Dresser-Rand, "Assessing Liquid Droplet Erosion Potential in Centrifugal Compress or Impellers", *Texas A&M Symposium #38*, USA.

[51] DeCorso, S.M., "Erosion Tests of Steam Turbine Blade Materials,", *Proceedings of ASTM, Vol. 64 1965*, USA.

[52] E. Kollar and Farzaneh, "Modeling the evolution of droplet size distribution in two-phase flows", *International Journal of Multiphase Flow 33 (2007) 1255-1270*, Canada, March 2007

[53] B. Massey and J. Ward-Smith, Mechanics of Fluids, 7th ed. UK: Nelson Thornes, 1998.

[54] Pai, I. Bermejo-Moreno, O. Desjardins, and H. Pitsch, "Role of Weber number in primary breakup of turbulent liquid jets in crossflow", *Centre for turbelent research, annual research briefs 2009*, 2009

[55] C. Baumgarten, H. Lrttman and G.P. Merker, "Modeling of Primary and Secondary Break-Up Processes in High Pressure Diesel Sprays", *Paper No. 7, CIMAC Congress*, Febrauary 2004.

[56] J.-P. Stalder, "Gas Turbine Compressor Washing State of the Art: Dield Experiences", *SAE Paper Vol. 123*, April 2001.

[57] P. Boyce and Gonzalez, "A Study of On-Lone and Off-Line Turbine Washng to Optimze the Operation of a Gas Turbine", *ASME Paper Vol. 129*, January 2007.

[58] A. Collin, P. Boulet, G. Parent, M.R. Vetrano, J.M. Buchlin, "Dynamic and thermal behaviour of water sprays", *International Journal of Thermal Sciences 47 (2008) 399–407*, July 2007

[59] FAN Jing-yu, " Large-Eddy Simulation of Three-Dimensional Vortical Structures For An Impinging Transverse Jet in the Near Regon ", *Journal of Hydrodaynamic 19(3):314-321*, August 2006.

[60] M. Pilch and C.A. Erdman, " Use of Breakup Time Data and Velocity History Data to Predict the Maximum Size of Stable Fragments for Acceleration-Induced Breakup of a Liquid Drop", *Int. J. Multiphase Flow, Vol. 13, No. 6, pp 741-757*, 1987.

[61] Iakunchak, "Performance Deterioration in Industrial Gas Turbines", *ASME J. Eng. Gas Turbines Power, 114, pp.*, 1992.

APPENDIX

Figures

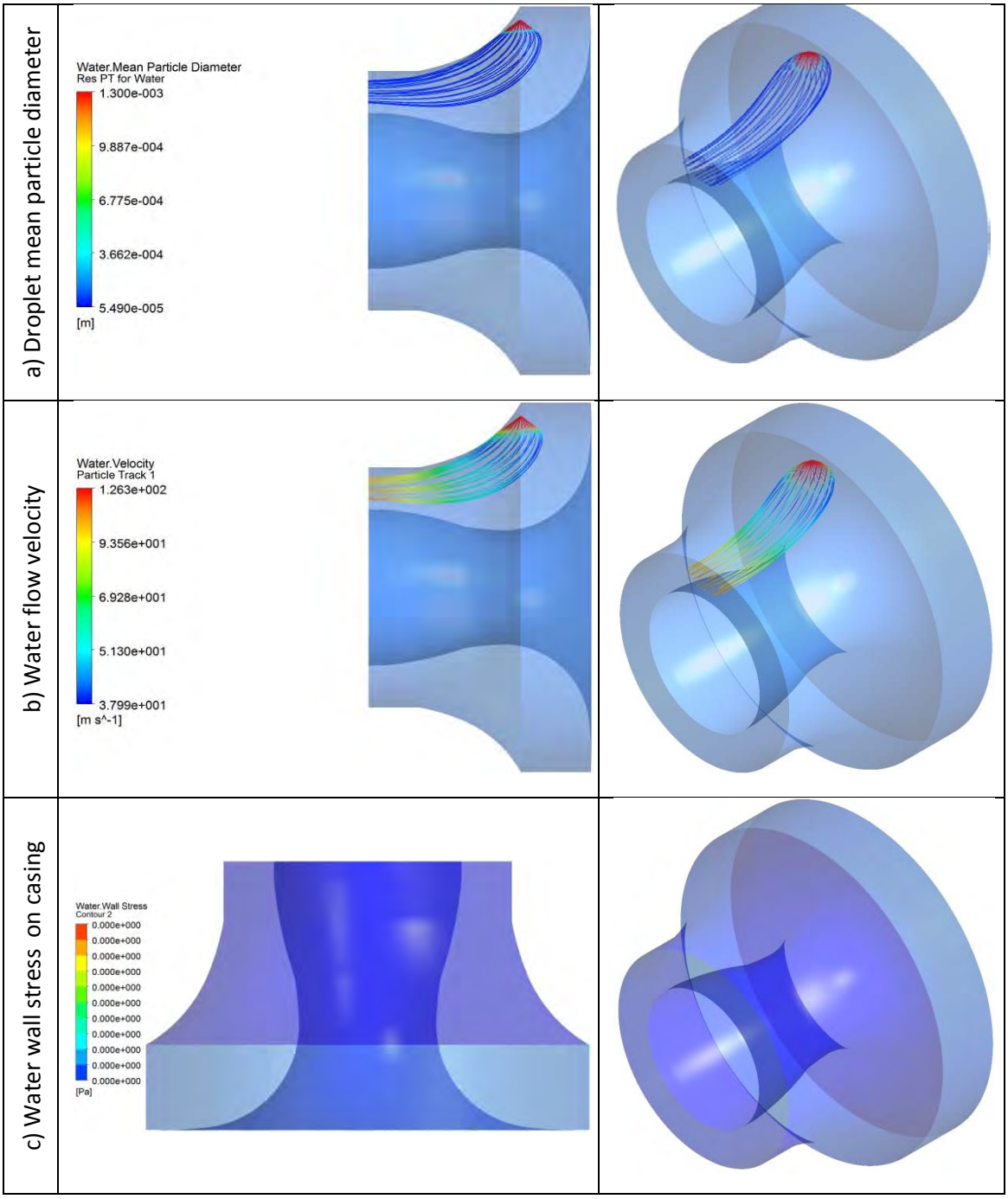

Figure A. 1, Water flow characteristics for optimum operation of radial nozzle and nozzle diameter of 1.3mm

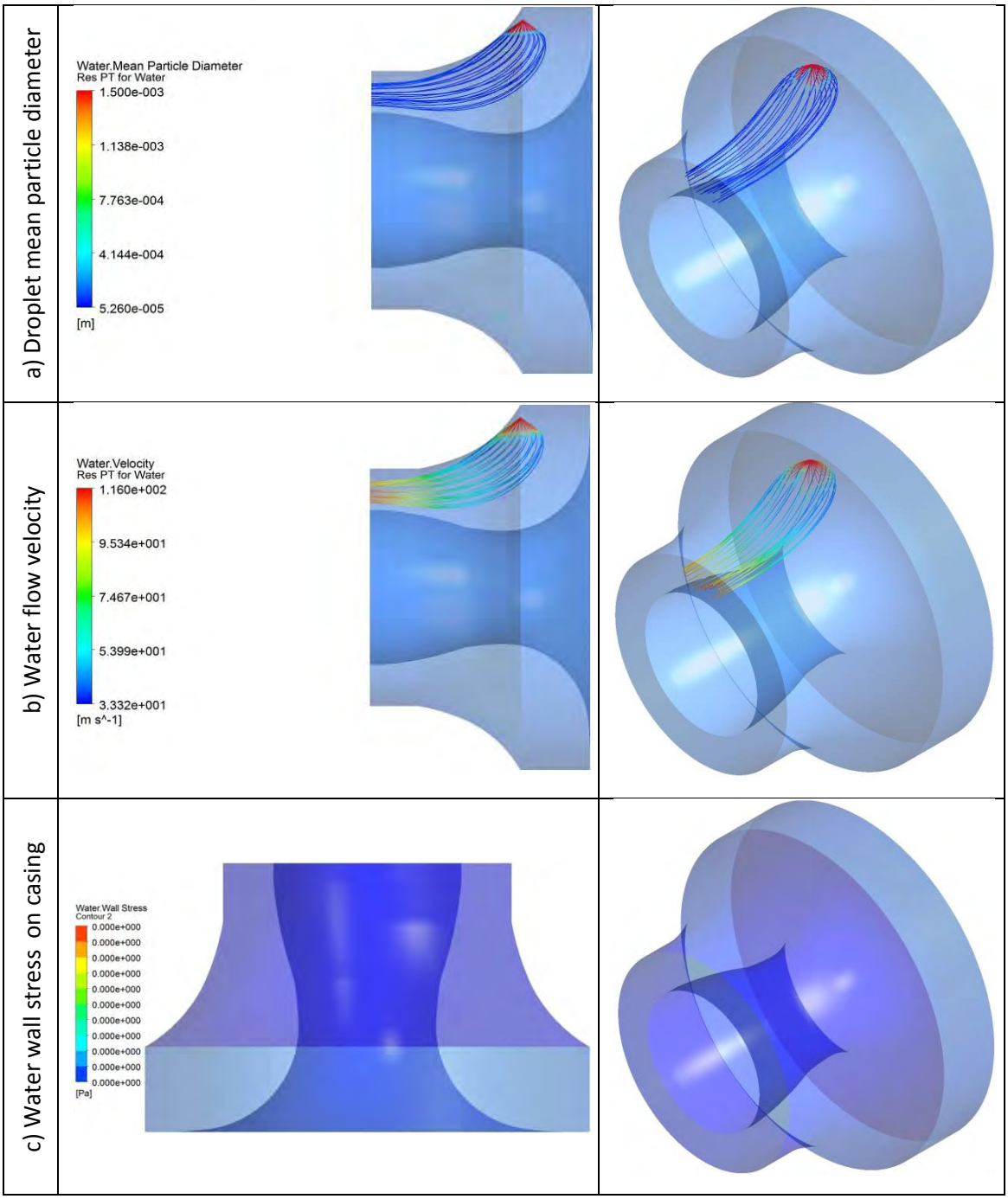

Figure A. 2, Water flow characteristics for optimum operation of radial nozzle and nozzle diameter of 1.5mm

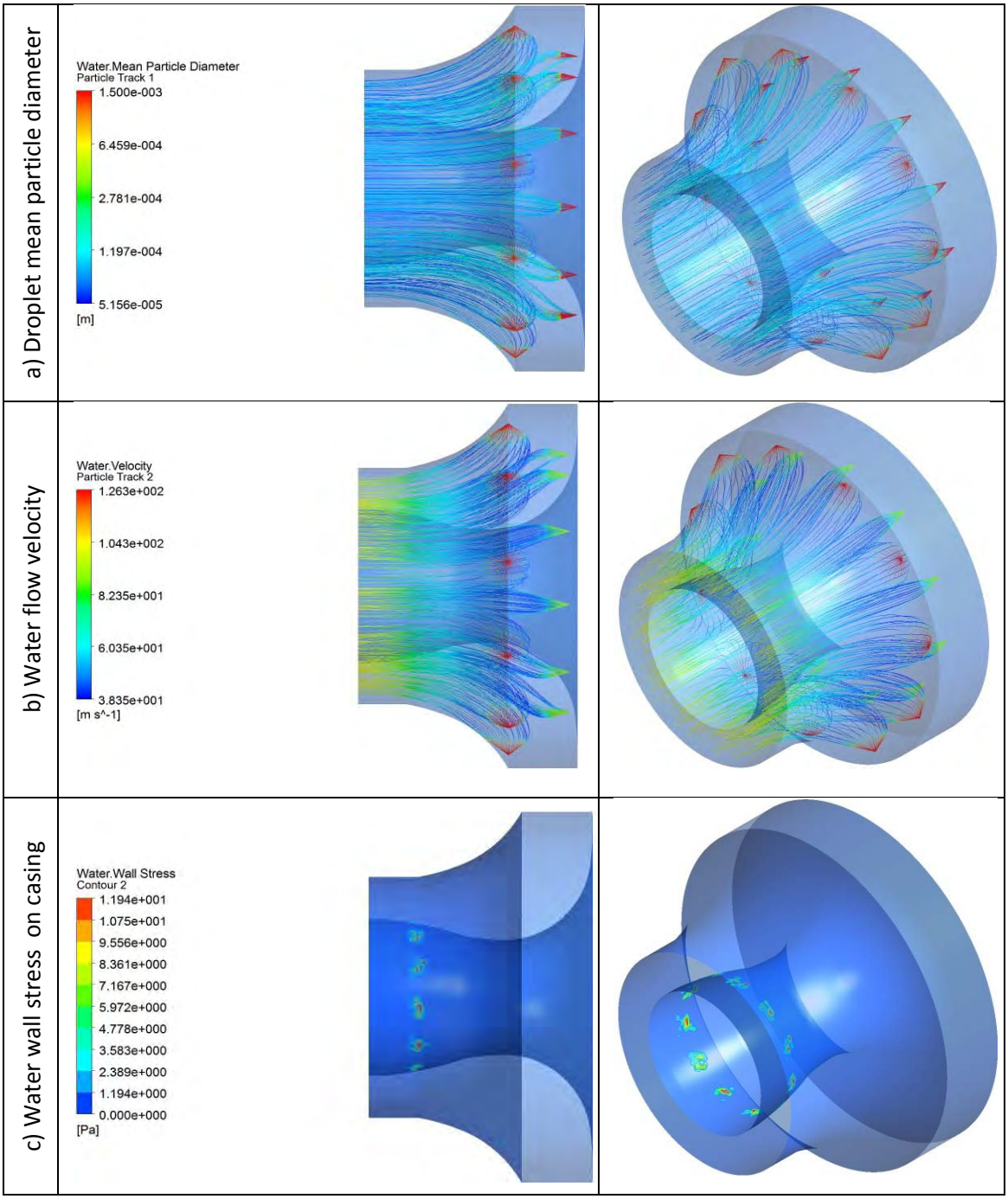

Figure A. 3, Water flow characteristics for optimum operation of radial nozzle ($\boldsymbol{d_n = 1.3mm}$) and axial nozzles ($\boldsymbol{d_n = 1.5mm}$)

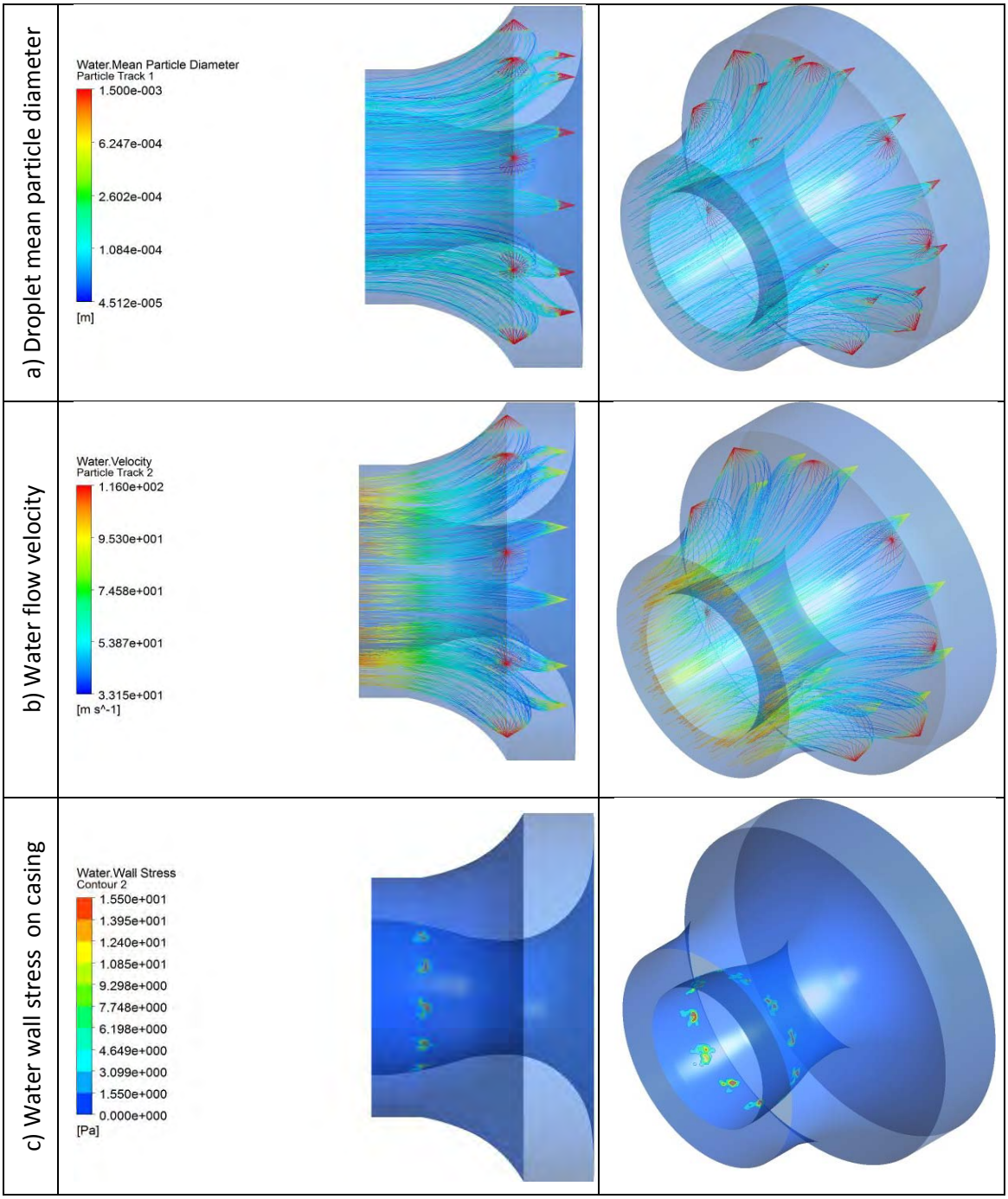

Figure A. 4, Water flow characteristics for optimum operation of radial nozzle ($\boldsymbol{d_n = 1.5mm}$) and axial nozzles ($\boldsymbol{d_n = 1.5mm}$)

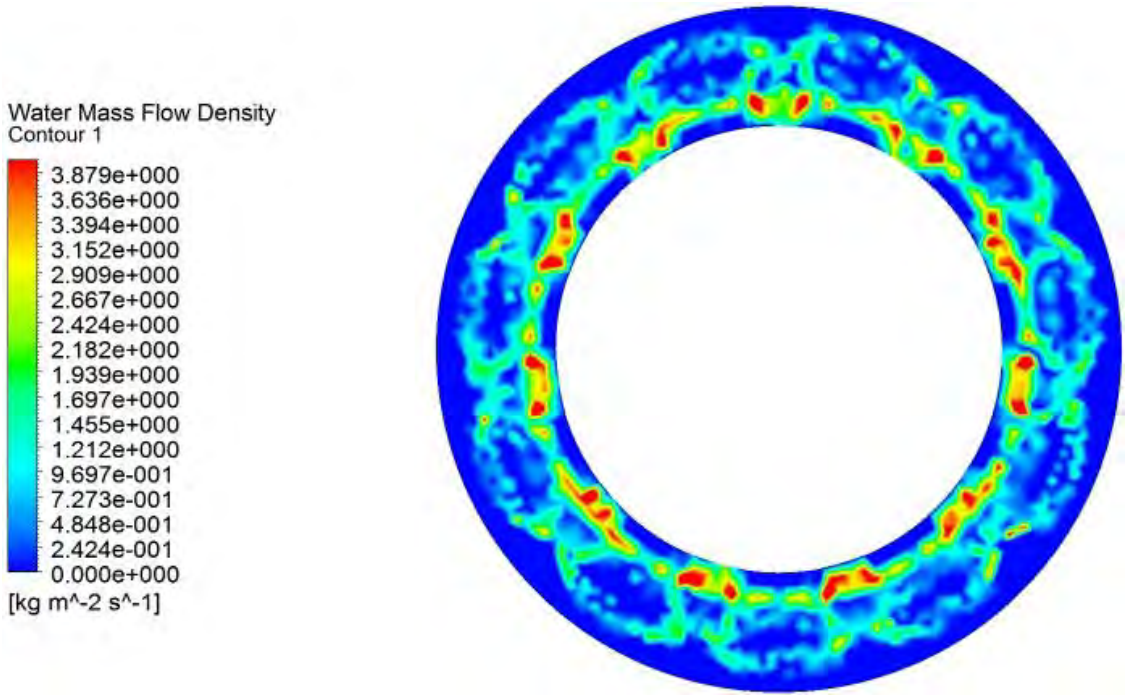

Figure A. 5, , Water mass flow density at the outlet boundary for for optimum operation of radial nozzle ($\boldsymbol{d_n = 1.3mm}$) and axial nozzles ($\boldsymbol{d_n = 1.5mm}$)

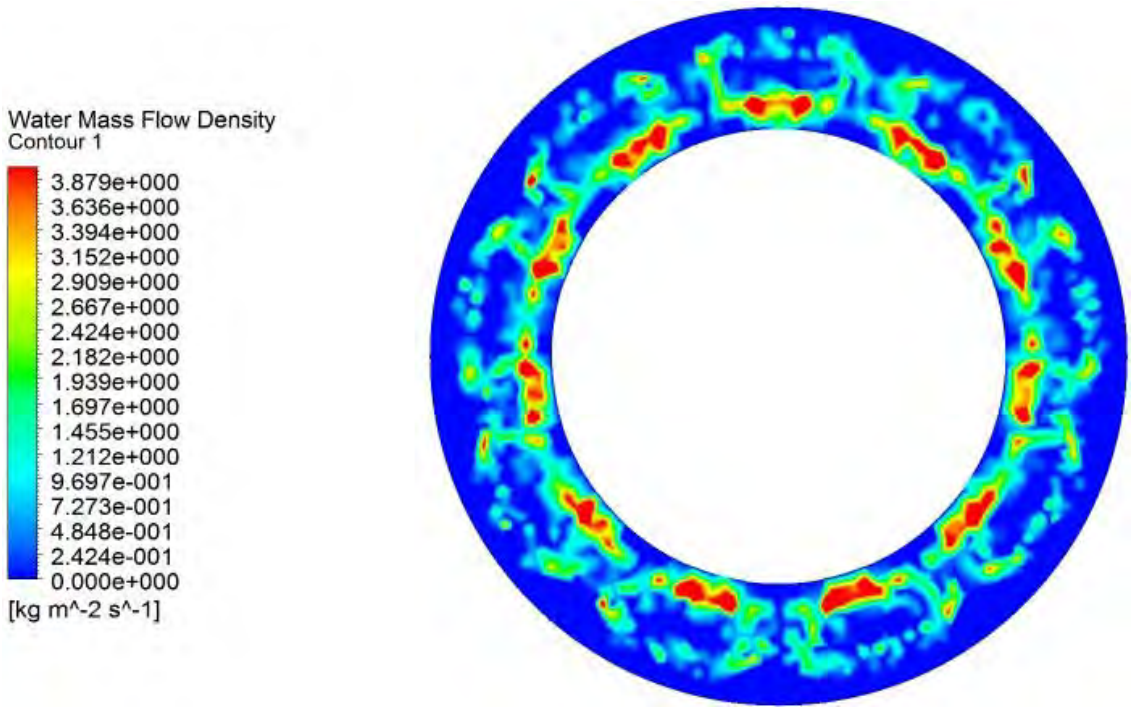

Figure A. 6, , , Water mass flow density at the outlet boundary for for optimum operation of radial nozzle ($\boldsymbol{d_n = 1.5mm}$) and axial nozzles ($\boldsymbol{d_n = 1.5mm}$)

VITA

Hamzeh Nawar was born in April 15, 1985 in Amman-Jordan, he started his education in a private school in Amman, then he moved to United Arab Emirates to finish his school education in 2004. He received a scholarship from Emirates Aviation College in Dubai-UAE from which he graduated in 2009. His Bachelor degree was in Aeronautical Engineering.

In fall of 2009, Hamzeh started his masters degree program in Science of Mechanical Engineering in the American University of Sharjah and worked as teaching assistant in American University of Sharjah for couple of years. Hamzeh is expected to graduate in 2011